UiT The Arctic University of Norway

Faculty of Engineering, Science and Technology (IVT)

Department of Industrial Engineering

Feasibility Study of Hydrogen Production from Wind Energy in Narvik

Christopher Odongo

Master's Thesis in Industrial Engineering, INE 3900

May 2021

Title: The Feasibility Study of Hydrogen Production from Wind Energy in Narvik, Norway	***Date:*** 15.05.2021
	Candidate Number: 13
Author: Christopher Odongo	***Number of Pages:*** 123
	Number of Attachments:
Subject Name: Master's Thesis	***Subject Code:*** INE-3900
Faculty: Engineering Science and Technology	
Master Program: Industrial Engineering	
Supervisor: Professor. Muhammad Shakeel Virk	
Co-supervisor: Professor. Mohamad Mustafa	
Keywords: Green Hydrogen Production, WRA, AEP, Wind Electrolysis, WindSim, Windographer, CFD simulation, Electrolysers.	

ABSTRACT

The use of renewable energy sources is gaining momentum globally as possible replacements for fossil fuels which have proven to be serial contributors to global warming. Hydrogen is one such environmentally friendly fuel with zero carbon emission proven to be reliable for use in the transport sector. Since hydrogen is an energy carrier, its mode of production has for a long time relied on high carbon emission fuels that negate its authority as emission-free fuel.

Therefore, this study investigates a green hydrogen production method based on water electrolysis using electrical energy from wind power. The project entails a detailed wind resource assessment around Narvik region through historical meteorological data analysis, and CFD simulations using Windographer and WindSim software programs to ascertain the viability of the wind power potential of the area. Thereafter, the project establishes suitable location(s) for appropriate wind turbine siting to generate optimal net AEP for use in the electrolysers. Subsequently, a detailed analytical calculation is conducted on the possible amount of hydrogen that can be produced when a water electrolyser system is installed at the Djupvik site based on the net AEP values obtained. Finally, there is determination of the probable cost estimates for such a venture.

ACKNOWLEDGEMENT

Foremost, I wish to express my sincere gratitude to my supervisors, Prof. Muhammad Shakeel Virk and Prof. Mohamad Mustafa, for all their support, motivation, and wise counsel during the entire project cycle, without which this thesis work would not have been successful.

Secondly, my utmost appreciation goes to the Northern Axis Barents Link (NABL) project and Hydrogen transport economy for the Northern sea region (HYTREC2) project for the financial support during the execution period and coming out as the main sponsors of this master thesis project.

I equally express special recognition to SAIH and DIKU for the sponsorship during the entire period of study. I sincerely thank Madam Hege Kristin Widnes for holding my hand for the whole period and seeing me through to the dead-end of this master's program.

Finally, I express my indebtedness to all my teachers and colleagues for the moral support and guidance during the entire life of studentship in Narvik.

May 15th, 2021

Ouma Christopher Odongo

UiT- The Arctic University of Norway

Table of Contents

List of Tables

List of Figures

Acronyms and Chemical Symbols

A/cm^2: Amperes per square centimeter

AC: Alternating Current

AE: Alkaline Electrolyser

AEP: Annual Energy Production

AP: Acidification Potential

ATR: Auto thermal Reforming

AVR: Automatic Voltage Regulator

CapEx: Capital Expenditure

CCS: Carbon Capture and Sequestration

CFD: Computational Fluid Dynamics

CG: Coal Gasification

CH_4: Methane

CO: Carbon monoxide

CO_2: Carbon dioxide

DC: Direct Current

DNS: Direct Numerical Simulation

EU: European Union

FCR: Fixed Charge Rate

GHG: Greenhouse Gas

GWEC: Global Wind Energy Council

GWh: Gigawatt hours

GWP: Global Warming Potential

H^+ Hydrogen ions

H_2: Hydrogen

HAWT: Horizontal Axis Wind Turbine

HER: Hydrogen Evolution Reaction

IEA: International Energy Agency

IGBT: Insulated Gate Bipolar Transistor

Kg/hr: kilograms per hour

KOH: Potassium hydroxide

KWh: Kilowatt hours

LCOE: Levelised cost of energy

LES: Large eddy simulation

MARS: Magenn Air Rotor Systems

MCP: Measure Correlate and Predict

MERRA: Modern-Era Retrospective analysis for Research and Applications

MSFD: Mixed spectral finite-difference

MW: Megawatts

MWh: Megawatt-hours

NABL: Northern Axis Barents Link

NaOH: Sodium hydroxide

NG SR Natural Gas Steam Reforming

Nm^3: Normal cubic meters

NREL: National Renewable Energy Laboratory

NWP: Numerical Weather Prediction

O & M: Operation and Maintenance

O_2: Oxygen

OER: Oxygen Evolution Reaction

OH^-: Hydroxyl ions

OpEx: Operational Expenditure

PEM: Polymer Exchange Membrane

POX: Partial Oxidation of hydrocarbons

RANS: Reynolds-Averaged Navier-Stokes

REDOX: Oxidation-Reduction reactions

SMR: Steam Methane Reformation

SPE: Solid Polymer Electrolyte

T: Temperature

UNEP: United Nations Environment Program

US: The United States

VAWT: Vertical Axis Wind Turbine

WEO: World Energy Outlook

WRA: Wind Resource Assessment

WRF: Weather Research and Forecast

Wt%: Weight percentage

WAsP: Wind Atlas Analysis and Application Program

1 INTRODUCTION

As the world races against time to mitigate the effects of climate change, every effort is put in place to minimize usage of any form of energy that immensely contributes to the emission of greenhouse gases. The International Energy Agency (IEA), in its annual World Energy Outlook (WEO) report of 2020, declared that the global carbon emissions must fall by 40% in this decade in order to revive the hope of achieving carbon neutrality by 2050 [1]. It, therefore, means that everyone must join hands in the war against carbon emission. This provided the motivation for this study to explore clean alternative energy sources with zero-emission of the environmental disastrous gases.

Carbon dioxide is considered the prime contributor to global warming and accounts for 64 % of the increased greenhouse effect [2]. Extensive use of fossil fuels continues to contribute to CO_2 gas emissions. Referencing the World Energy Outlook publications, the emission is projected to increase to more than 45 billion metric tons in 2040. Among the fossil fuels, coal is the primary culprit and accounts for more than 44% of the CO_2 emissions, and this is projected to increase to more than 47% in the decade of 2020-2030; while liquid fuels and natural gas cumulatively contribute to over 22% of the global emissions [3].

Since it is universally agreed that the main contributor to the overall emission of greenhouse gases is the usage of organic fuels, every focus and attention should be geared towards eradicating the use of fossil fuels. Topping the list of the most coveted new sources of energy are the renewable sources targeted to assist in balancing the global energy demand as well as to pilot the replacement of the fossil fuels since the IEA net-zero emission report outlines that the subcritical and supercritical coal plants should shut down by 2030. The significance of this study is attached to the global call for a reduction in carbon emissions as outlined by the IEA 2020 world energy outlook, which aims for net carbon neutrality by 2050 and negative carbon emission by 2070 [1].

Therefore, this master thesis project entails a comprehensive study of how to produce electricity from wind energy, which is eventually used to calculate the possible amount of hydrogen that can be generated through a green process of water electrolysis. The project targets the Djupvik site in Narvik, located at the latitude and longitude coordinates of 68.4485568°N and 17.5213884°E, respectively, as a reference point where the hydrogen refueling unit is installed. This is also where study begins by analysing the wind power potential of the area to predict the net AEP that can be generated to ascertain the possible hydrogen production capacity on site.

Figure 1-1 shows the pictorial view of the proposed hydrogen refueling site in Djupvik as of November 2020, while figure 1-2 shows the geographical map of the proposed area of the hydrogen production site.

Figure 1-1: *Photo showing the proposed hydrogen refueling site at Djupvik in Narvik.*

Figure 1-2: *Geographical map of the proposed hydrogen production site in Djupvik.*

1.1 Background Information

The use of fossil fuels such as oil, natural gas, and coal have been of great concern globally for decades because of their widespread application as essential energy sources for transport, industrial, and residential services. Our World in Data report reveals that 73.2% of the global greenhouse gas (GHG) emissions come from energy usage in industrial, residential buildings, and transport sectors [4]. Therefore, reducing emissions from any of these three top contributors will significantly impact the amount of carbon dioxide in the atmosphere.

Currently, all efforts are directed towards combating the looming global warming crisis led by the world's political leaders, researchers, and environmentalists who are in the forefront against climate change and possible ways of mitigating the current situation. During her New Year 2021 address to the nation [5], the Norwegian prime minister outlined her government's climate policy plans, which are geared towards achieving the targets for reducing emissions in non-ETS sectors by reducing greenhouse gas emissions in Norway, in line with the Paris agreement. Further, she explicitly echoed the importance of investing in hydrogen production as emission-free fuel and expressed her government's plan of investing in more hydrogen-powered ferries to promote the development of green shipping [5].

In the same spirit, the United Nations Environment Program (UNEP) calls upon every individual, institution, company, society, and all agencies worldwide to join hands in the war against carbon emission. In a detailed report, UNEP proposes that CO_2 emission must reduce annually by 7.6% between 2020 and 2030 to mitigate the anticipated temperature increase of 1.5°C by the end of the decade [6]. The global call for reducing the rate of carbon emission started in the last century but became more pronounced in the previous two decades with several proposals and ideas put forward to help combat the menace and forecast the timeframe when negative carbon emission will be achieved. For instance, in 2015, the Research Council of Norway, Innovation Norway , and Enova jointly established a PILOT-E funding scheme to incentivize companies to create innovative zero and low-emission technologies as a way of reducing greenhouse gas emissions within the next ten years [7]. This scheme has received widespread support from the intended stakeholders, and in 2019 the scheme awarded a whooping NOK 95 million to four projects that purpose to establish a hydrogen supply chain and reduce emission in construction sites.

The HyWays report by the European Commission [8] forecasted that the global CO_2 emission from road and rail transport would reach an all-time high in 2020 and whatever happens thereafter will determine the fate of the net-zero emission plan by 2050. This is further confirmed by the UNEP emission gap report, which shows that carbon emission has been on an upward trajectory since 1990, with a meteoric rise between 2010 and 2019 [6]. The reports suggest that robust support policies and systems coupled with high learning and innovation in the implementation of the end-use application of hydrogen energy in road transport will reduce 25-50 metric tons of CO_2 emission in the year 2050. Figure 1-3 shows the HyWays' analysis of CO_2 emission from the EU member states and the significance of implementing hydrogen support policies and skills.

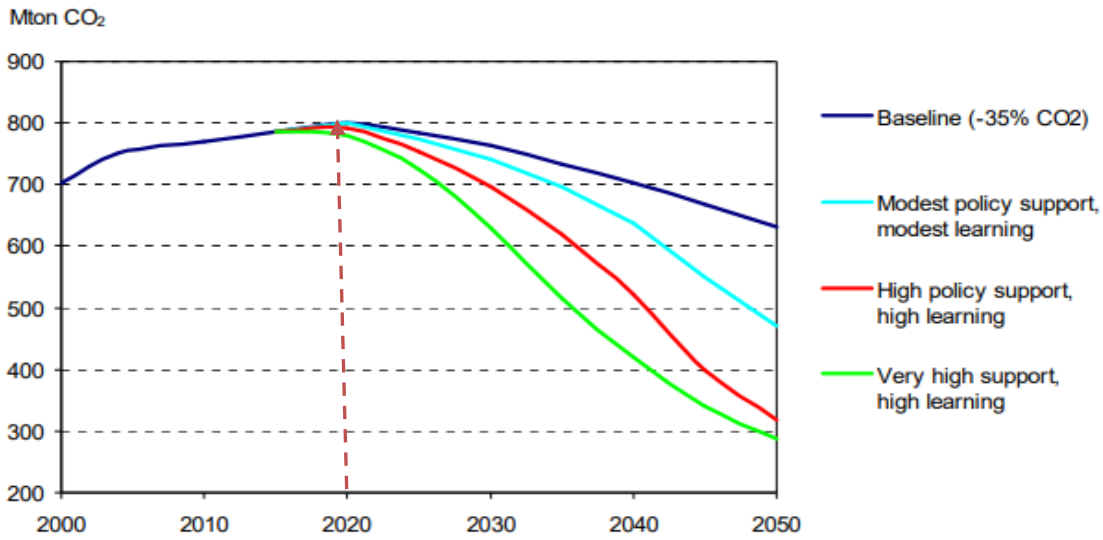

Figure 1-3: *Illustration of the prediction of road transport CO_2 emission by the EU member states and significance of hydrogen technology application as outlined by HyWays* [8]

Since transport sector is a major culprit of carbon emission, technologies must be developed to curb the usage of such fuels in this sector and replace them with more effective and environmentally acceptable means of locomotive power. Further, the most significant proportion of carbon emission from the transport sector comes from road transport. As reported by Ritchie and Roser of Our World in Data [4], 75% of the transport sector emission is from road transport. Therefore, tackling emissions from road transport will contribute a greater deal in combating the overall emission from the transport sector. The IEA report of 2020 continues to outline that in order to attain carbon neutrality by 2050, half of all cars globally should be electric by the end of 2030 [1]. Due to these findings, there is pressure to develop alternative sources of energy that are clean, efficient, and reliable for use in the transport sector, more specifically in road transport. This is anticipated to unfold new investment potentials in large scale renewable energy sources, electric cars, and new technological innovations. In this regard, there has been a critical mission to eliminate fossil fuel vehicles on roads and replace them with non-emission vehicles. In this aspect, hydrogen has been recommended as one better alternative to fossil fuel since it is a high-efficiency energy carrier with zero emissions at its point of use [9, 10]. Actually, the by-product of hydrogen combustion is just water.

Studies by the National Renewable Energy Laboratory (NREL), USA have shown that hydrogen can be used for transportation, heating, and power generation and has the potential to replace fossil fuels in all their contemporary applications, thereby getting accolades as the panacea for global warming [11]. Further, hydrogen ranks higher as the perfect replacement to fossil fuels in cars, buses, and other motor vehicles [11, 12]. However, for a long time, a major hindrance to green hydrogen production has been the feedstock and energy source since

hydrogen production is highly energy-intensive [13]. Over the years, hydrogen production has heavily relied on fossil fuel combustion processes such as steam methane reformation (SMR), partial heavy oil oxidation (POX), and gasoline reforming, among other techniques. These are high carbon emitting processes which negate the merits of hydrogen as non-emission fuel [9]. However, a paradigm shift is eminent from fossil fuel sources to the green production of hydrogen. One such method is hydrogen production from electrolysis using electrical energy from renewable sources such as hydropower, solar power, and wind power.

Electricity production from wind energy has been on the upward trend globally due to technological innovations, governments' incentive programs, cost reduction, and public demand for clean energy [14]. According to the Global Wind Energy Council (GWEC) 2019 report [15], the global total wind energy installed capacity by the close of 2019 stood at 651GW, translating to 5% of total global electricity generated. In addition, GWEC Market Intelligence is forecasting that by 2024, over 355GW of new capacity wind power will be installed globally, translating to nearly 71GW of new installations every year until 2024, with developing nations and offshore installations as the major contributors to the new growth [15]. As a result, wind energy and hydrogen form a vital part of clean sources of energy that must be attentively monitored to help in minimizing the over-reliance on fossil fuels.

Since 2010, research and development has been extensively applied to support in rolling up large-scale technologies for the anticipated takeover of the hydrogen economy and the looming crisis due to shut down of the fossil fuel plants. Figure 1-4 shows the chronological events of innovative occurrences in the past ten years with regard to introducing new hydrogen and fuel cell technologies in road transport and the expected technological progress towards attaining the net-zero emission as outlined by the HyWays - an integrated project to develop the European Hydrogen Energy Roadmap. This is coupled with the IEA publication in October 2020 on World Energy Outlook that will guide energy demand discussions in this decade and beyond as a roadmap to achieving net-zero emission by 2050 [1].

Consequently, with the projected shutdown of many organic fuel production plants in the future, alternative clean and reliable energy sources have to be implemented with urgency in the energy sector. Therefore, this is the opportune time to conduct this study when everyone is on board concerning CO_2 emissions' reduction, and all efforts are geared towards achieving a sustainable green economy in all sectors.

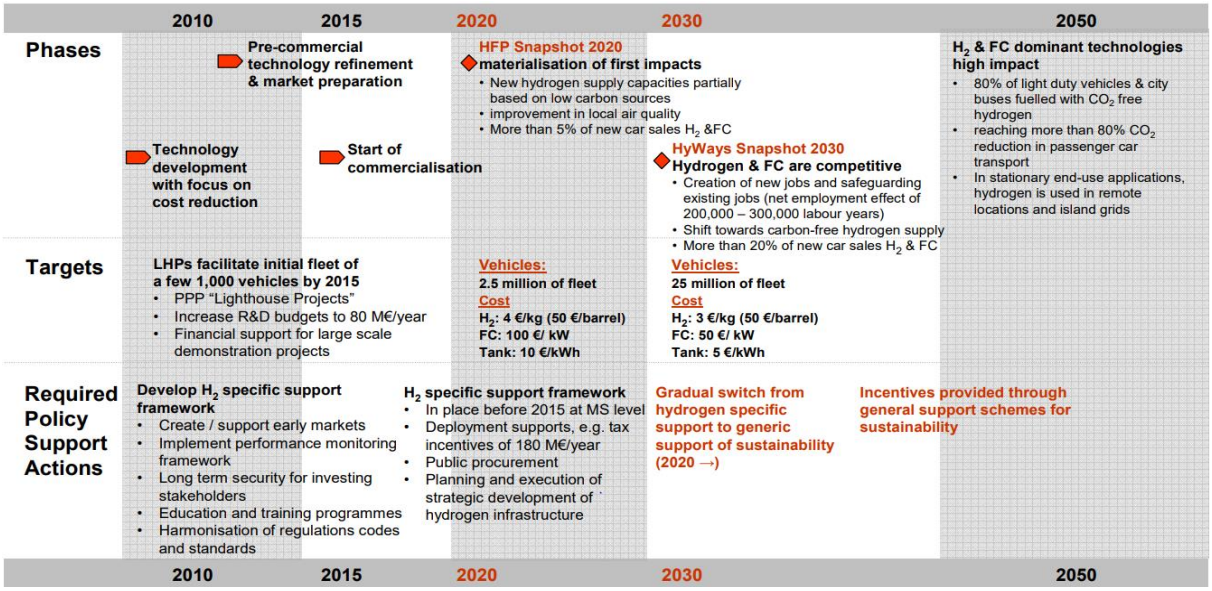

Figure 1-4: *Summary of an action plan towards technological innovations in eliminating carbon emissions as proposed by the HyWays* [8]

1.2 Problem Statement

The Arctic Technology & Icing Research group and the Building, Energy and Material Technology research group of UiT the arctic university of Norway is seeking to establish a hydrogen refueling station to join in the global clarion call for mitigating the effects of climate change. The station already under construction at Djupvik in Narvik, is planned to receive hydrogen from an external source in the short-term, but in the long run, the group intends to establish a hydrogen production system onsite to navigate the logistical challenges of transporting hydrogen to Narvik. Given that the vision and mission of the research groups is to minimize any fossil fuels' usage as a way of combating the emission of CO_2 gases, the hydrogen production process must be from 100% approved clean technology. One of the popular methods of producing pure hydrogen free of CO_2 emission is the electrolysis method. Others include photolysis, thermolysis, and thermochemical reactions.

The electrolysis method requires electrical energy for its operation to be ultimately successful. The central and popular sources of clean and renewable energy that can be used to produce electrical energy for such projects include solar energy, hydropower, and wind power. Given the geographical location of Narvik, solar energy is not a practical option. This is because Narvik is one of the northernmost cities globally, and hence solar is very seasonal and unreliable. Such regions have approximately less than three months of solar in a year during the summer months of June, July, and August. The next significant electricity source is hydropower. However, according to reports from Nordkraft, the agency in charge of electrical

power production and distribution in northern Norway, hydropower is overstretched by power supply demands from industries and residential homes, and they are venturing into alternative sources of renewable energy like wind power going into the future [16]. As a result, wind power harnessing remains the best opportunity for generating electricity for hydrogen production. This is also backed by recent studies that have extensively revealed that the onshore and offshore wind power potential around the arctic region is high and virgin for exploitation to provide novel electricity solutions in the region. On the backdrop of such findings, this research chose to delve into the exploration of harnessing wind energy as a renewable source of electricity for use in the water electrolysis process. This research study examines the possibilities of using the wind power potential of the Djupvik site and its environs to supply the electrical energy demand for hydrogen production.

1.3 Project Description

This master thesis project seeks to prove that it is possible to produce hydrogen at 100% CO_2 emission-free. The project explored one primary approach i.e., producing hydrogen from water through the electrolysis method. Since the electrolysis method requires electricity to produce hydrogen, electrical energy must be produced from a renewable source to guarantee sustainability and conserve the environment. Both electrical energy and hydrogen are energy carriers, and as such, their sources must be 100% clean; otherwise, the end product will not be regarded as emission-free. In this case, the source of electricity for use in the electrolysis process has been identified as wind power. Therefore, the first task was to conduct thorough research on wind resource assessment around the specified site. This mission was possible by obtaining the climatological historical data of the site and its environs followed by profound analysis of the data to forecast the possible mean wind speed and direction of the site and prediction of the areas with more substantial wind speed for wind turbines micro-siting. Besides the data analysis, the project involved aspects of terrain analysis, area classification, and wind fields simulation. All these converged to facilitate prediction of the wind power potential of the area and the possible amount of electrical energy that can be generated per year, otherwise called annual energy production (AEP) potential.

The information on AEP contributed to the calculation of the amount of hydrogen that could be generated from the site in order to make the judgment if the project would be worth pursuing or not. Therefore, the second phase involved analysis of the net AEP information and calculations on hydrogen production to give the final recommendations. Figure 1-5 shows the flow outline of this master thesis project framework.

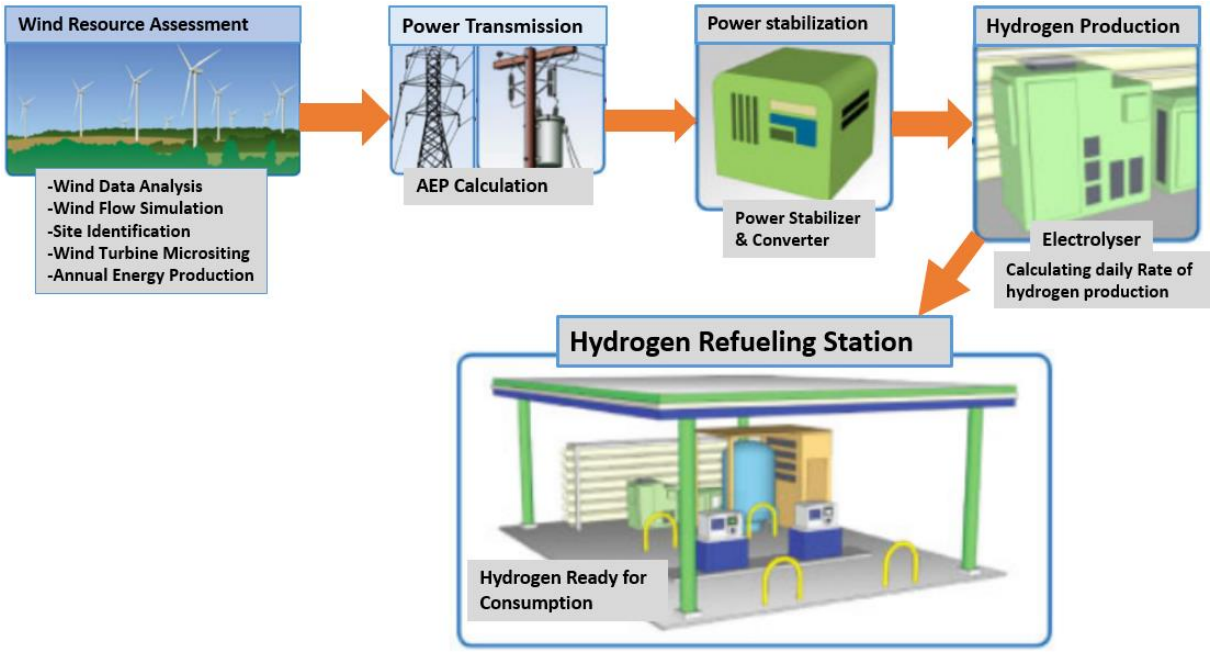

Figure 1-5: *Flow outline of the Master Thesis Project*

This study is part of the bigger mission of UiT on establishing a hydrogen production plant in Djupvik near Narvik as part of the activities of the Hytrec2 project to demonstrate green hydrogen utilization in the transport sector and Northern Axis Barents Link (NABL) project, where the focus is on wind energy production at cold climate sites in Arctic Regions. The goal of this master thesis theme is the onsite production of hydrogen from electricity generated from wind energy. Finally, this project will be linked with the other ongoing mainstream research activities of Arctic Technology & Icing Research group and the Building, Energy, and Material technology Research Group.

1.4 Research Design

Elements	Descriptions
Project title:	Feasibility Study of Hydrogen Production from Wind Energy in Narvik.
Project sponsors:	- UiT The Arctic University of Norway - HyTrEc 2 project - Northern Axis Barents Link (NABL) project - Arctic Technology & Icing Research group - Building, Energy, and Material Technology Research Group
Project Supervisors:	Supervisor: Prof. Muhammad Shakeel Virk Co-Supervisor: Prof. Mohamad Mustafa

Theory/hypothesis:	- Hydrogen is the future fuel for transportation. - Green hydrogen production is the ultimate panacea to global warming. - Wind power is the focal source of electricity for the future.
Assumptions:	➢ It was assumed that this project would be completed on schedule, and no delays would be encountered in the project cycle. ➢ Further, it was assumed that all software programs planned for use in this project would work optimally, and any challenges would be addressed in time. ➢ Lastly, I was hopeful to remain focused and healthy to see this project to its ultimate conclusion.
Risks/constraints:	- Unforeseen effects of the ravaging Covid19 restrictions - Sickness during the project execution period - Risks of losing vital files due to program crashing.
Specific objectives:	• To conduct a thorough feasibility study of wind power potential around Djupvik site, Narvik. • To establish very precise estimates of the amount of electrical energy that can be harnessed from the onsite wind power. • To calculate the hourly and daily proportional amounts of hydrogen that can be produced compared to the daily demand.
Scope:	1. Initial work/literature study with refinements and definitions. 2. Definition of the research problem, methodology, and objectives. 3. Study of wind resource assessment as the prerequisite for establishment of the wind park project using numerical tools and other field data. 4. Study and analysis of currently available system solutions i.e., analysis of the available data for the Djupvik site as a roadmap for estimation of the wind power potential of the area. 5. Feasibility study of onsite hydrogen production using wind power at the Djupvik site based on the findings of 3 and 4 above. 6. Presentation of the results of the research work 7. Production of a scientific article/paper based on the master thesis report.

1.4.1 Research Project Plan

This master thesis project was scheduled for about eight months, from October 2020 to May 2021. To accomplish all the outlined tasks and objectives, the following Gantt charts tables 1-1 and 1-2 show the scheduled plan for execution of every section of the project.

MASTER THESIS PLAN
GANTT CHART 2020/2021

TASKS/ TIMELINES	Oct. 18th-31st	Nov.	Dec.	Jan.	Feb.	March	April	May 1st-15th
Introduction and Task Description								
Literature Review								
Research methodology								
Wind Data Analysis using wind flow model software								
Feasibility study of onsite hydrogen production								
Writing Project Report								
Writing Scientific Paper								
Presentation of Research findings and reports								

Table 1-1: *Master thesis execution plan*

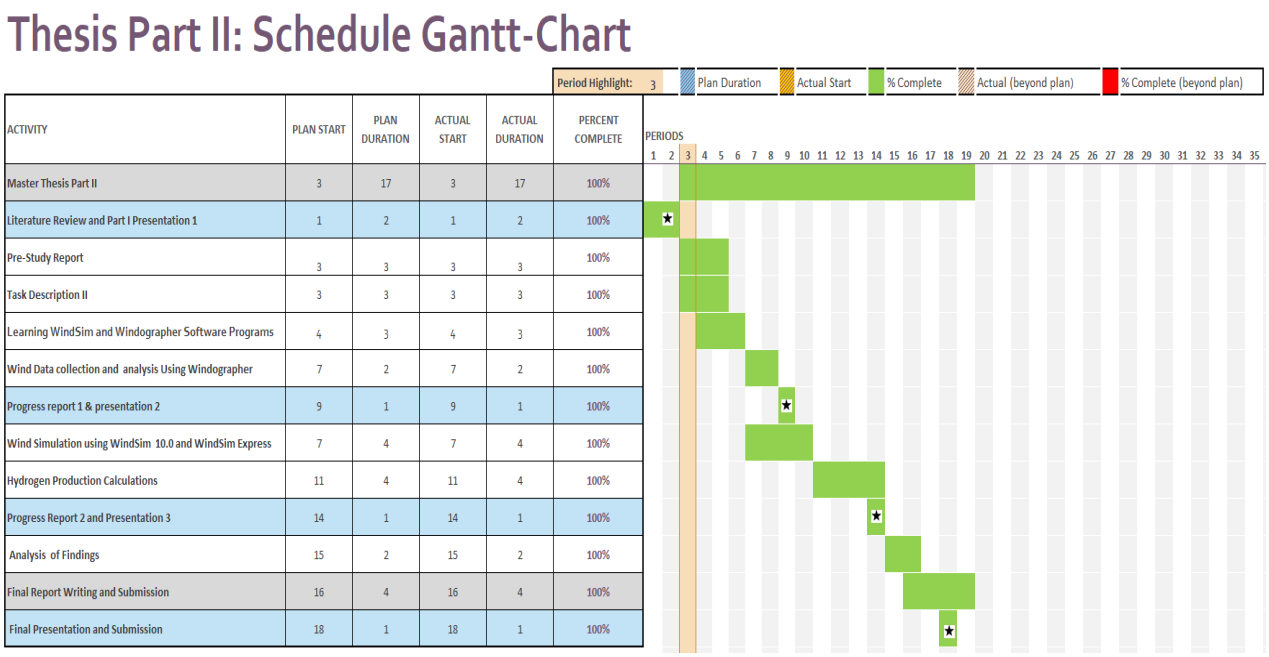

ACTIVITY	PLAN START	PLAN DURATION	ACTUAL START	ACTUAL DURATION	PERCENT COMPLETE
Master Thesis Part II	3	17	3	17	100%
Literature Review and Part I Presentation 1	1	2	1	2	100%
Pre-Study Report	3	3	3	3	100%
Task Description II	3	3	3	3	100%
Learning WindSim and Windographer Software Programs	4	3	4	3	100%
Wind Data collection and analysis Using Windographer	7	2	7	2	100%
Progress report 1 & presentation 2	9	1	9	1	100%
Wind Simulation using WindSim 10.0 and WindSim Express	7	4	7	4	100%
Hydrogen Production Calculations	11	4	11	4	100%
Progress Report 2 and Presentation 3	14	1	14	1	100%
Analysis of Findings	15	2	15	2	100%
Final Report Writing and Submission	16	4	16	4	100%
Final Presentation and Submission	18	1	18	1	100%

Table 1-2: *Master Thesis Part II Execution Plan*

2 LITERATURE REVIEW

This section entails the comprehensive study of the subject matter and combing through different literary works in the recent past from various authors in the fields of hydrogen production technologies and wind energy production methodologies. The topic is subdivided into two main phases, i.e., the literature review on hydrogen production technologies and the literature review on elements of wind resource assessment. The literature review on hydrogen production begins by briefly outlining the non-renewable methods that have been applied over the years in producing hydrogen, such as steam reforming practices, partial oxidation of heavy hydrocarbons (POX), and coal and biomass gasification. Thereafter, a deep and extensive look into the modern and emission-free methods used in producing hydrogen is outlined, coupled with an in-depth analysis of different classifications of water electrolysis as a method for producing clean hydrogen.

Given that water electrolysis method requires electrical consumption, the desired source of electricity in this project would be wind power. As a result, a comprehensive study on elements of wind resource assessment is mandatory. Therefore, the subsequent section is a discussion of the wind resource assessment methodologies, which involve site analysis and topographical features of the project site, analysis of different numerical wind flow models, wind turbine technologies, micrositing, and wind power conversion systems.

2.1 Hydrogen Production Technologies

The ravaging effect of climate change has resulted in the implementation of alternative sources of energy that are clean, efficient, reliable, and renewable. Hydrogen has gained prominence in the recent past as a novel energy carrier that can be generated for use in various sectors of the economies. Several tests have proven that hydrogen is indeed an environmental-friendly energy source, if and only if it is generated from a clean source. Some of the advantages of hydrogen that makes it desirably stand out as the fuel for the future include [10, 17]:

- Hydrogen is the most abundant element on earth and with the highest energy content per unit weight.
- It can be produced from several feedstocks, both renewable and non-renewable sources.
- It can supply the energy needed for transportation, electric power, and thermal requirements.
- It has very high efficiency in utilization and conversion, i.e., fuel cells can convert 40-65% of hydrogen's energy to electricity unlike internal combustion engines 15 – 20%.

- If handled appropriately, it is safer, convenient, and clean fuel for transportation than gasoline.

Hydrogen is an energy carrier and not a primary energy source. This means that hydrogen is not directly extracted from the earth but produced from feedstocks constituting hydrogen elements in their composition, e.g., water or hydrocarbons, which are either clean or unclean sources as displayed in figure 2-1.

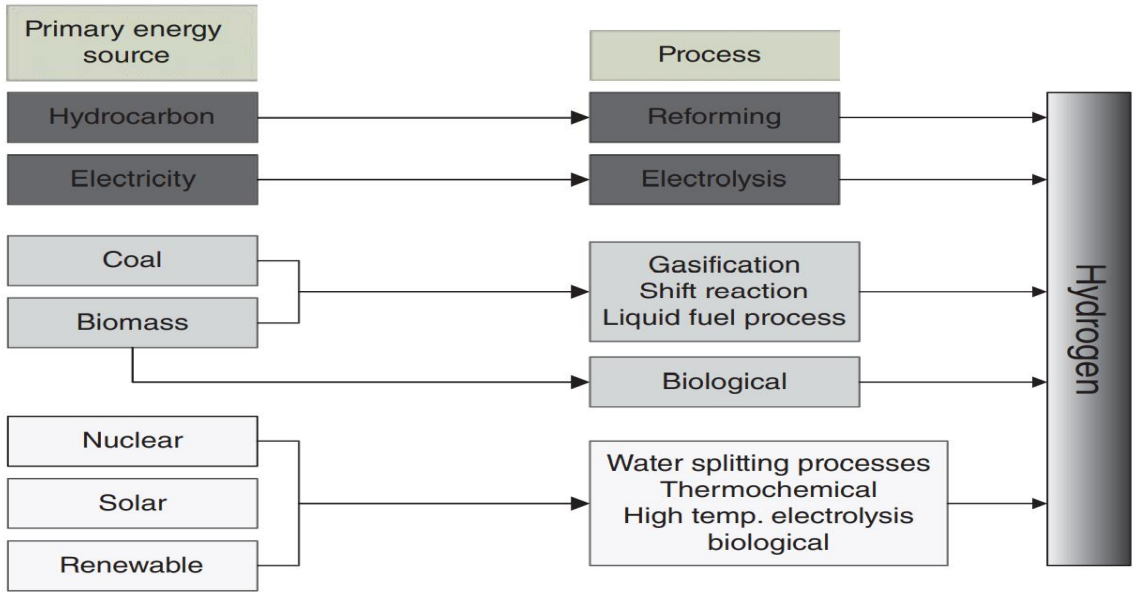

Figure 2-1: *Showing the primary energy sources of Hydrogen* [18]

For the longest time, hydrogen has been majorly produced from non-renewable fossil fuels through steam reforming of natural gas, thermal cracking of natural gas, partial oxidation (POX) of heavy oils, or coal gasification. This is because of lower cost of production due to high maturity level of such industrial processes as a result of long-standing establishment over the years [9]. Such processes negates the entire concept of hydrogen as an environmentally friendly fuel, since for it to be considered completely clean energy, the production processes must be entirely clean from the onset to contribute to the reduction of CO_2 emissions into the ecosystem [19]. The other methods of hydrogen production include, biomass by burning, fermenting, pyrolysis, gasification followed by liquefaction, and water by electrolysis, photolysis, thermochemical processes, and thermolysis [13].

Figure 2-2 shows some of the primary techniques used to extract hydrogen from their feedstocks. It is worth noting that the cost of hydrogen generation from renewable sources is

relatively higher than non-renewable sources since such technologies are still in their early stages of development, but the long-term benefits are far much greater than the present costs.

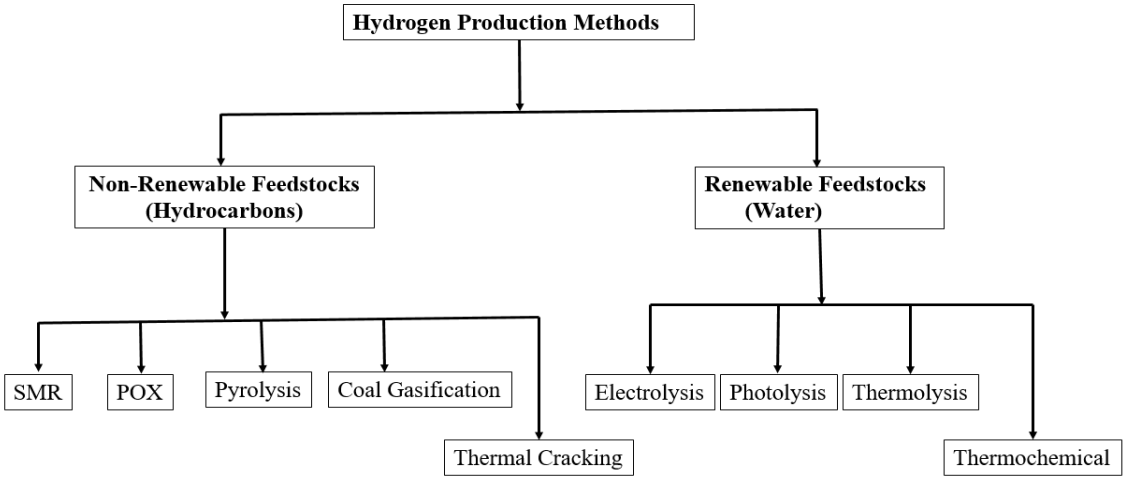

Figure 2-2: *Illustration of the main processes of hydrogen production.*

The subsequent sections look into some of the different technologies that have been used in producing hydrogen and further highlights the most appropriate methods for achieving the hydrogen economy, being cognizant that to attain hydrogen economy, then hydrogen must be produced in a sustainable, efficient, and environmentally friendly manner.

2.1.1 Steam Reformation of Natural Gas

This method is also called steam methane reformation (SMR), and it is the most established, popular, and least expensive method for the commercial production of hydrogen [20]. The method accounts for about 48% of the global hydrogen market [21]. The technique is a simple three-step process whereby methane (CH_4) as a feedstock is reacted with steam at a temperature between 700˚C to 1100˚C to produce syngas. Syngas is a mixture of hydrogen (H_2) and carbon monoxide (CO) [9]. Thereafter, the carbon monoxide component of the syngas reacts with steam to produce additional H_2 and carbon dioxide (CO_2) [19]. This is a water-gas shift reaction that aims to increase the yield of hydrogen content. Finally, hydrogen and CO_2 are separated in a gas purifier using different methods like pressure swing absorption, wet scrubbing, membrane separation or carbon capture and sequestration (CCS). Generally, it is estimated that SMR produces hydrogen with a purity of approximately 96 - 98% [9, 22, 23] with an operating efficiency of around 68-73% [18, 24]. However, this method is associated with the release of a vast amount of CO_2 into the atmosphere. In fact, according to a suggestion from the US Energy Information and Administration department [25], for every metric ton of hydrogen produced

through hydrocarbon reformation, 2.5 metric tons of CO_2 is released into the atmosphere. Figure 2-3 illustrates the process of steam methane reformation.

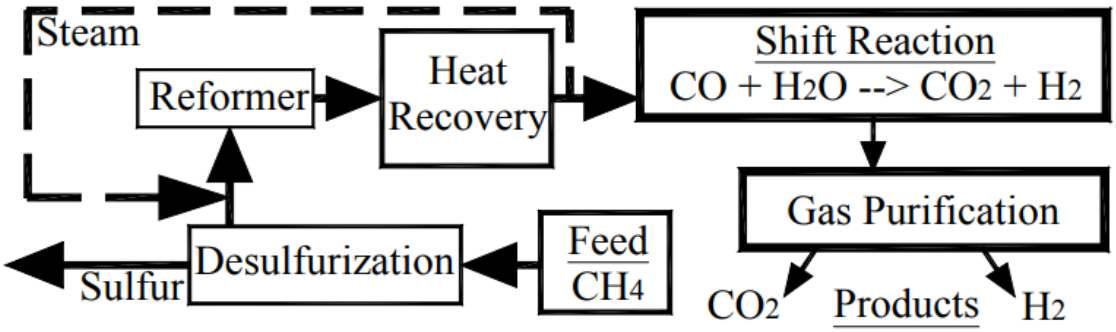

Figure 2-3: *Block diagram of hydrogen production by SMR process* [17]

2.1.2 Partial Oxidation (POX) of Heavy Hydrocarbons

The feedstock for this process is any liquid or gaseous hydrocarbon, for instance, heavy oil obtained from the treatment of crude oil. The feedstock is catalytically reacted with steam and oxygen at a temperature of about 600˚C to give a mixture of hydrogen, CO_2, and Carbon monoxide [24]. The mixture is then subjected to a shift reaction whereby hydrogen content is boosted then finally separated to form the hydrogen product stream. To provide energy for the entire process, the feedstock itself is burnt in the air, and as such pollutant gases such as Nitrogen Oxides (NO_x), Sulphur Oxides (SO_x), and Carbon Oxides (CO_x) are released into the atmosphere [10]. To avoid the formation of NO_x gases, air constituents must be separated to obtain pure oxygen used in the reformer. This will require an air separation plant, which will add to the cost of the entire POX process, hence making the process expensive. The efficiency of the POX process is estimated to be about 50% [23], and this process supply 30% of hydrogen to the global market [21]. Figure 2-4 shows the flow of the POX process.

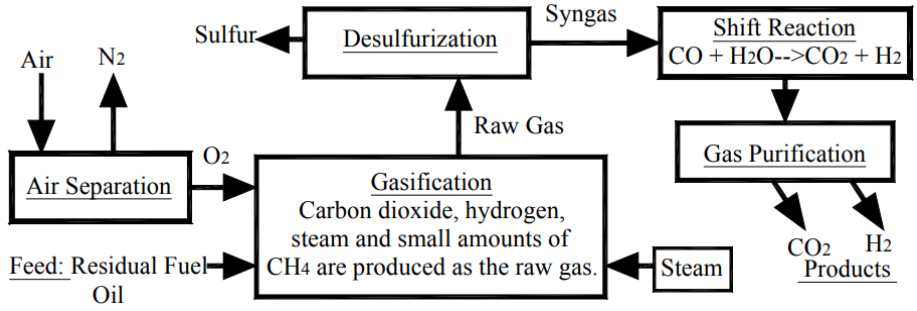

Figure 2-4: *Block diagram showing hydrogen production from POX process [24]*

2.1.3 Coal and Biomass Gasification

Gasification is another method of producing hydrogen that is well anchored over the years and is equally linked to the high release of CO_2 gas into the atmosphere. The process occurs at a much higher temperature than the POX process, usually between 1100°C and 1300°C [23]. In this process, different kinds of solid feedstocks such as coal and biomass are used, which are subjected to high temperature and pressure in the reactor where they react with oxygen or steam to produce syngas (CO and H_2) [19]. The carbon monoxide part of syngas is then subjected to water-gas shift reaction like in POX and SMR processes to boost the hydrogen yield. The conversion process is efficient though any unconverted feedstock is removed as molten slag. Coal is the most abundant fossil fuel, and coal gasification is the oldest method known for producing hydrogen with purity levels of about 97% [10] and takes 18% of the global hydrogen market share [21]. Figure 2-5 shows a flow chart of hydrogen production through the gasification process.

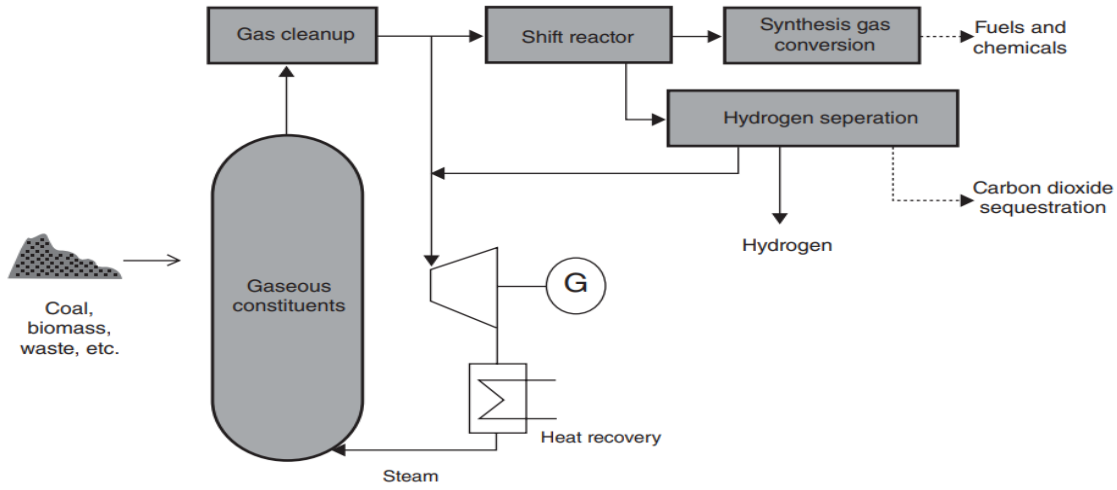

Figure 2-5: *Flow chart showing gasification processes [19]*

Generally, the three hydrogen production processes discussed above are the most popular and well-established methods. The feedstocks used in those processes are fossil fuels (hydrocarbons and coal) that are associated with the emission of a lot of CO_2 into the atmosphere. El-Shafie et. al.[26] and Vaes [21] argue that for a long time, over 96% of the hydrogen produced in the world came from fossil fuel feedstocks, and this has derailed the entire essence of using hydrogen as a clean source of energy. This has become a stumbling block in achieving a hydrogen economy. In order to produce environmentally friendly hydrogen, the method of production must use feedstock that does not release CO_2 into the atmosphere. Several methods have been proposed as the replacement to the already established methods that use fossil fuel feedstocks as a way to mitigate overall carbon emission during hydrogen production. However,

most of the methods under consideration are either too expensive in comparison to those using fossil fuels or are in their very early stages of development. Some of the methods under consideration include electrolysis, photoelectrochemical, photocatalytic, photobiological, and thermal decomposition, as shown in figure 2-6. All these methods use water as the feedstock, and they involve direct splitting of water which requires a very high temperature of over 2,000°C [3, 26].

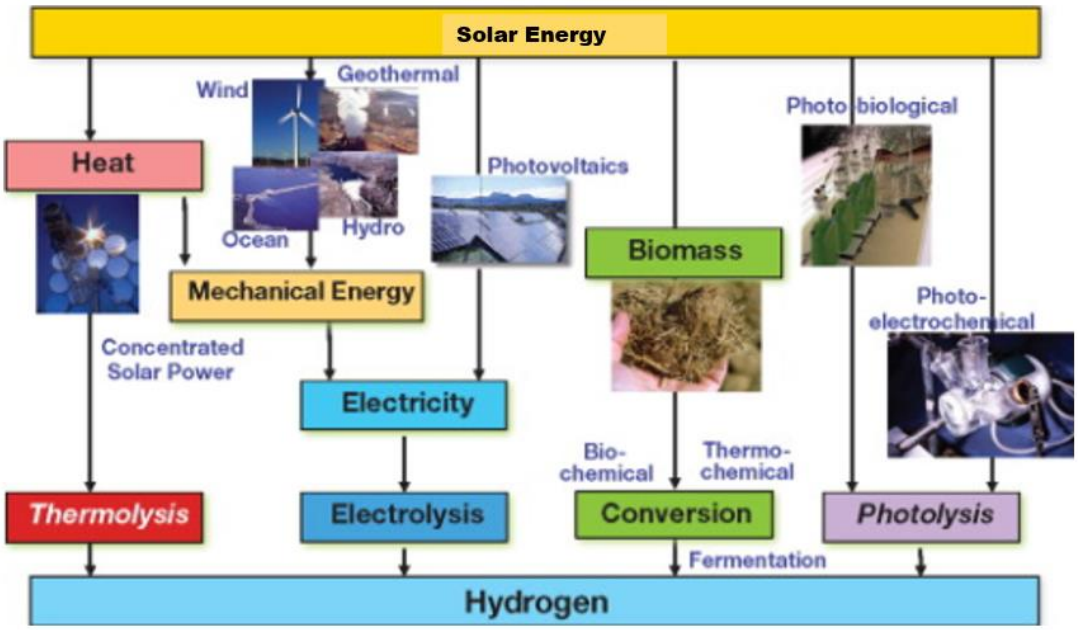

Figure 2-6: *Renewable pathways for green hydrogen production* [12, 27].

Different studies and research have shown that of all the methods outlined, water electrolysis has the potential of viability in large scale production of hydrogen in line with growth towards hydrogen economy. This is because water electrolysis has favourable efficiency of over 75% even though the cost is far much higher than that from fossil fuels [9, 13]. The following subsection is a discussion of the electrolysis production method that uses water as the feedstock.

2.1.4 Water Electrolysis

This technological process involves splitting water molecules into its constituent chemical elements of Hydrogen and Oxygen gases in the presence of an electrolyte, suitable electro-catalytic electrodes, and optimal temperature under the established Michael Faraday's laws of electrolysis. The process is very energy-intensive, and therefore electrical energy is used hence the name electrolysis. Other similar methods like photolysis and thermolysis occur through the use of solar and heat energy, respectively. This particular study focuses on the electrolysis of water, and as such other methods like water photolysis, thermolysis, and thermochemical reactions will not be considered.

Water electrolysis technology is not as widespread as the hydrocarbons reforming technologies, but a lot of attention is now directed towards it as the first port of call to producing clean hydrogen, free of CO_2 emissions. Records have indicated that the global hydrogen production from water electrolysis stands at only 4%, which is the highest in ranking compared to other green hydrogen production methods [3, 18, 26].

Given that water electrolysis is energy-intensive, the electrical energy used in this process can come from any source. However, it is imperative that electricity used should come from renewable sources for it to be considered sustainable [20]. This is why, this study explores the option of harnessing wind energy for the production of electrical power to be used in water electrolysis. According to [20, 28], wind electrolysis has the highest potential among renewable sources for producing emission-free hydrogen, but its impediment is the high cost of wind turbines and electrolysers.

There are different types of water electrolysis technologies depending on the type of the electrolyte and the operating temperature of the electrolyte. Water electrolysis technologies can also be classified into low-temperature processes (T<150°C), medium temperature processes (200°C < T < 600°C), and high-temperature processes (T >600°C) [22]. The most popular technologies are the alkaline water electrolysis method and polymer electrolyte membrane (PEM) electrolyzer method discussed in the next subsections. It is worth noting, that electrolysis cells are named based on their electrolytes, e.g., alkaline electrolyzer or solid polymer electrolyte (SPE) electrolyzer. Others include Saltwater Electrolysers, Solar Powered Electrolysis, and Solid Oxide Electrolysers. Figure 2-7 shows the general pathway of hydrogen production through electrolysis.

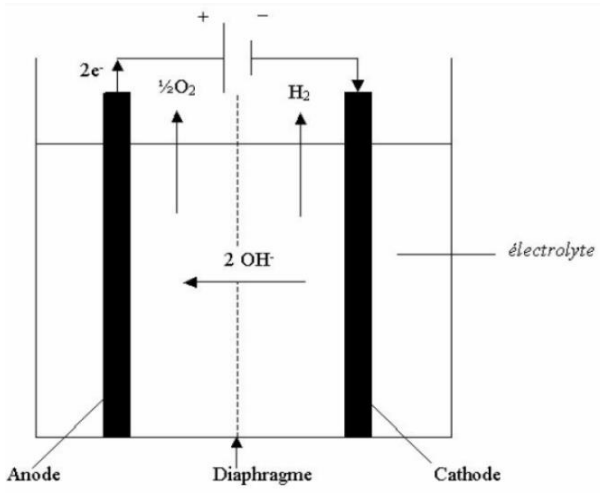

Figure 2-7: *General pathways of hydrogen production water electrolysis.*

2.1.4.1 Alkaline Water Electrolyzers

This method is used in large-scale systems where potassium hydroxide (KOH) or sodium hydroxide (NaOH) solutions are used as the possible ionic conductors (electrolytes). The most preferred electrolyte type is the aqueous solutions of KOH. This is because it has the highest specific conductivity than NaOH reaching optimal conductivity at a concentration of 30wt% (weight percentage) [12]. Besides, the electrolyte can perfectly operate at any concentration level within the range of 20wt% to 40wt% [9]. The standard operating temperature is between 60°C and 80°C even though it can increase up to a maximum of 100°C without any hitch, while the allowable pressure is anything between 1-30bars [24]. Another essential factor of consideration in alkaline water electrolyser is the choice of material for the electronic conductors (electrodes). The electrode material chosen must have high electrical conductivity, high catalytic activity, and good corrosion resistance, with regards to the two half-cell reactions of interest, i.e., the hydrogen evolution reaction (HER) at the cathode and the oxygen evolution reaction (OER) at the anode [23]. For a long time, steel grids have been used as the electrodes because of their low costs. However, they were found to be chemically unstable at high voltage in highly concentrated alkaline solutions [3]. To improve the electrochemical active surface area of the steel grid electrodes, they are covered with a porous layer of Raney Nickel (nickel–silicon alloy) or nickel-iron alloy, or nickel-zinc alloy [29]. Different research works have been conducted to find the best electrodes for use in the sector of alkaline water electrolysis, with some proposals suggesting that Nickel-Sulphur alloy as the excellent material for HER on cathode electrode [22].

When an electric DC is passed through an electrolysis cell, the water molecule is split into hydrogen ions (H^+) and the hydroxyl ions (OH^-) at the cathode. The hydroxyl ions are then attracted to the anode, where they get oxidized. The electrochemical oxidation-reduction (REDOX) reactions occur at various electrodes where electrons gain and lose take place to produce hydrogen and oxygen gases, as shown in figure 2-8.

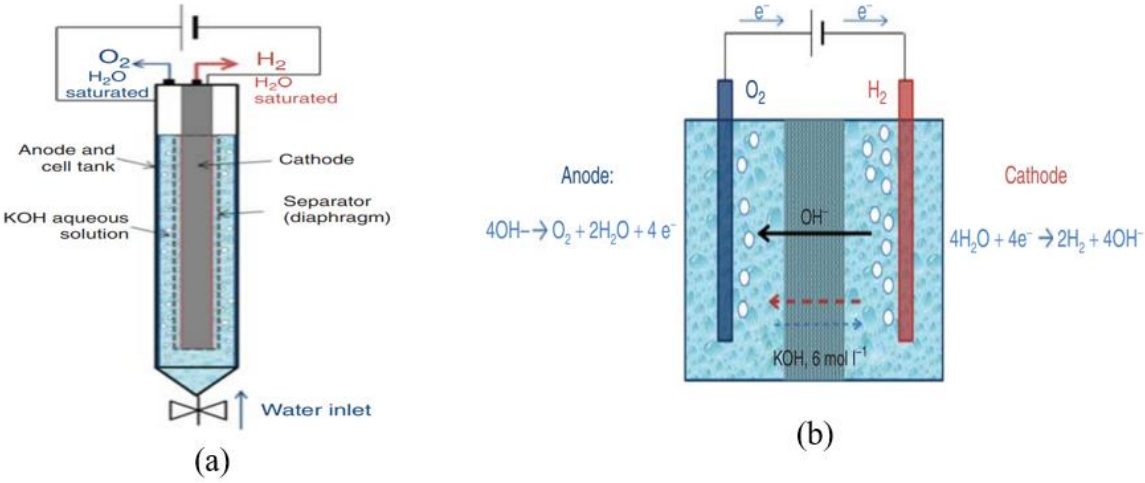

Figure 2-8: *Unipolar alkaline water electrolysis cell with a clear view of a diaphragm in (b)* [18]

Reaction at Cathode Electrode

At the cathode, the hydrogen ions (H^+) get reduced by gaining electrons to form hydrogen gas, as shown by the half-cell equation [12].

$H_2O + e^- \longrightarrow H^+ + OH^-$

$2H^+ + 2e^- \longrightarrow H_2$

Reaction at Anode Electrode

At the anode, the hydroxyl ions (OH^-) get oxidized by losing electrons to form Oxygen gas and water, as shown by the half-cell reaction equation.

$4OH^- \longrightarrow O_2 + 2H_2O + 4e^-$

Overall Reaction Equation

The overall reaction can be expressed as: -

$2H_2O \longrightarrow 2H_2 + O_2$

The lowest voltage needed to drive the water-splitting electrochemical reaction at room temperature, and pressure is 1.229V, which is called equilibrium voltage, and the required electrical energy to electrolyze water under the same conditions is 236.96KJ [17, 18].

As the electrolysis process takes place in the cell, water molecules get depleted, and therefore the concentration balance and volume of the electrolyte keep changing. The electrolyte volume in the electrochemical cells is determined by the gap between the anode and cathode electrodes [18]. Therefore, it is advisable to adjust the amount of electrolyte in the cell to take care of gaseous losses and change it regularly to avoid the accumulation of impurities from water and electrolyser for an extended period.

To prevent hydrogen and oxygen gases from recombining and to avoid any short circuit between electrodes in the electrolysis cell, a porous diaphragm (separator) is used between the electrodes [17]. Figure 2-8 (b) shows a clear view of the diaphragm, which should be a highly ionic conductor to permit the passage of hydroxyl ions from the cathode to the anode while preventing the mix-up of either gas. In the initial stages, asbestos was used as the preferred material for the porous separators, but the major stakeholders abandoned it due to its corrosive nature at high temperatures in strong alkaline solutions. Besides, asbestos is also highly poisonous that resulted in European Union banning its commercial usage in 1999 [18]. However, different separator materials are being developed from organic and inorganic materials by various stakeholders with surety that non-asbestos porous separators are getting into the market for use by the electrolyser producers. Today, the major electrolyser producers like the Nel Hydrogen (Norway), Hydrogenics (Canada), Teledyne Energy Systems (USA), and De Nora (Italy) are using non-asbestos separators, with the chemical composition of their separators remaining a hidden secret as their competitive advantage [26].

Commercially, two types of alkaline water electrolysis cells are commonly used. They include the tank cell unipolar configuration, which is the simplest and reliable (figure 2-8 (a)), and the bipolar configuration filter-press cells, which are more compact, have lower ohmic losses and require less energy supply [24] hence highly recommended and preferred as shown in figure 2-9.

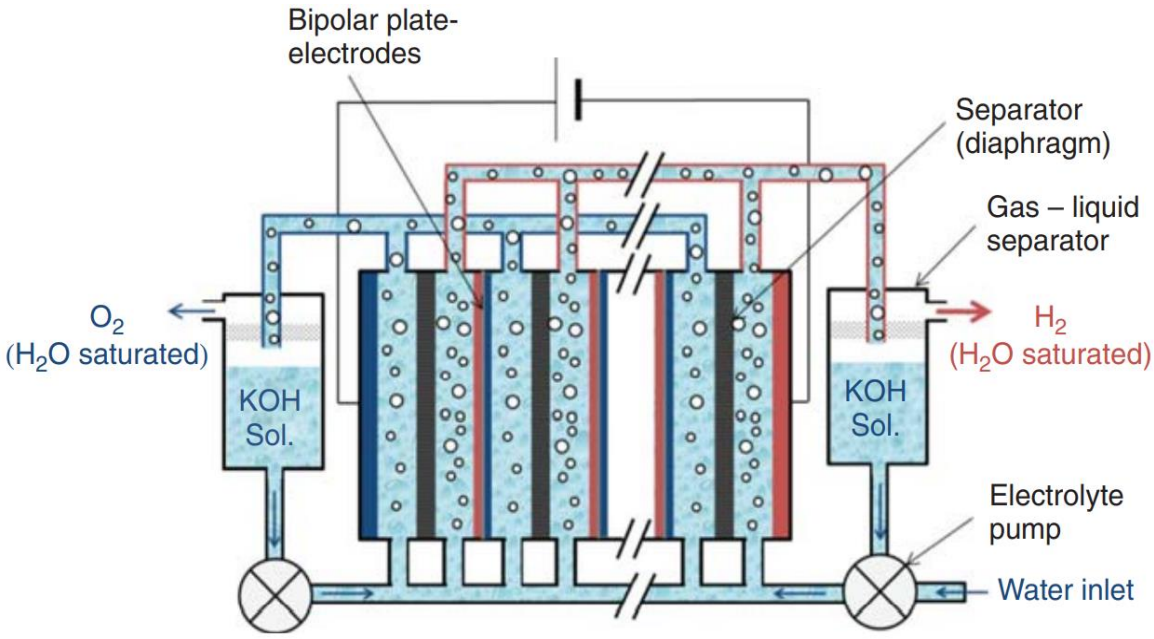

Figure 2-9: *Schematic diagram of a bipolar alkaline water electrolysis cell [18]*

The alkaline electrolyser processes have operational efficiency of between 50% - 60% at a current density range of 0.1- 0.3Acm^{-2} [26]. The demerit of the alkaline water electrolyser method is the corrosion problem of the diaphragm resulting from the use of the alkaline solutions [13]. Because of this problem, new materials are being developed for use as the alternatives to the diaphragm materials.

2.1.4.2 Polymer Exchange Membrane (PEM) Water Electrolyser

This method is also called a solid polymer electrolyte (SPE) water electrolyser. They use solid polymer electrolytes that are made of special materials called perfluorocarbon ion-exchange membranes [18]. The ion exchange membrane is sandwiched between catalyst-loaded electrodes. Water is fed to the anode of an electrolysis cell, where it splits into oxygen and protons (hydrogen ions). The protons move past the ion exchange membrane to the cathode, where they are reduced to hydrogen molecules [19]. The development of PEM water electrolyzers started in the 1960s at General Electric Co. (USA) for space application when chemically stable proton-conducting polymers became commercially available [22].

In PEM water electrolysis, Iridium (metal or oxide) is the most efficient and stable catalytic electrode used on the anodic side for the Oxygen Evolution Reaction in acidic media. Therefore, the unsupported iridium oxide particles impregnated with polymeric ionomer chains are used to form the anodic catalytic layer, which acts as the electronic carrier to aid the half-cell reaction at the anode as shown in the equation [12]:

$$2H_2O \longrightarrow 4H^+ + 4e^- + O_2$$

At the cathode, electro-conductive carbon blacks are used as electronic carriers, which means that carbon-supported platinum nanoparticles are used as the electro-catalytic electrode at the cathode for the promotion of Hydrogen Evolution Reaction as shown by the half-cell cathode reaction equation:

$$4H^+ + 4e^- \longrightarrow 2H_2$$

Figure 2-10 is an illustration of the PEM water electrolysis cell with the half-cell reactions at each electrode in (b).

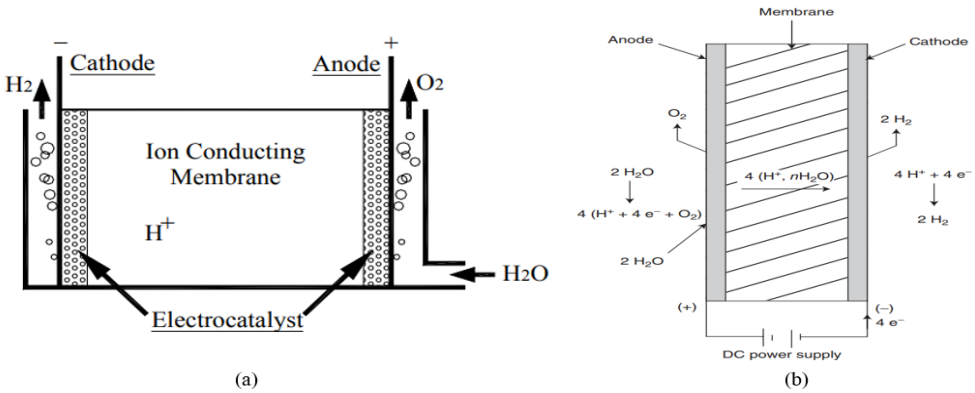

Figure 2-10: *(a) PEM electrolyser and (b) shows the cross-section of PEM cell and the half-cell reactions [9, 24]*

Electrolysis systems based on PEM have several advantages compared to the traditional water-alkaline electrolysers. They include; ecological cleanliness, considerably smaller mass-volume characteristics and power costs, a higher degree of gases purity, an opportunity of obtaining compressed gases directly in the installation, and the increased level of safety [13]. Furthermore, because of using solid polymer membranes as electrolytes, PEM electrolyzers exhibit good chemical and mechanical stability, high protonic conductivity, and gas impermeability characteristics compared to conventional alkaline electrolyzers [23]. The solid polymer membrane is also an excellent gas separator, allowing small cell construction with a very thin gap between anode and cathode, which improves its conductivity and allows high current densities at higher cell efficiencies [3]. Similarly, a reduction in the number of moving parts is an advantage that results in easier system maintenance [24]. These merits and many more make the PEM electrolysers more applicable commercially than the alkaline water electrolysers. However, the high cost of the system, which is due to the high cost of the membrane and acid-resistant noble metal catalysts, is one of the demerits of the PEM electrolyser methods, limiting the commercial development of these systems [26].

Figure 2-11 shows the commercial set-up of the 13MW PEM electrolyser hydrogen production plant by the proton onsite gas generation, which uses low voltage to drive the water-splitting process. Figure 2-12 shows the subsequent flowchart of PEM commercial hydrogen production.

The mature technologies of producing hydrogen through water electrolysis are alkaline and PEM technologies discussed above. However, many more technologies in this area are sprouting and are in the research and development stage. Table 2-1 shows the comparison of the existing technologies of water electrolysis methods.

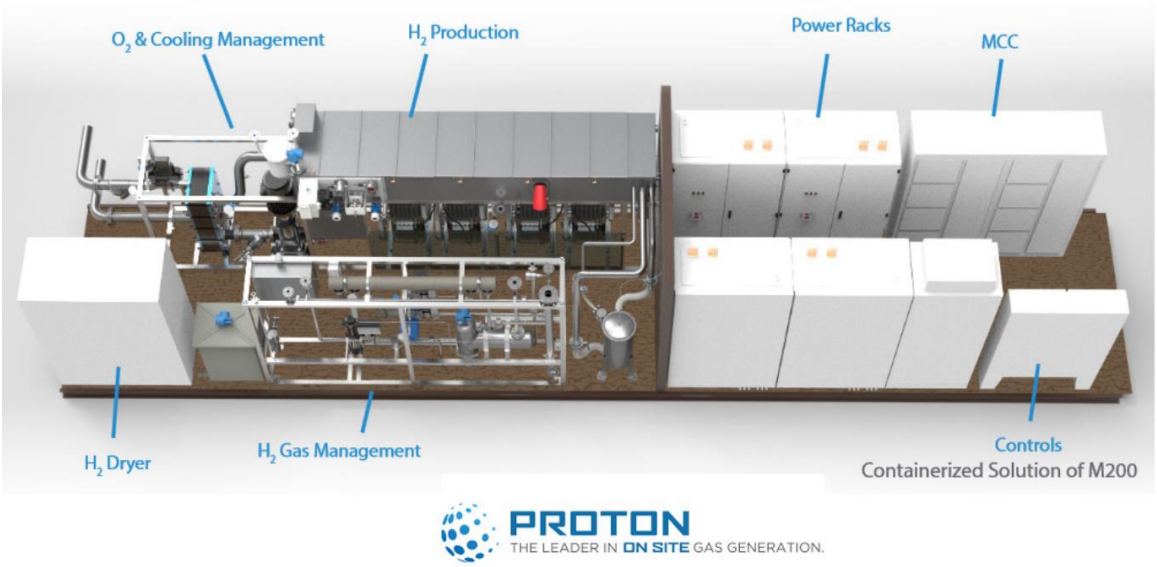

Figure 2-11: *Set up of commercial hydrogen production through PEM electrolyser [18].*

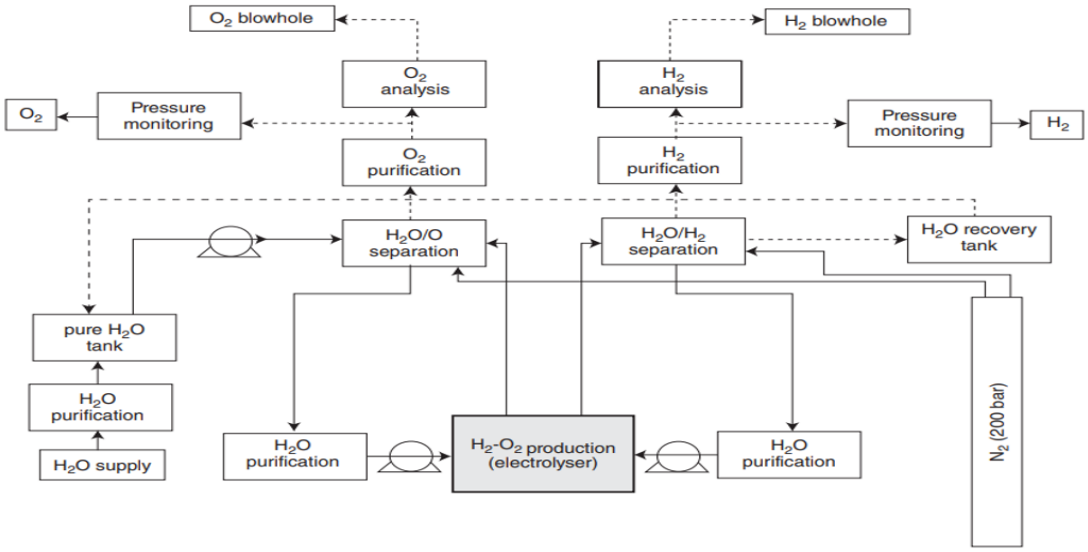

Figure 2-12: *Shows process flowsheet of a PEM water electrolysis unit [3].*

	Alkaline	PEM	Medium T	Solid oxide
Technology status	mature technology		lab-scale, R&D	
T range (°C)	ambient / 120	Ambient / 90	250 / 600	800 / 1,000
Electrolyte / pH	25–30 wt% $(KOH)_{aq}$	PFSA[1]	polymer or $Sr[Ce_xZr_{1-x}]_{0.95}Yb_{0.05}O_3$, $La_{0.6}Ba_{0.4}ScO_{2.8}$	Y_2O_3-ZrO_2, Sc_2O_3-ZrO_2, MgO -ZrO_2, CaO-ZrO_2
Mobile species	OH^-	H_3O^+	H_3O^+	O^{2-}
Cathode catalyst	nickel foam/Ni-SS[2]	platinum	Ni-YSZ or Ni-DC Cermet with proton conducting electrolyte	Ni-YSZ or Ni-GDC Cermet
Cathode carrier	nickel foam/Ni-SS Ni-Mo/ZrO_2-TiO_2	carbon		
Anode catalyst	Ni_2CoO_4, La-Sr-CoO_3, Co_3O_4	Ir/Ru oxide	(La,Sr)MnO_3, (La,Sr)(Co,Fe)O_3	(La,Sr)MnO_3, (La,Sr)(Co,Fe)O_3
Anode carrier	–	–	–	Gd-doped Ceria
Separator	asbestos, PAM[3], ZrO_2-PPS[4], NiO, Sb_2O_5-PS[5]	electrolyte membrane	electrolyte membrane	electrolyte membrane
Sealant	metallic	synthetic rubber or fluoroelastomer	glass and vitro-ceramics	glass and vitro-ceramics
Current distributor	nickel	titanium	–	ferritic SS (Crofer APU[6])
Containment material	nickel plated steel	stainless steel	stainless steel	stainless steel
P range (bar)	1–200	1–350 (700)	1	1–5
Conventional current density (A/cm^2)	0.2–0.5	0–3	0–0.1	0–2
Efficiency (%) (at i A/cm^2 / U_{cell} V / T °C)	60–80 0.2–0.5 / 2.0 / 80	80 1.0 / 1.8 / 90	lab-scale tests	100 3.6 / 1.48 / 950
Capacity (Nm^3/hour)	1–500	1–230	1	1
Durability (hours)	100,000	10,000–50,000	500	500–2,000
H_2O specification	liquid	ρ > 10 MW.cm	steam	steam
Load cycling	medium	good	no data av.	no data av.
Stop / go cycling	weak	good	no data av.	weak

Table 2-1: *Comparison of leading water electrolysis technologies* [18, 22, 29].

Given that the universal standard for producing hydrogen through any of the water electrolysis methods discussed above requires an electrical energy supply, there is a need to investigate the potential sources of electrical energy that can be harnessed for use in the industrial production of hydrogen through such methods. By and large, the source of electricity for use must be from a renewable and environmentally friendly source in order to guarantee 100% CO_2 emission-free production.

So far, three primary renewable sources of energy can be exploited based on their reliability, i.e., solar, wind, and hydropower. As mentioned in chapter one, the geographical location of Narvik does not permit the exploration of solar power as a source of electricity. In addition, hydropower is equally overstretched due to high exploitation for domestic and industrial power supply in the region, as reported by the Nordkraft Narvik [16]. As a result, wind power

harnessing remains the lone opportunity for generating electricity for use in hydrogen production in this project. In addition, this is coupled with recent GWEC studies that have extensively revealed that the onshore and offshore wind power potential around the arctic region is high and virgin for exploitation to provide novel electricity sources in the region [15].

On the backdrop of such findings, this research chose to delve in exploring the wind energy as a renewable source of electricity for use in the water electrolysis process. As a result, this research study explored the possibilities of using wind power potential around the Narvik area to supply the electrical energy for hydrogen production. Therefore, the next section, 2.2, is the detailed literature review of the wind resource assessment detailing all the elements of investigating the wind power potential of a given area with the bullseye on the Djupvik site and its environs.

2.2 Wind Resource Assessment

Wind resource assessment (WRA) is the art and science of estimating wind conditions based on available wind data in addition to topographical and meteorological features of a given site [30]. For any wind power plant to generate electricity, it requires wind that acts as the fuel for the plant. Therefore, wind resource assessment is basically the determination of how much fuel available for a wind power plant to optimally operate for the period of its useful life. The WRA forms the backbone of any wind power project investment success since it is the most critical step for determining how much energy the plant will produce and the monetary returns of the project. The success of the wind power project is wholly and entirely dependent on the accuracy and precision of the wind resource assessment, given that the projects are usually very capital intensive. For the projects to earn any profits in the future, the earnings must be predicted before wind parks are established, and risk premiums must be thoroughly evaluated [31]. In short, every element of WRA must be done right the first time to avoid any miscalculations and ensure that every aspect is up to the required standards. Such investigations have proven to be of immense help for installing different wind energy technologies such as nano, micro, small, medium, and large scale for wind energy generation.

The act of studying wind resources with the aim of establishing a wind power plant to produce electrical energy is called wind energy meteorology [32]. The realm of wind resource assessment encompasses site analysis, wind turbine selection, wind data analysis, wind turbine siting (micro-siting), wind flow modelling, power production estimates, wind park optimization, and the analysis of uncertainties [30]. To clearly provide detailed information

about the research in wind resource assessment for better understanding, an exhaustive literature review comprising the different techniques, preliminary assessment methodologies, and uncertainties connected to wind resource assessment must be put into serious consideration [33]. The subsequent sections of this research paper investigate different aspects of wind resource assessment with the bullseye on establishing a cost-effective and efficient wind park.

2.2.1 Preliminary Site Identification and Analysis

Site identification is the most crucial initial step in the long route to establishing a wind park in an area or region to ensure effective utilization of the wind resource. It is the concept of selecting a suitable location for putting up a wind power project based on the wind power potential, wind flow patterns, and other environmental and communal features. The economic viability of the wind park project is pegged on the effective assessment of the existing wind resource over the site to identify the areas with stronger, moderate, and weaker winds [30]. In ancient times, the technique that was extensively used for identifying regions with good wind power potential was the wind deformed conifer trees [34]. This technique entailed observing the conifer trees as the biological indicators to forecast the wind speed and prevailing wind direction to estimate the wind power potential in the monsoon and the winter seasons. Flagged trees, in this case, offer inexpensive, simple, and quick ways of identifying slightly suitable locations for the wind resource availability and therefore act as indirect indicators for identifying potential sites. Actually, Murthy and Rahi [35] opine that flagged trees can solely be used to identify the location for small-scale wind applications since they offer sufficient quantitative evidence to justify the installation of the wind energy conversion systems.

In contemporary times, the local vegetation like flagged trees such as the Douglas-fir and Ponderosa pine are only used as indicators to give a rough idea of the wind power potential of a particular area. Thereafter, modern instruments are installed and monitored for a specific period to provide detailed and actual information on the wind power potential of the specified area [31]. Different kinds of software programs are currently used to analyse the already available wind speed data collected over time from the nearby weather stations or airports closer to the potential site to help forecast the potentiality of a given area for setting up a wind power project.

Once the potential site has been identified, the immediate step to follow is the site analysis which is the artistry of looking into the possible factors that may affect the optimal harnessing of the wind power on the identified site. The wind resource evaluation of the site involves

identifying the topographical and meteorological features that may have a potential influence on the wind flow. The topography components include the terrain (orography), the obstacles, and the roughness of the site, while the meteorological features include atmospheric stability, boundary layer structure, and weather system [35].

2.2.1.1 Surface Roughness on Wind Flow

The measure of the magnitude of the surface roughness is known as the roughness length. The earth's surface, both water bodies and landmass, offer some element of resistance to the blowing wind on top of it. The frictional magnitude is due to the size and distribution of the roughness elements on the earth's surface, and they vary from place to place. The roughness length changes only with the change in the roughness elements of the land surface, e.g., height and coverage of vegetation, urban development, and deforestation [30]. However, roughness length is not affected in any way by wind speed, stress, and atmospheric stability. Even though water surfaces also depict some friction elements on wind flow at different sections of water bodies due to tides, the roughness length of water is very low and is assumed to be constant. Table 2-2 below shows the roughness length of different surfaces.

Terrain surface characteristics	Roughness length, Z_0 (m)	Roughness class
Forest and urban areas	0.7~ 1.0	4
Suburbs and sheltering belts	0.3 ~ 0.5	3
Farmland with closed appearance, many trees, bushes	0.1	2
Farmland with open appearance, few buildings, trees	0.02 ~ 0.05	1
Mown grass and airport runway areas	0.01	0
Smooth snow surface	0.001	0
Smooth sand surface	0.0003	0
Water area	0.0002	0

Table 2-2: *Roughness length and class for typical surface characteristics* [30]

2.2.1.2 Effect of Terrain on Wind Flow

Terrains cause speed-up effect on the blowing wind. Speed-up effect of the terrain is whereby the wind speed blowing just above the hilly or mountainous area is drastically reduced, and the streamline flow is affected up to a particular height when the wind flow resumes normalcy [31]. The terrain influence on wind flows decreases as the height increases above ground level until a certain height where the wind blows horizontally without change in speed [35]. The wind flowing past a hilly or mountainous area usually tends to squeeze through a narrow pass that ensures that the wind speed must increase for the same amount of air mass to move past the terrain [30]. This is what is called the speed-up effect of the terrain. Due to the speed up effect

of terrain, wind turbines are usually sited at the peak of mountainous or hilly terrains. The level of orographic complexity of the terrain is measured in terms of ruggedness index, which shows that the higher the ruggedness index value the more complex is the terrain and vice versa [36]. Ruggedness index and Linearised flow models have been extensively applied in wind resource assessment and siting in complex terrains. The figure 2-13 illustrates the effect of terrain on flow of wind. Figure 2-13(a) depicts the speed-up effect by the density of the streamlines, i.e., denser streamlines show higher wind speed past the simple hilly terrain. Figure 2-13(b) shows the maximum height, *l*, where the maximum speed-up effect is found beyond which wind flows normally without change in speed.

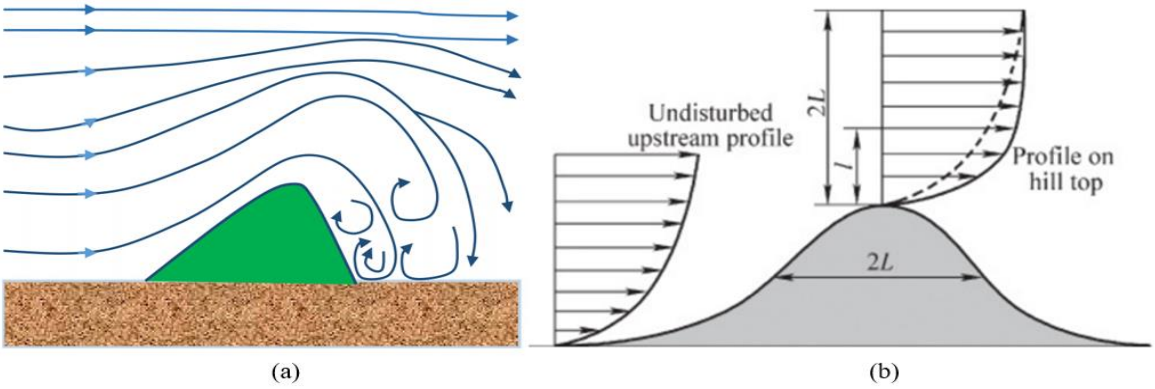

***Figure 2-13**: (a) wind acceleration effect of hilly terrain on wind flow (b) Display maximum height, l where the maximum speed-up effect is found [31, 35].*

2.2.1.3 Effect of Obstacles on Wind Flow

The presence of obstacles like housing, trees, and fences in an area have adverse effects on wind flow, hence affecting the optimal operation of the wind turbines or met masts [30]. The obstacles tend to lower the wind speed and also increase the turbulence intensity in their vicinity. The wind speed reduction influence of obstacles on a potential site is called the shelter effect. It depends on the porosity of the obstacles, height of the site, geometrical shape, and orientation of the obstacle [35]. The sheltering effect decreases with an increase in both length and height away from the obstacle. In fact, as a rule of thumb, the three-times-fifty principle dictates that the shelter effect from an obstacle vanishes when the distance from the obstacle is longer than 50 times the height of the obstacle and the height of the site is taller than three times the height of the obstacle [31]. The three-times-fifty principle is conservative and rudimentary and only applies to two-dimensional obstacles. Realistically, obstacles such as buildings and trees are three-dimensional with comparable dimensions in length, width, and height, in which case the two-times-twenty principle applies [30]. The principle suggests that the wind reduction effect is likely to be felt within a height of 2 times the height of the obstacle and distance of 20 times the height of the obstacle, and all depends on the girth and porosity of the obstacle [37].

It is worth noting that obstacles are in all kinds of shapes and patterns with unclear boundaries compared to other topographical elements. For example, forests and urban centers are highly ranked as roughness elements, but they behave as obstacles in some scenarios and hence produce shelter effects on the potential sites. Figure 2-14 shows the shelter effect of obstacles for both two-dimensional and three-dimensional obstacles.

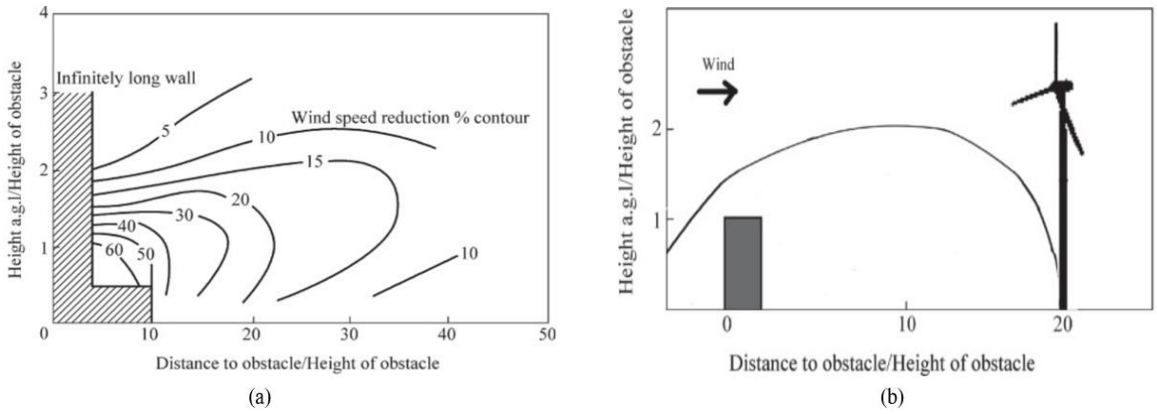

Figure 2-14: *(a) The percentage reduction of wind speed with height and distance from the obstacle (b) shows the sketch of the shelter effect zone by a three-dimensional obstacle [31].*

Other than reduced wind speed due to the shelter effect of the obstacle, the turbulence intensity is also significantly enhanced by shear forces exerted on the wind flow by the obstacles [37]. The turbulence intensity is the wind flow distortion around the obstacle, and it is estimated to be felt at a distance of 3 times the height of the obstacle [30]. Due to increased turbulence intensity and shelter effect, wind parks should never be established in sites with obstacles without detailed investigations to verify that such conditions are within the design limits, as demonstrated in figure 2-15.

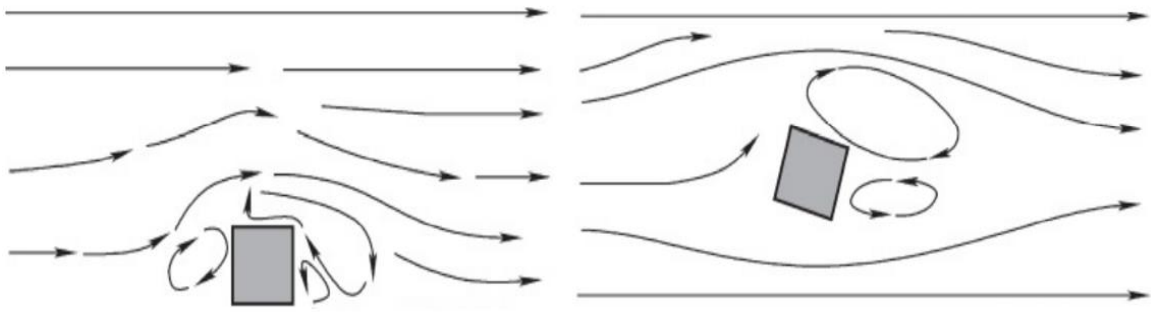

Figure 2-15: *Shows the wind flow around an obstacle, indicating turbulent airflow [30].*

2.2.2 Numerical Wind Flow Modelling

Once the site has been selected and analyzed, the immediate step to follow is the estimation of the wind resource at the proposed site so that reliable prediction can be made on the overall

energy production of the wind park. Different methods exist and are used in modelling wind flows. However, the wind flow models work on the principle of some outstanding assumptions in order to permit smooth calculations. Such assumptions include [32]:

- Wind flow is considered inviscid and very turbulent flow due to its higher Reynolds number.
- It is assumed that the wind flow is steady because of the tractability nature of wind.
- Similarly, wind flow is assumed to be incompressible in the atmospheric boundary layer since its change in temperature and pressure is negligible to affects its density.

Wind flow modelling help in simulating variations of wind flows as a result of the different topographical features and conducting flow interactions amongst the neighbouring wind turbines [38]. In the subsequent subsections, I look into different classifications of the numerical wind flow modelling methods, with great emphasis on computational fluid dynamic (CFD) models, which will form the basis of the entire study, together with their merits and demerits as well as the uncertainties associated with the wind flow modelling.

2.2.2.1 Equations Governing Wind Flow

The governing equations of flow dynamics apply to atmospheric flows, which are synonymous with meteorological variables like wind speed, temperature, air pressure, density, and moisture content, etc., which makes it nearly impossible for the wind flow modelling to solve all the equations simultaneously [31]. However, wind speed is the cardinal variable in wind engineering, and as such solving momentum equations become the nucleus of any wind flow models [39]. Therefore, the governing equations have two main components, i.e., the mean flow equations and the turbulence fluctuations.

(i). Mean Flow Equations.

Mean flow equations consist of the laws of conservation, i.e., mass, momentum, energy, etc., and the ideal gas laws. The governing equations in this category include [32]:

- The Navier-Stokes' equations (equation of motion). Initially derived for laminar flows, they describe momentum equations for Newtonian fluids that are nonlinear sets of differential equations. They describe the fluid flow by relating the changes of velocities to the pressure gradient, friction, thermal buoyancy, and the Coriolis force.
- Continuity equation (conservation of mass). It shows that mass can neither be created nor destroyed in a control volume.
- Thermodynamic equation (energy conservation). It explains the changes in temperature due to heating, cooling, compression, or rarefaction.

- Gas law equations. They relate to pressure, temperature, and density.
- Water continuity equation. It expounds that water is neither created nor destroyed but may change phase.

(ii). Turbulence Fluctuations

The component of turbulence fluctuation is the turbulent fluxes, also called Reynolds stresses, that include Reynolds shear stresses and Reynolds normal stresses [32]. The inclusion of these unknown Reynolds stress terms into a Navier-Stokes equation results in a problem called turbulence closure which makes the equation unsolvable [39]. In order to solve the turbulence closure, a technique must be employed. Such technique is called the turbulence closure technique, which involves introduction of turbulence models that help sort the flow problems. As a result, the Navier-Stoke equations are renamed as the Reynolds Averaged Navier-Stokes (RANS) equations [31]. Turbulence models usually deal with relatively large turbulence eddies, while RANS models solve the continuity and momentum equations excluding the conservation of energy equation [32].

2.2.2.2 Linearised Numerical Flow Models

Jackson and Hunt were the pioneer proposers of the linearised model of the Navier–Stokes equations that described the 2D turbulent airflow over low hills in the boundary layer [40]. The model was named Jackson–Hunt Model that used the Navier–Stokes equation to describe the terrain shape in terms of Fourier equations solved in inverted numerical Fourier transformation to give results in real Fourier space [38]. The model had its fair share of weakness, like the mismatch between the turbulence closures in the inner and outer layers of the longitudinal approach flow velocity [41]. To improve such shortfalls, different models were developed due to the inspiration from the Jackson–Hunt theory [42]. Mason and Sykes came up with a three-dimensional model, an extension of the Jackson–Hunt Model that introduced an alternative approach of the wavenumber scaling technique to account for the large range of horizontal scales of real terrains. The developed model was called MS3DJH (the Mason and Sykes three-dimensional extension of the Jackson–Hunt model), which was later adopted by the Wind Atlas Analysis and Application Program (WAsP) [37].

WAsP was developed at the Risø National Laboratory in Denmark in 1987. It is a spectral model that solves the linearised Navier–Stokes equations with only first-order velocity perturbation induced by the terrain considered in a Fourier space [32]. It is very quick and accurate in flat to mildly undulating terrains but poorly performs in complex orography [32,

43]. Actually, the WAsP tools give good results in areas with less than an 18° terrain slope, or approximately 30% [43]. For over three decades now, the success of the WAsP model makes it to be regarded as the industrial standard for wind resource assessment such that renowned products like WindPRO and WindFarmer directly use results from it [38]. The only limitations of the WAsP model are those inherited from the Jackson–Hunt models, such as the first-order turbulence closure, neutrally stable steady-state flow, small velocity perturbation, and linear advection, which have been understood over the years and formed part of the improvement process of the model [40].

The other newly proposed linearised flow model is the RAMSIM (Risø Atmospheric Mixed Spectral-Integration Model) model advocated by Corbett in his Ph.D. thesis after getting inspiration from the linear theory of the Jackson-Hunt model and MSFD (mixed spectral finite-difference) family of models [32]. According to Corbett [32], the RAMSIM is steered by two equations: steady-state Reynolds-Averaged Navier-Stokes (RANS) equations for incompressible flow and neutral thermal stratification, which entails transport equation for momentum and transport equation for mass (the continuity equation). In contrast, the other equation is the turbulence closure equations consisting of the transport equation for the turbulent kinetic energy (TKE) and the transport equation for the dissipation of turbulent kinetic energy.

2.2.2.3 Mass Consistent Models

Mass consistent models are diagnostic models just like the Jackson-Hunt models, which means that they are capable of reconstructing a steady-state wind field from a set of initial experimental data [33]. They model the mean wind flow by simply solving only one governing equation of motion, i.e., the mass conservation equation, thereby limiting the amount of computational data required [41]. The variable data of mass consistent models are defined on the three-dimensional wind field numerical grid of Δx, Δy, and Δz, which are then interpolated and adjusted to satisfy the incompressible state of mass conservation [44, 45]. The model is highly susceptible to the method of interpolation used such that the same data may give totally different wind fields when the interpolation method is changed. The mass-consistent models are specialised in simulating stationary three-dimensional wind fields in complex terrains [39]. The limitation of such models is that they cannot describe thermally induced wind systems, like land-sea breezes and mountain-valley circulations [37]. The most commonly used example of a mass consistent model is the openWind model (WindMap) software developed by the AWS Truepower [43]. Others include the NOABL (Numerical Objective Analysis Boundary Layer) model software

[44], MATHEW (Mass-adjusted three-dimensional wind field) model [45], MINERVE model, COMPLEX model, and WINDS model [46]. Table 2-3 below summarises the diagnostic wind flow model types and their main characteristics.

Wind Flow Model Types		*Main Characteristics*	*Meteorological Data Required*	*Examples*	*Computer resources*	*Remarks*
Diagnostic models	***Linearised Numerical Flow models***	-Based on linearized solutions of the dynamic equations for boundary layer -logarithmic wind profile	- Wind speed and direction at a given height, or wind and temperature-profile	-FLOWSTAR -LINCOLM -MS3DJH/3R -MSFD -NLMSFD -WAsP -RAMSIM etc.	Minimal computer power (Personal Computers)	*-They cannot be applied over steep slopes and very complex terrain*
	Mass consistent models	-Interpolated wind fields are adjusted to satisfy mass conservation	- Wind speed and direction from ground stations and vertical profiles - in some cases, temperature data	-ATMOS1 -COMPLEX -CONDOR -MASCON -MATHEW -MINERVE -NOABL -NUATMOS -WINDS WOCSS etc.	Limited computer power (new generation PC or workstations)	*-They can be applied to any kind of terrain, but attention is required when applied to very steep slopes*

Table 2-3: *Diagnostic wind flow models, characteristics, and examples* [33].

2.2.2.4 Computational Fluid Dynamic (CFD) Models

Computational fluid dynamic (CFD) wind flow models are considered to be prognostic models given that they are capable of forecasting the time evolution of the atmospheric system through the space-time integration of the equation of conservation of mass, momentum, heat, water, and other substances like gases or aerosols [33]. As such, they solve time-dependent equations that help in describing time-evolving three-dimensional wind fields [41].

The computational fluid dynamics was brought forth in trying to find an approximation and assumptions that would help in simplifying the Navier-Stokes equations for numerical solutions to be feasible with modern computers [38]. The CFD models primarily solve complete forms of RANS and continuity equations without linearization, making them capable of simulating nonlinear flow occurrences like recirculation and flow separation with highly better performance in complex orography [39]. They operate under the assumptions of steady-state flow, conditions of prescribed equilibrium inflow, neutral stratified atmosphere, and logarithmic law of vertical wind speed profile because of the unresolved thermal conditions with respect to atmospheric stability and thermally induced circulations [37].

The CFD methods are classified into three categories, i.e., DNS (Direct Numerical Simulation), which attempts to simulate all the scales of a given flow, from the largest flow, through the mid-size turbulent fluctuations, down to the smallest turbulent eddies [39]. The second category is the LES (Large-eddy simulation), which uses a coarser computational grid to determine the

main features of a flow by fully simulating larger eddies while approximating the effect of the smaller eddies on larger flows [44]. Lastly, the RANS (Reynolds-Averaged Navier-Stokes) model describes the mean flow variables such that the impact of the turbulent eddies on the mean flow is modelled using turbulence closures while individual eddies remain unresolved [32].

Some of the general-purpose CFD model packages are expensive and require high-level prowess. They include OpenFOAM, PHOENICS, CFX, FLUENT, and STAR CCM+, among others [31]. Equally, some organizations have established the necessary facilities and expertise to develop and run their own customised CFD modules based on the general-purpose CFD packages. For instance, Vestas CFD is based on the open-source OpenFOAM toolkit [43] and WindSim software package is based on the PHOENICS code [39]. In this master thesis, WindSim software will be the application tool for simulation, and therefore more details about it are discussed in chapter four of this paper.

2.2.2.5 Meso-Scale Numerical Weather Prediction (NWP) Models

Mesoscale NWP models are prognostic, just like the CFD models, which enables them to generate long-term wind data time series based on over 30 years of global weather data archives [43]. They also solve the RANS equations, like CFD models, in addition to describing atmospheric equations in detail [38]. The mesoscale NWP models are considered realistic in the sense that they are capable of simulating wind flows in very complex terrains and simulating processes such as land-sea breezes, downslope winds, and mountain–valley circulation. This is because they incorporate thermally driven forces [43], which makes them unique tools for investigating extreme winds like typhoons and windstorms and other adverse weather conditions [39]. Because of these features, mesoscale NWP models are costly to operate, require high-level expertise, and run on very complex computer systems. In addition, they employ a nested grid, which means that the outputs of the larger domain are the boundary conditions of the smaller grid [33]. Table 2-4 shows prognostic wind flow models, their characteristics, and possible examples.

2.2.3 Wind Turbine Technologies

This section looks into different wind turbine components and how they operate in tandem with each other. Also, it looks into different types of available choices of turbines in the market. Wind turbines operate by converting the kinetic energy in the wind into mechanical energy, which drives the generator to produce electrical power [47]. The use of wind turbines to extract

wind energy began in the 1880s, with a small turbine equipped with a 12-kilowatt (kW) direct-current (DC) generator.

Model Types		Main Characteristics	Meteorological Data Required	Examples	Computer Resources	Remarks
Prognostic Models	*CFD Models*	Simplification of the non-linear equation of motion (RANS equation)	-Vertical profile of wind, temperature, and humidity Gridded meteorological fields provided by large scale models	-OpenFOAM -PHOENICS -CFX -FLUENT -STAR CCM+ -Meteodyn WT -WINDSIM	Variable computer requirements (generally workstations)	*They cannot be applied over very complex terrain and for small grid sizes*
	MesoScale NWP Models	Use of a complete set of equations describing the atmospheric motions	Vertical profile of wind, temperature, and humidity Gridded meteorological fields provided by large scale models	-ADREA -FITNAH -GESIMA -GRAMM - KAMM - MEMO -MERCURE - MESOSCOP - MM5 - RAMS -WRF	Considerable computer requirements (new generation work-stations, supercomputer & parallel machines)	*They are the most suitable models to describe the atmospheric flow over complex terrain*

Table 2-4: *Prognostic wind flow models, characteristics, and examples* [33]

The advancement in technology gradually improved over the years such that by the 1980s, the technological expertise had reached a penultimate level that the first 50-kW utility-scale wind turbines were commissioned [14]. Over the 40 years, there have been gradual development in wind turbine technologies with increasing sizes of wind turbines. The most contemporary and world's largest 12MW capacity wind turbine of its kind was recently developed by US conglomerate General Electric with tower height of 260m and is due for commissioning in this year 2021 [48].

2.2.3.1 Components of Wind Turbines

The components of wind turbines are classified as either mechanical or electrical components. Four main components are essential in a wind turbine: the tower, blade, generator, and nacelle. Figure 2-16 shows the main components of the wind turbine and the inner parts of the nacelle.

(i). Main components of Wind Turbines

The main parts of a wind turbine include [14]:-

- Rotor that generates aerodynamic torque from the wind
- Nacelle contains electrical and mechanical components, and it protects them from adverse weather conditions. It also includes a set of gears that connects blades to a generator that converts torque into electrical energy.
- Tower holds nacelle and the rotor blades off the ground up to where they access better wind speed conditions. Most wind turbines have hub height ranging from 20m to 200m

though General Electrics have developed the world's largest wind turbine due for commissioning in this year 2021 with a hub height of 260m [48].

- Foundation ensures that the turbine stays strong and upright against all conditions of extreme weather.

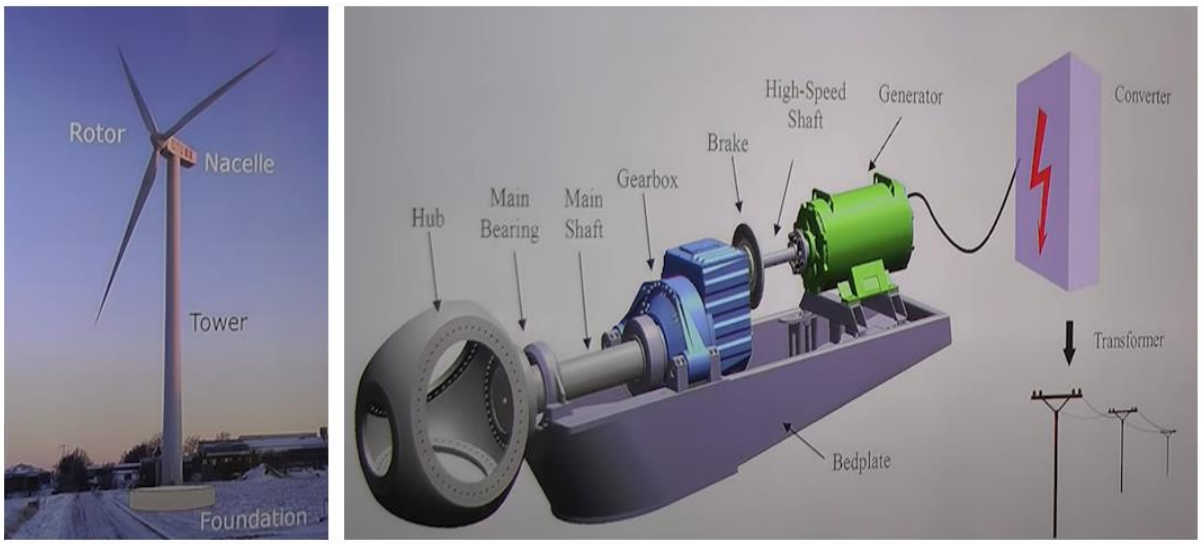

Figure 2-16: *(a) Components of the wind turbine (b) Parts of Nacelle with drivetrain and power electronics [47].*

(ii). Parts of the Rotor

The components of a rotor include:

- Rotor Blades are air-foil shaped to help in converting wind kinetic energy to mechanical energy [48].
- Rotor hubs are made of cast steel to support the rotor blades and convert the transverse motion of the blades into torque input for the gearbox.
- The Pitch bearing system connects the rotor blades and the hub and provides coupling support between the hub and the main shaft [14].

(iii). Parts of Nacelle

It consists of the drivetrain that consists of the [14, 48]:-

- Main shaft, also called a low-speed shaft, connects the rotor hub to the gearbox to transmit mechanical energy through large moments of inertia. It operates on very low speed and high torque.
- Mechanical brakes are used to abruptly stop the wind turbines in times of emergencies like fault conditions or high wind gust.

- The gearbox is used to couple the main shaft to the generator shaft, which is of high speed and low torque.
- Generators use the potential difference to create change in voltage which acts as the driving force for the electrical current. The current is then passed through power lines to the converter that ensures electrical energy is distributed in DC or AC to the grid.

2.2.3.2 Wind Turbines Classifications and Selection

Wind turbines are classified into two major categories based on their wind generator and drivetrain shaft orientation with respect to the ground. The major categories are HAWT (Horizontal Axis Wind Turbine) and VAWT (Vertical Axis Wind Turbine). The HAWT has the generator shaft parallel to the ground level and the major mechanical and electrical components are placed in a nacelle where the tower elevates their height to allow sufficient space for the blades to rotate [14]. The VAWT has wind generator shaft perpendicular to ground level and generator and gearbox, are close to the ground which makes them easier to install and maintain unlike HAWT [14]. However, with advancements in technology, new generational wind turbines have cropped up in the market in the last decade. The new generational turbines include Kite generation turbines and MARS (Magenn Air Rotor Systems) turbines [35]. Figure 2-17 shows different classifications of wind turbines.

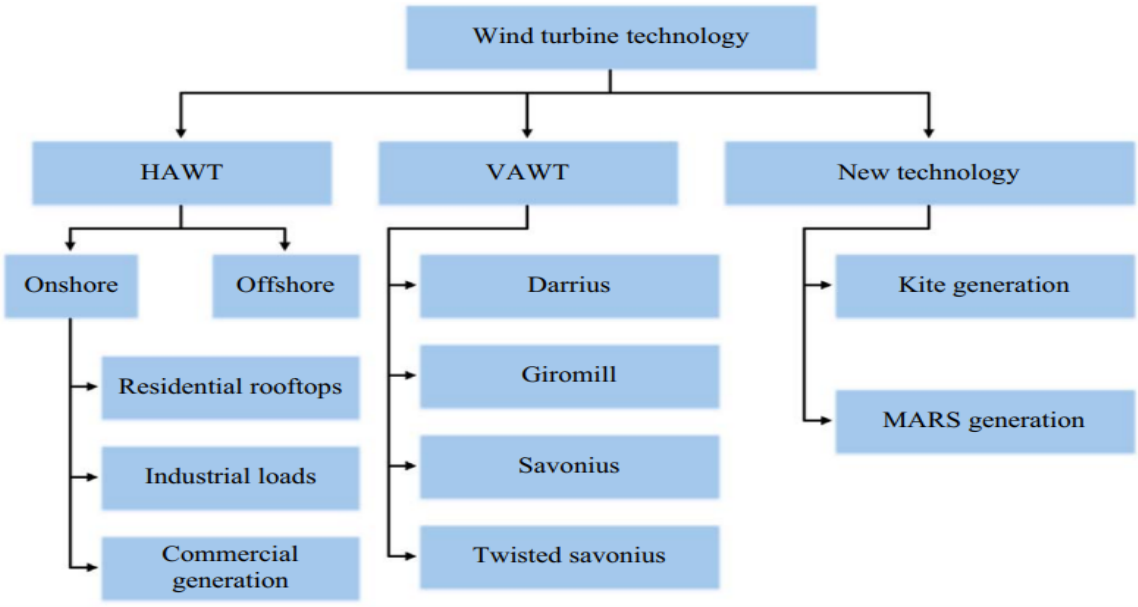

Figure 2-17: *Classification of commonly available wind turbine technologies [35].*

The most commonly used wind turbine for large-scale and small-scale power generation is the HAWT turbines which are further sub-classified into large, medium, domestic, mini, and microscale wind turbines based on their rotor diameter as shown in table 2-5 [35]. VAWT

turbines are primarily considered in small-scale power generation, e.g., below 100kW, because of lower wind energy conversion efficiency caused by rotor blades getting subjected to varying wind speeds [14]. Figure 2-18 shows the pictorial view of the categories of wind turbines.

The primary factor to consider while selecting the wind turbine for siting is to match the site-specific wind conditions with the design classification of the model, including rotor size, tower heights, reliability, and efficiency [30]. Other factors to consider include design configurations, operational mechanisms, and physical structure appearances such as the orientation of axis, aerodynamic forces, rotor position and speed, number of blades, transmission, power control, yaw orientation, and hub type. Besides, general commercial factors can also come into play when making considerations such as analyst's familiarity with the models, track record and reputation of the manufacturer, technical advantages, and fair prices and warranty [31].

S. no.	Technology Type	Rotor diameter range (m)	Rotor swept area range (m^2)	Standard Nominal power range (kW)	Wind speed regions	Suitable Applications
1	**Large scale**	50-100	1963–7854	1000–3000	Very high	***Large scale grid power generation (onshore and offshore wind farms)***
2	**Medium scale**	20-50	314–1963	100–1000	High	***Mini wind farms (micro grid application in remote areas, village power).***
3	**Small scale**	10-20	79–314	25–100	Good	***Residential purpose, rural electrification, water pumping, and telecommunication sites***
4	**Domestic scale**	3-10	7–79	1.4–16	Moderate	***Hybrid systems***
5	**Mini scale**	1.25-3	1.2–7.1	0.25–1.4	Low	***Building-integrated rooftop applications***
6	**Micro scale**	0.5-1.25	0.2–1.2	0.004–0.25	Very low	***Low power applications***
7	**Nanoscale**	May come under < 0.25 kW (standard definition not yet defined)				

Table 2-5: *Classification of HAWT models* [35].

(a) **3-Bladed HAWT** (b) **Savonius VAWT**

Figure 2-18: *Pictorial view of (a) HAWT and (b) VAWT wind turbines* [30].

The categorization of the wind turbine models is based on the standard specifications of the International Electro-technical Commission (IEC), which defines the technical standard for wind turbines [31]. According to "IEC 61400-1:2019" standards, wind turbines are classified based on the annual average speed, turbulence level, and extreme 50-year gust data [14]. Table 2-6 shows the wind turbine classes derived from IEC 61400-1 standard.

Wind Class	Annual Average Wind Speed	Turbulence Level	Extreme 50-Year Gust
IA	High Wind Speed – 10 m/s	High Turbulence – 18%	High Gust – 70 m/s
IB	High Wind Speed – 10 m/s	Low Turbulence – 16%	High Gust – 70 m/s
IIA	Medium Wind Speed – 8.5 m/s	High Turbulence – 18%	Medium Gust – 59.5 m/s
IIB	Medium Wind Speed – 8.5 m/s	Low Turbulence – 16%	Medium Gust – 59.5 m/s
IIIA	Low Wind Speed – 7.5 m/s	High Turbulence – 18%	Low Gust – 52.5 m/s
IIIB	Low Wind Speed – 7.5 m/s	Low Turbulence – 16%	Low Gust – 52.5 m/s
IV	6.0 m/s	–	42 m/s

Table 2-6: *Shows the wind turbine classes derived from IEC 61400-1 standard* [14].

2.2.4 Wind Power Conversion

The wind turbines extract kinetic energy from wind and convert it into mechanical energy and then to electrical power [49]. Figure 2-19 is a schematic diagram showing the conversion of kinetic energy to electrical energy.

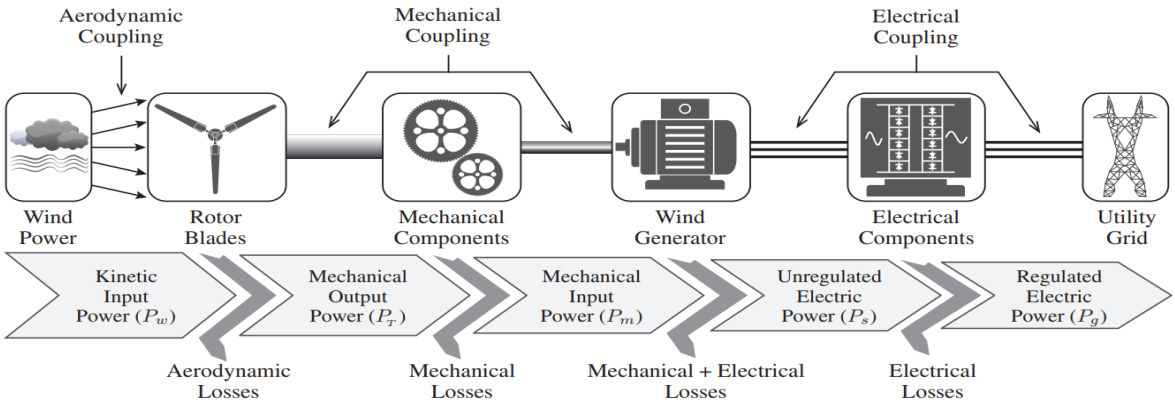

Figure 2-19: *Wind turbine conversion system of wind kinetic energy to electrical energy* [14].

It is possible to determine the maximum amount of energy that can be extracted from kinetic wind energy in open flow, irrespective of the design of wind turbines, using Betz's limit law. The Betz's limit is a theoretical model that operates under some major assumptions, i.e., the rotor is an ideal plate without a hub and with no mass, blades are infinite in number with zero drag, the rotor inflow and outflow is axial, the flow is incompressible with constant air density, and there is no heat transfer between the rotor and the flow [50]. In the wind turbine power conversion process, the kinetic energy is first converted into mechanical energy, as illustrated

by equation 2.1 and equation 2.2. The wind kinetic power (P_w) flowing through an imaginary area (A_T) at a speed *Vw* is given by: -

$$Kinetic\ Power, P_w = \frac{1}{2}\ \rho\ A_T\ v_w^3, \quad \text{Given that} \quad A_T = \pi r_T^2 \qquad (2.1)$$

Where ρ = air density in (kg/m^3), A_T = rotor swept area (m^2), r_T = blade radius (m) and v_w is the wind speed (m/s).

Based on Betz's law, the mechanical power P_T extracted from wind kinetic energy is given by [35]:-

$$Mechanical\ Power, P_T = P_w \times C_p = \frac{1}{2}\rho A_T v_w^3 C_p \qquad (2.2)$$

C_p = The power coefficient of rotor blades, and the value of P_T increases proportionally with the increase in its value.

According to Betz law, the theoretical maximum value of $C_P = \frac{16}{27}$ or ≈ 0.593, and practically no wind turbine can convert more than 59.3% of the wind kinetic energy to mechanical energy because of aerodynamic losses experienced by the blade during its operation. Different wind turbines have different C_p values, with the modern high power utility wind turbines having values from 0.32 to 0.52 [35].

After the conversion of the wind kinetic power to mechanical power, the slow speed wind turbine rotor is mechanically coupled to a high-speed generator through the drivetrain and main shaft while in the process, there are mechanical losses which represents the difference between mechanical output power (P_T) and mechanical input power (P_m) [50]. Thereafter, the wind generator is duty-bound to convert the mechanical input power (P_m) into electrical energy (P_s). The electric output power (P_s) is unregulated because the generator voltage and frequency fluctuate with variation in wind speed. In order to stabilize frequency and voltage, a power converter is used, which regulates the electric power; hence the regulated electric power (P_g) is fed to the utility grid. In order to connect the wind turbines to the utility transmission network, a step-up transformer is usually used to boost the output voltage of the power converter [49].

2.2.5 Wind Turbine Power Curve

From the findings in section 2.2.4 above, it is clear from Betz's law that it is impossible to convert all the kinetic energy to the actual electrical output by a wind turbine at a given wind speed. To determine the actual electrical output of any wind turbine, the wind turbine power curve must be used to forecast the actual amount of electrical energy that the wind turbine will be able to generate at any particular wind speed.

The wind turbine power curve is the indicator of each wind turbine's electrical energy production potential at different wind speeds and varies from one wind turbine to another [13]. The manufacturer sets the power curve of any wind turbine following the strict guidelines of the international standards set by the IEC 61400-12-1: Power Performance Measurements of Electricity Producing Wind Turbines [51]. In order to determine the wind turbine power curve (P_e), we need to start by finding the electrical power coefficient (C_e), which is the representation of the actual amount of kinetic wind energy that is converted into electrical energy by a wind turbine [50].

$$Electrical\ Power\ Coefficient, C_e = C_p \eta_m \eta_e, \quad (2.3)$$

Where C_p is the power coefficient of the rotor blade, η_m is the rotor blade mechanical efficiency of converting kinetic energy into electrical energy, and η_e is the electrical efficiency of the generator. It is worth noting that at rated power, η_m range from 0.95 to 0.97 while η_e range from 0.97 to 0.98 [50].

$$Wind\ Turbine\ Power\ Curve, P_e = \frac{1}{2}\rho A v^3 C_e, \quad (2.4)$$

The C_e replaces C_p in the mechanical power, P_T equation 2.2 above.

The wind turbine power curve equation 2.4 is usually used to determine the power ratings of wind turbines hence help in classifying the wind turbines.

2.2.6 Wind Turbines Wake Effects

Given that wind turbines extract kinetic energy from blowing wind, the wind speed and pattern change after passing through the wind turbine path, i.e., the wind speed reduces, and turbulence intensity increases. This kind of behavior is called the wind turbine wake effect, as illustrated in figure 2-20, showing the wake structure of a HAWT [52]. From figure 2-20 below, it can be deduced that the near wake zone is approximately two rotor diameters, and it is where a lot of air mass has been blocked by the rotor. The intermediate wake zone is about 2-3 rotor diameters, while the far wake zone is estimated to be five rotor diameters, where there is the recovery of wind flow velocity until it normalizes [53].

Suppose several wind turbines have to be installed in a park, care must be taken to ensure that neighboring adjacent wind turbines don't influence wind flow velocity that passes each other. Otherwise, it will result in profound production loss in a wind power plant [54]. To alleviate the risk of wind turbine wake effect in a wind farm, wind turbine layout optimization must be thoroughly conducted. There are different kinds of wake models that have been developed over the years to help ease the upsets of the wake.

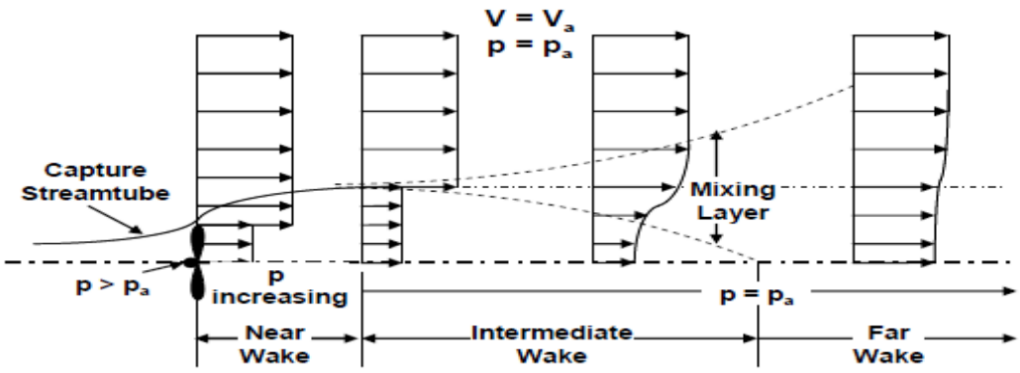

Figure 2-20: *Illustrates wake structure of HAWT* [31, 52].

The wake effects of wind speed loss and amplified turbulent intensity are modelled separately to obtain an optimal wind turbine layout that maximises the economic yield of the wind power project [52]. Some of the existing models for both wake effects include Jensen, Larsen, Ainslie, Elliptic, UPMWAKE, Frandsen wake, open Wind DAWM, GH WindFarmer, and Werle's wake models, etc. [52, 53]. To tone down the wake effects, Chen and Agarwal [52] propose that the optimised wind turbine layout and safety threshold must be at least five rotor diameters in the prevailing wind direction and three rotor diameters in the perpendicular direction for the onshore wind parks. For offshore wind farms, the recommended safety requirements for wind turbines are a minimum of 9 rotor diameters in the prevailing wind direction and seven rotor diameters in the perpendicular direction [31, 54].

2.2.7 Wind Turbine Micro-siting

Wind turbine micrositing is the process of optimising wind turbine layout whereby the wind turbines are strategically arranged to inspire maximised net annual energy production of the wind farm while minimising wind turbine loads and wake effects in a wind park area [31]. This process is a balancing act between the numbers of wind turbines in a site area versus the average output per wind turbine. For instance, to maximize land use, many wind turbines will have to be installed in an area, which might be translated to mean increased overall energy production. However, this act is likely to compromise on the productivity of individual wind turbines due to aggravated wake effects, hence hurting the wind farm's overall productivity.

Several factors have to be put into consideration while conducting the wind turbine micrositing layout. They include understanding the specific wind conditions of the site (mean wind speed, turbulence intensity, inflow angle, and wind shear), topographical conditions of the site, wind turbine loads, installation costs, availability and capacity of the power grid, the present and future land use, and environmental and health concerns [30].

3 METHODOLOGY

In this chapter, the outline of executing the project is discussed and the procedures in which every step was undertaken. Basically, this section discusses how the whole project was accomplished. The topic is a conglomeration of subsections like the design of the experiment, research procedures, data collection and the collection procedures, and data sorting.

3.1 Design of Experiment

From the literature review chapter, it is evident that hydrogen production is very energy-intensive. The amount of energy required must come from any source as long as it is a clean and renewable source. This project was intended to develop a clear roadmap that would culminate in determining the possible amount of hydrogen that can be produced per hour at the Djupvik site through the process of wind electrolysis. As earlier discussed, the water electrolysis process is accompanied by an electrical energy source, and in this project, the source was wind energy. At the Djupvik site, there is an installation of a hydrogen refueling unit that would be used for a short run to receive hydrogen from an external source to satisfy the existing demand in Narvik and its environs. However, the long-term plan is to produce hydrogen in-house through the water electrolysis system to mitigate the logistical challenges associated with the transporting of hydrogen from the external source to the refueling location. Figure 3-1 is a sectional view of the hydrogen refueling unit under installation at Djupvik.

Therefore, this master thesis project was to establish and determine the possible amount of electrical energy that could be harnessed from wind power to accomplish the benevolent idea of 100% emission-free hydrogen production. This entire project was performed in four intertwined stages, which involved a number of software programs for data and site analysis. The primary software programs applied in this project were Windographer 4.0 and WindSim version 10.0 and WindSim Express software programs. Windographer was used for data sorting and analysis as well as obtaining satellite data, while WindSim versions were used for wind flow CFD simulations, as extensively explained in chapter 4. Similarly, Google Earth and Google Maps were extensively used in this project to assist in getting the exact coordinates of the wind turbines and climatology locations during CFD wind flow simulations. The hydrogen production calculation and analysis were accomplished using the MS excel program in chapter 5. Figure 3-2 is an illustration of the design of the research experiment execution stages.

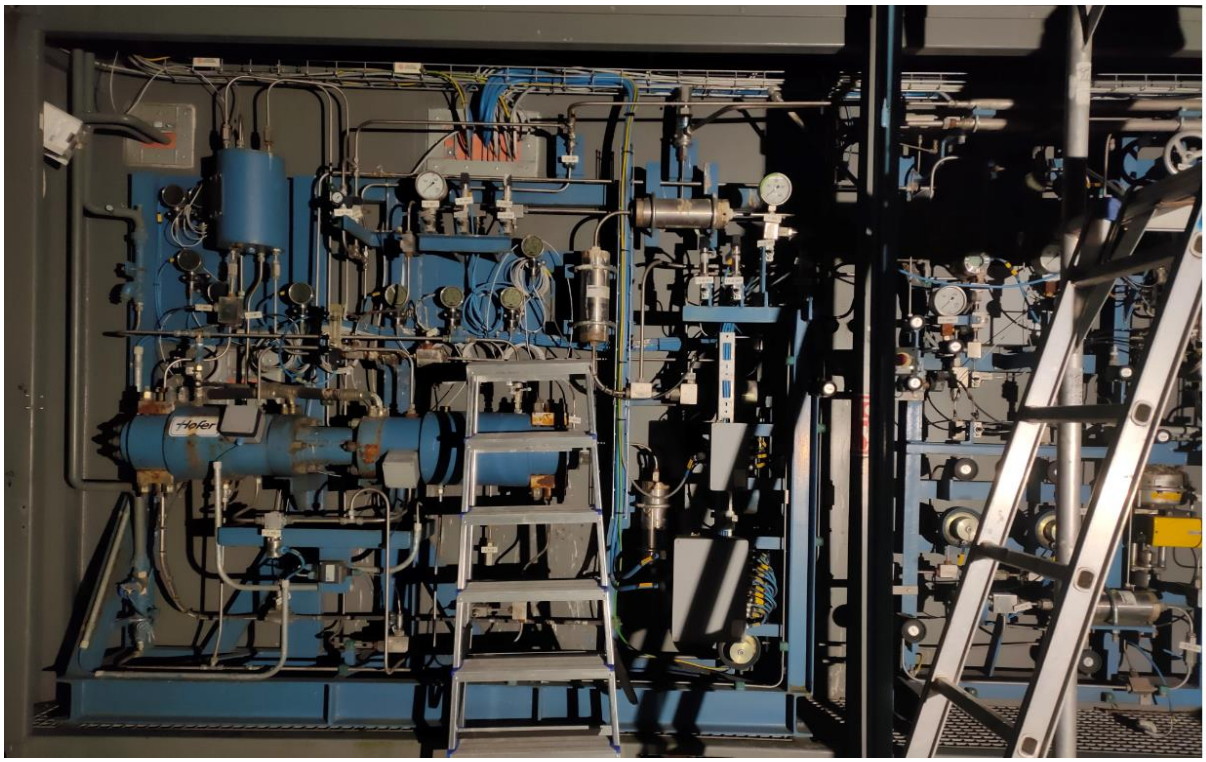

Figure 3-1: *A section of Hydrogen Refuelling unit during installation at Djupvik site.*

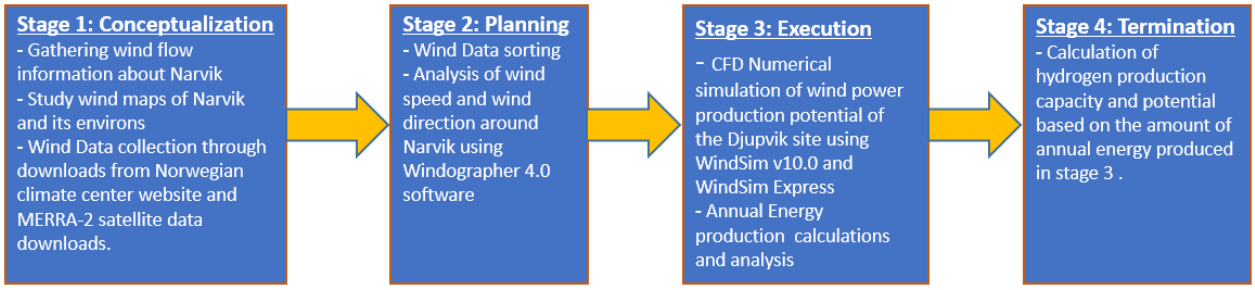

Figure 3-2: *Stages involved in the research design execution of the project experiment.*

3.2 Data Collection

This project's first step was to obtain and analyse the wind speed and direction historical data of the Djupvik site and its environs. The sources of data used in this project were; the data from the Norwegian Meteorological Institute (Norsk KlimaServiceSenter) and the data downloaded from satellite sources. From the Norwegian Meteorological Institute website, it was possible to download the mean wind speed and direction data from the weather stations nearest to the site, which in essence are similar conditions to the project site [55]. For the purposes of this study, there were four weather stations around Narvik from where data was collected by downloading the wind speed and direction data from the "Norsk KlimaServiceSenter" website. The weather stations include Straumsnes, Narvik-Fagernesfjellet, E6 Hålogalandsbrua, and Narvik Sentrum.

The periodic hourly wind speed and direction data were downloaded, and such data seemed more reliable since they were obtained from an authentic source. The wind speed and direction data downloaded was a record for the past ten years since 2010.

Another source of wind flow data used in this project was the download from the satellite sources. Windographer version 4.0, apart from data sorting and analysis, has the option of MERRA-2 (Modern-Era Retrospective analysis for Research and Applications, Version 2) downloader where one can easily download the historical meteorological wind speed and direction data for an area of choice of which in this case was Djupvik site in Narvik.

3.2.1 MERRA-2 Data

The data obtained in this source was from 1980 to the present, showing hourly recordings of the data for over 40years. To download the satellite data from Windographer MERRA-2 downloader, simply go to **<tools bar>** in Windographer 4.0 program, then to the **<Data downloader>** option where a page similar to one in figure 3-3 will appear. After which, you set the location of interest for which the data is needed, then select data source **<MERRA-2>** from the available options of MERRA-1, MERRA-2, and ERA 5. Lastly, select the **<request data set>** section, and the data needed will download after a short while for saving into a personal computer.

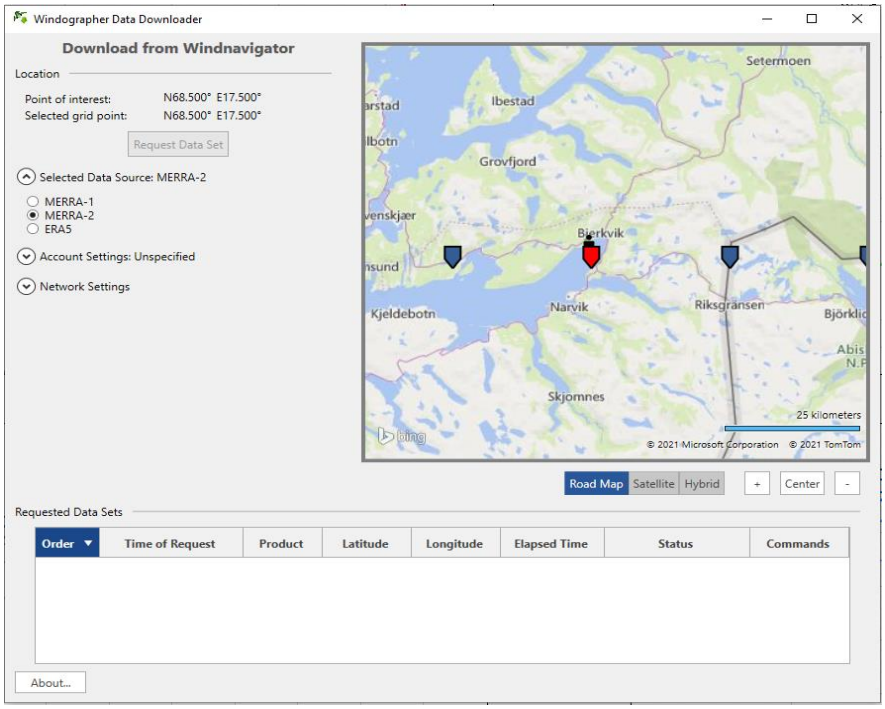

Figure 3-3: *Windographer Data downloader within the software.*

It must be noted that the request data button will not activate if the account setting is unspecified. Therefore, one must ensure that the account setting is active to allow for the request data set. Equally, the lower versions of Windographer, such as version 3.0 and lower, do not have the option of data downloader. As a result, a suitable software version must be purchased to enable this service to be available.

In MERRA- 2 data set downloader, a number of different variables can be generated, such as wind speed and direction at particular heights, the temperature of a place at different heights, and precipitation. Table 3-1 contains some of the variables that can be generated from the MERRA- 2 data set downloader in a periodic hourly sequence values of the data. The MERRA-2 satellite data used in this project was hourly data for the past 40 years from 1980 till January 2021, while the Narvik meteorological data was from December 2010 to January 2021.

Variable	Units	MERRA-2 Name	Column Name
Wind speed @50m above ground	m/s	Computed from U50M and V50M	Speed_50m [m/s]
Wind direction @50m above ground	°	Computed from U50M and V50M	Direction_50m [degree]
Temperature @ 10m	°C	T10M	Temperature_10m [degrees C]
Temperature @ 2m	°C	T2M	Temperature_2m [degrees C]
Pressure at ground level	kPa	PS	Pressure_0m [kPa]

Table 3-1: *Variables generated from MERRA- 2 data set downloader.*

The MERRA-2 wind data was recorded and collected from a height of 50m while the "Norsk klimaservice senter" data was recorded and collected from 10m height above ground level. However, these data could be synchronized to any height required for analysis. Once the data had been gathered from all the sources mentioned, the next step was to sort and analyse the data for use in the simulation stage, as discussed in the next chapter. Therefore, the subsequent section of this topic is a discussion on data sorting and analysis using Windographer software.

3.3 Data Sorting and Data Analysis

In this section, the data obtained was analyzed using the Windographer 4.0 software program to assist in determining and forecasting the mean wind speed and direction of the area under investigation and its surrounding. The two sources of data, once obtained and analysed, were compared and the correct forecast of the wind speed of the site was acquired for use in decision making in the subsequent sections of the project. The primary data variables used in this project were the wind speed and direction, and this was the data which was extensively applied. Since the data collected was a combination of several parameters, the Windographer was able to sort

and capture the data of wind flow which was required in this case. The data analysis was equally performed in the Windographer program, and the final results were downloaded for interpretation. Given that two data sources were used in this project, the first step was to study the data from both sources and observations on the similarities and differences were made. This was well executed in the Windographer 4.0 where data was fed into the program and then measuring and correlating the two data sources conducted.

In the program's Measure, Correlate, and Predict (MCP) column, you import the first data as the target data of which the MERRA-2 satellite data was taken as the target data because it was covering a more extended period while the data from the "Norsk KlimaServiceSenter" was taken as the reference data since its source could be authenticated. Figure 3-4 is an illustration of the imported data sources.

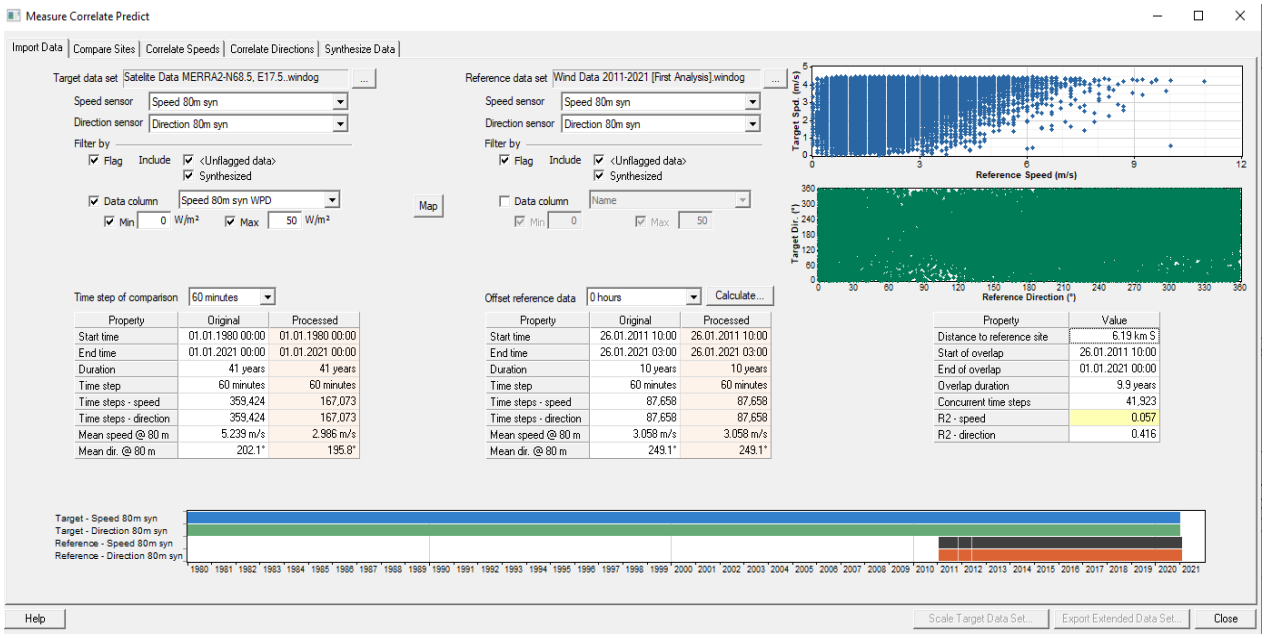

Figure 3-4: *MCP target and reference data importation.*

The comparison of the two data sources in terms of average wind speed and direction is illustrated in figure 3-5. Looking at figure 3-5, both the data sources depict constant and stable wind direction as indicated in the wind rose. Moreover, the mean monthly wind speed profile curve also showed a predictable pattern whereby high winds were recorded in winter seasons and lowest recorded in summer seasons. The highest average wind speeds were recorded between the months of December and March while the lowest average wind speeds recorded in July for both the target (MERRA-2 satellite data) and reference data (Norwegian metrological data).

However, there was a notable variation in the average monthly wind speed across the year i.e., the general mean monthly wind speeds were higher in target data than in the reference data. This was due to the elevation difference in which the two data sources were collected and recorded. The MERRA-2 satellite data was recorded from an elevation of 50m above ground level while the Norwegian metrological data was collected from a height of 10m above ground level. This explains why the MERRA-2 satellite (target) data had a higher average wind speed than the Norwegian Met (reference) data since the higher the data collection height the lesser the interference on wind flow from obstacles, surface roughness and terrain hence higher wind speeds. Generally, both the data sources showed that the average wind speed of the area is oscillating between 2m/s and about 7m/s.

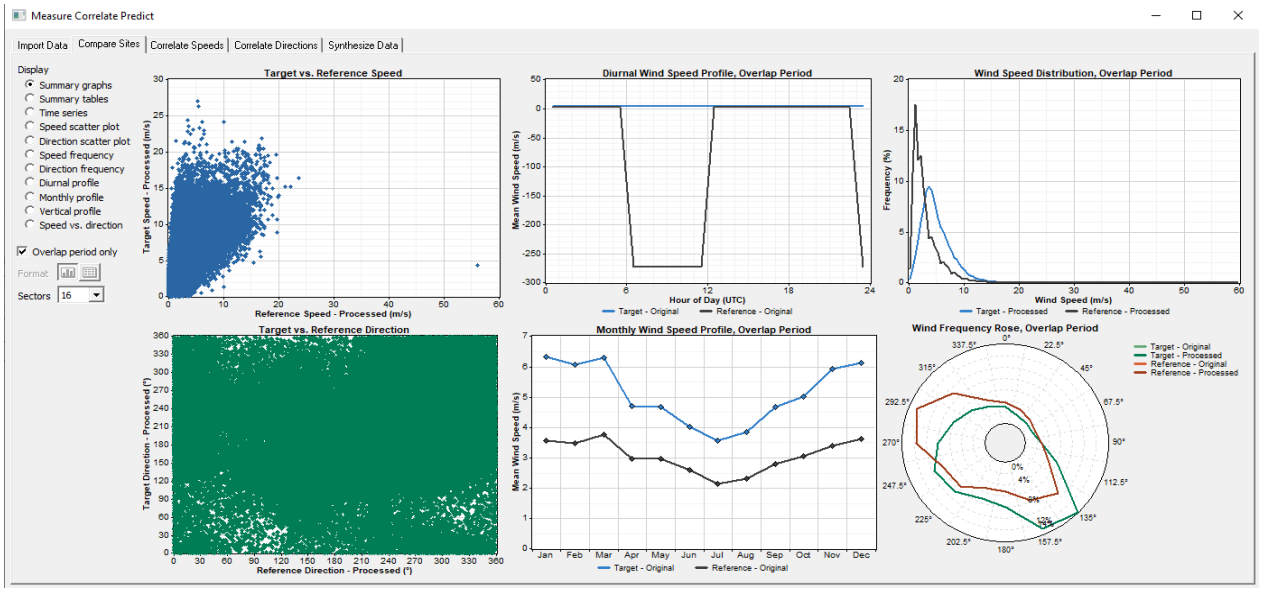

Figure 3-5: *Comparative analysis of the target and reference data.*

There were much more similarities in the data sources based on the comparative analysis. Therefore, using any of the sources for further research was assumed to be a representation of the other and so on. The data fed into Windographer was of any file extension since Windographer is designed to interpret any data from any file extensions like (.txt), (.xlsx), among others which were then sorted and tabulated.

After the comparative analysis, the data of choice was fed into the Windographer for further research. Figure 3-6 illustrates the data set configuration after the data file was loaded into the Windographer, showing the mean, maximum, and minimum wind speed, and direction at different heights. The details generated were presented in various formats for further analysis. The wind rose for directional analysis, and the mean monthly and mean diurnal wind speeds were obtained from the Windographer for scrutiny and decision making on the best wind power

production site. Figure 3-7 shows the mean monthly speed curves, a wind rose, mean diurnal profile, and the vertical wind shear profile.

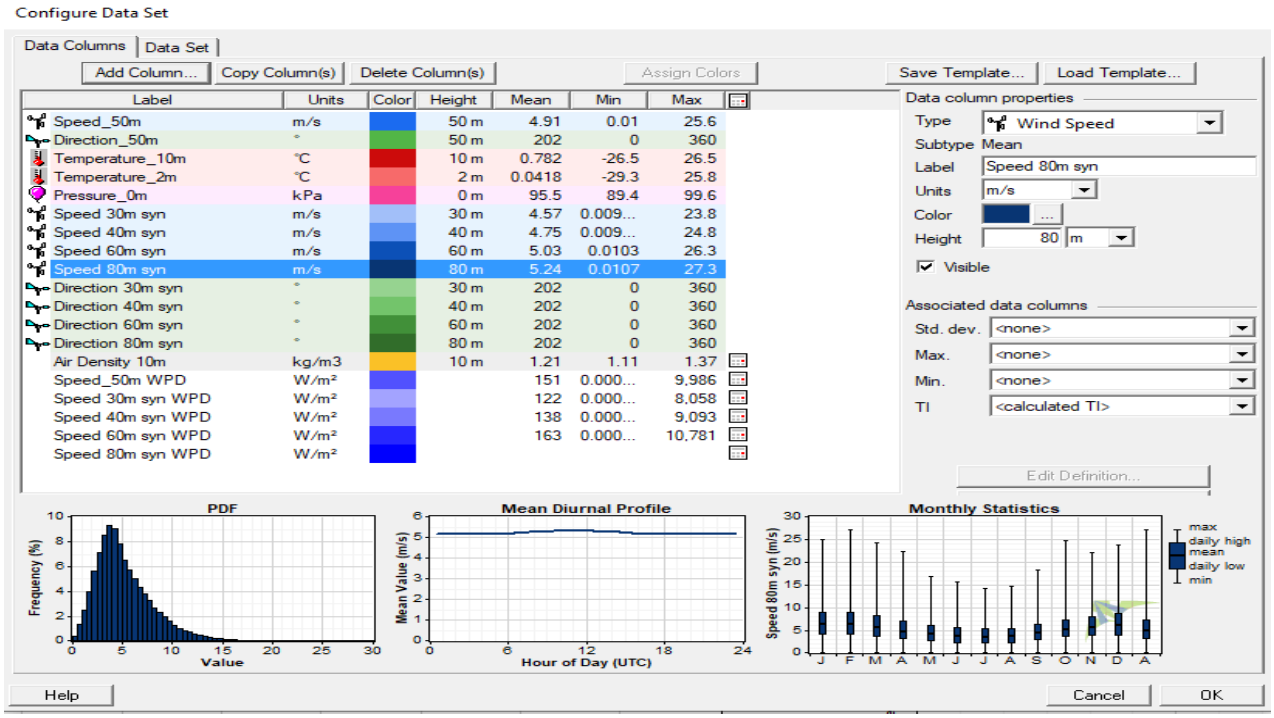

Figure 3-6: *Windographer mean wind speed data configuration at different hub heights.*

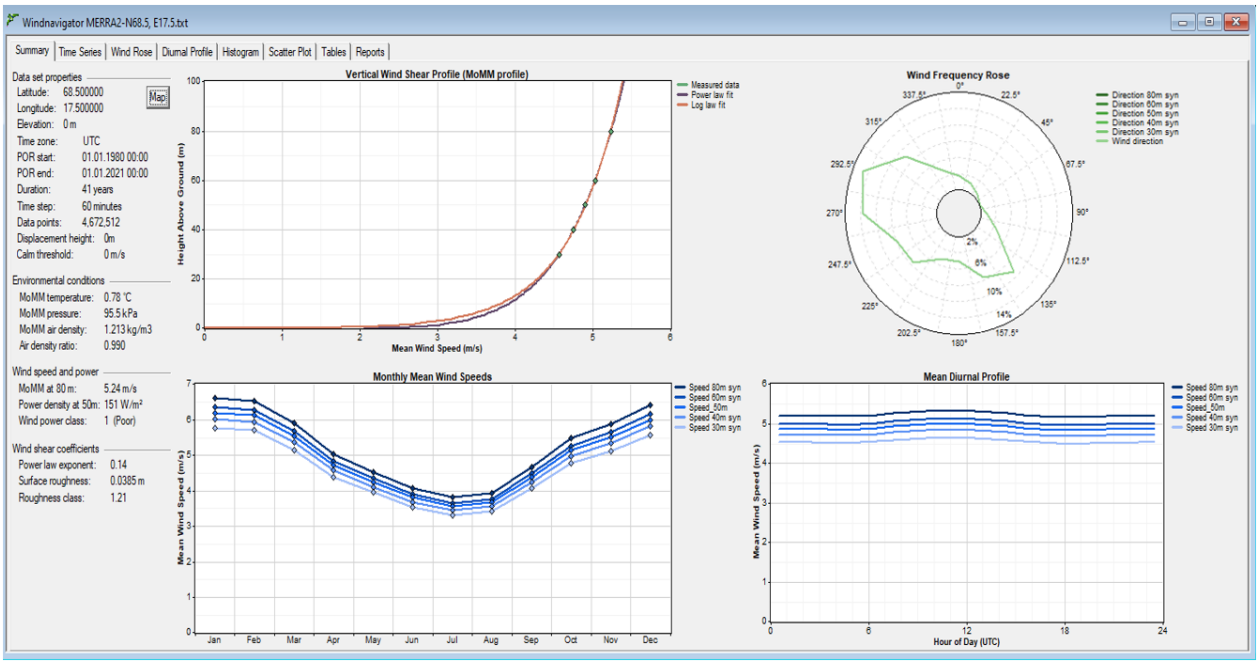

Figure 3-7: *Windographer mean monthly wind speed curves at varying height and wind rose frequency curve.*

From figure 3-7, it was observed that the area under study had its highest wind speeds during the winter months and lowest during the summer season. This could be seen in the mean monthly wind speed curve, which showed high wind speeds between January and March and

then a gradual decline to all time low values in July. Thereafter, the wind speed values started rising steadily to the highest level in December. Therefore, maximum wind power production will be highly experienced in the winter months. The determination of the wind speed was demonstrated by analysis of the wind speed distribution frequency curve shown in figure 3-8, which showed the mean wind speed based on different measurement algorithms such as OpenWind and WAsP. The mean wind speed of the area was found to be between 3m/s and 7m/s based on the measurement algorithms at the height of 60m above ground level. This was further justified by the wind speed frequency distribution curve in figure 3-9.

The vertical shear curve was also a testament that the mean wind speed increased with an increase in height above ground level. This was attributed to the presence of obstacles and other roughness factors on the lower ground levels than high above the ground. It is also interesting to note that in height above 60m, there was minimal change in mean wind speed in respect to an increase in the height above ground levels. This can be a justification that the higher you go, the lesser the obstacles and hence no interferences that increase the turbulence intensity. The wind rose showed a relatively constant wind direction, as was observed in figure 3-5 and confirmed in figure 3-7.

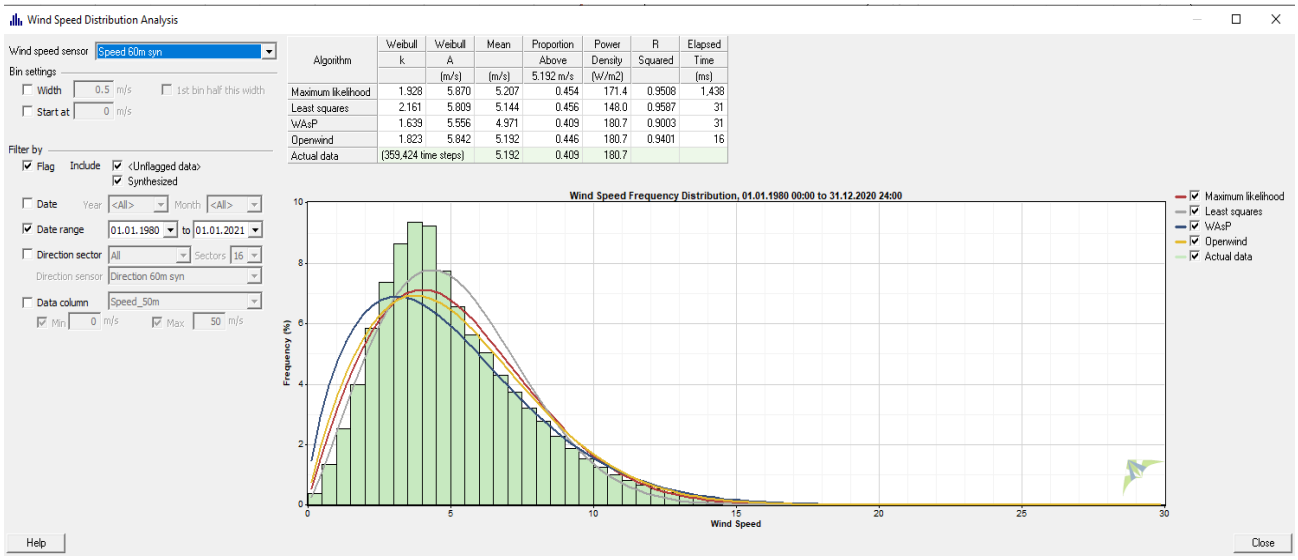

Figure 3-8: *Wind speed distribution Analysis*

Given that the data was analysed for future installation of the wind turbines, it was also necessary to make some long-term forecasting of the wind speed at different heights. Using the MCP tool, it was possible to make critical analysis and prediction on the future average annual wind speed to decide on the wind speed trends based on the forecasts found. Figures 3-10 and 3-11 demonstrate the long-term forecasting of the mean annual wind speeds at different heights

of 40m, 50m, 60m, and 80m above ground. Based on the regression analysis, it was observable that the mean annual wind speed has been on the decline since 1980. Therefore, going into the future there would be a possibility of wind speed decline. This information will be essential to assist in making decisions while siting wind turbines in the area.

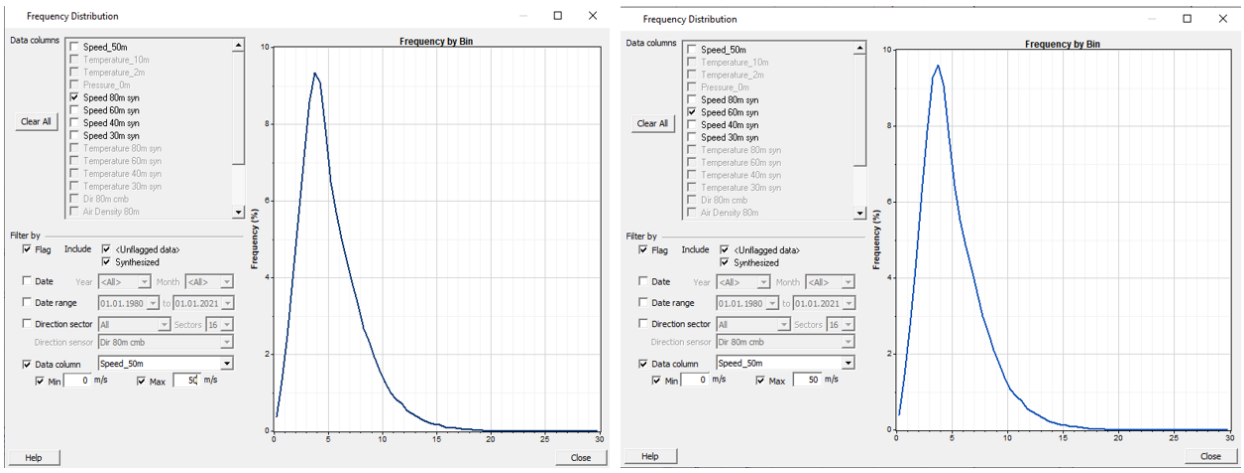

Figure 3-9: *Frequency distribution of wind speed at height 60m (right) and 80m (left).*

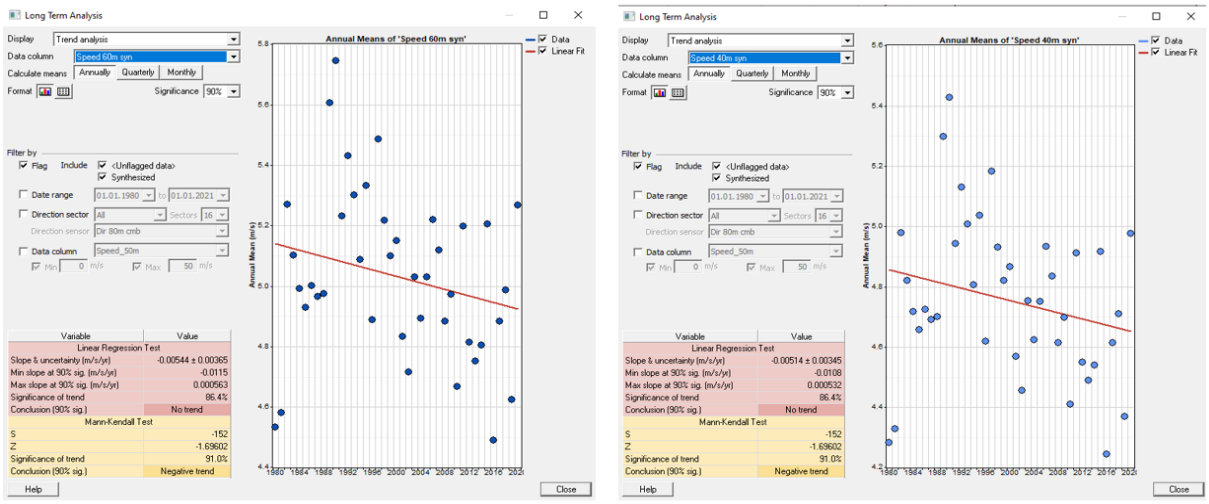

Figure 3-10: *Long term analysis of annual mean wind speed at height 40m (right) and 60m (left)*

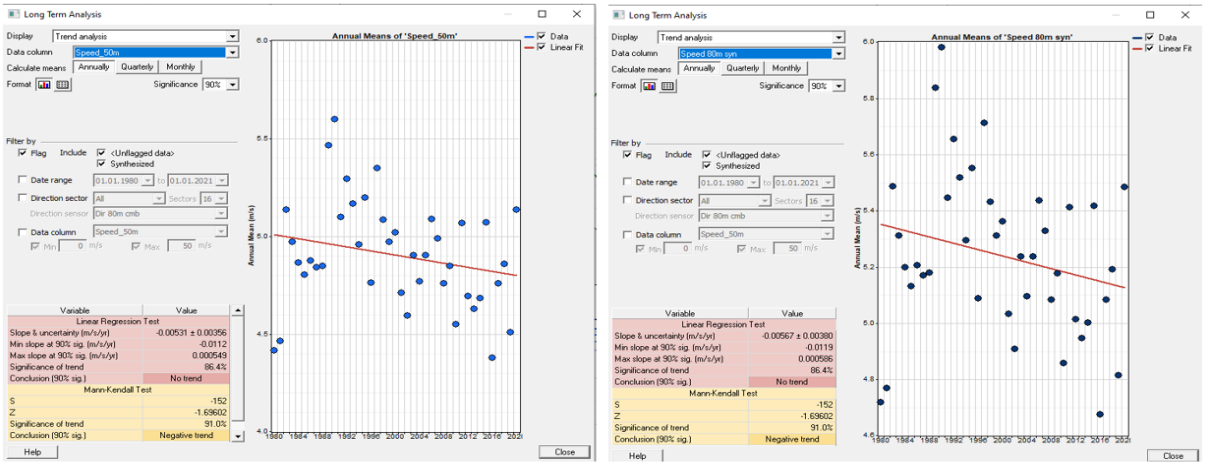

Figure 3-11: *Long term forecast analysis of wind speed at height 50m (left) and 80m (right)*

The long-term forecasting margin of error analysis for height 80m above ground is shown in figure 3-12, where the percentage of mean biased error (MBE) and the mean absolute error (MAE) was at 6.8%, while that of root mean square error was at 7.76%.

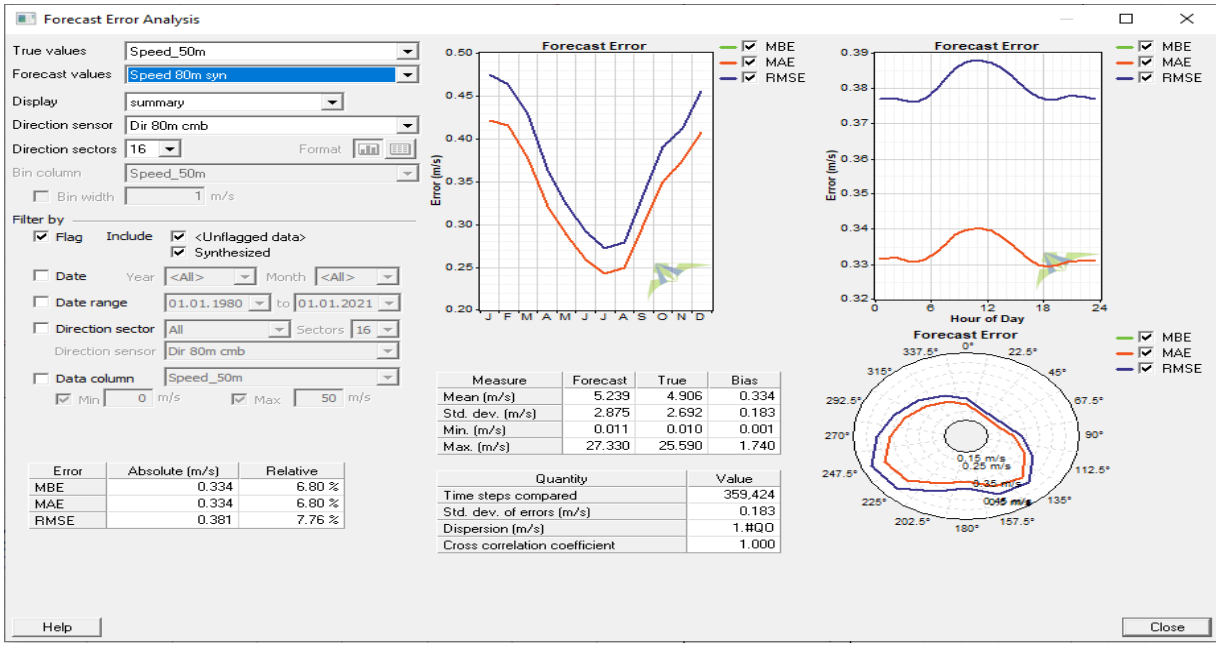

Figure 3-12: *Forecast error analysis for wind speed at 80m above ground*

Once all the investigations were concluded in the Windographer and all the wind speed and direction data synchronized to the required heights for analysis, the data was exported in (.TWS) files or (.WWS) files which was then stored in personal computers for use in the WindSim software during CFD numerical simulations. The data obtained in this chapter was used as the raw material in the next chapter to estimate the possible amount of annual energy production (AEP) from wind energy potential of the area.

4 CFD-NUMERICAL WIND FIELD SIMULATIONS

This chapter entails the analysis of the wind pattern behavior in Narvik and its environs for the sole benefit of describing the possible amount of renewable wind energy that could be tapped for use in the Djupvik site. The site is already pre-selected a few miles from the Narvik central business district (CBD), and the honour was on this study to establish the nearest location with optimal wind speed and predictable wind direction. Therefore, this chapter looked into different methodologies that could be applied to help in breaking the deadlock of wind flow patterns around the Narvik area using computational fluid dynamic simulations. As a result, it was possible to select the location with optimal wind speed and a suitable wind turbine for installation. Thereafter, the resultant findings and the general issues that would impede or accelerate the power production were outlined.

4.1 Wind Resource Methodologies

These are techniques that are employed to predict and estimate the wind resource. In this master thesis, the method used was the computational fluid dynamics simulation employed in the WindSim software program. The WindSim version 10.0 and WindSim Express were engaged in this project to help in finding the suitable site location for optimal generation of wind energy. The prerequisite of this topic was the sources of data used, data collection, and sorting methodologies which are found in chapter three.

Therefore, the preamble of this topic involved importing the analysed data from Windographer 4.0 software program as used in the previous chapter. Thereafter, the data was fed on the WindSim Express to simulate on terrain and object modules before exporting the data to WindSim 10.0 for the final wind flow simulations. As an introduction, the next subsection is a brief overview of the WindSim software.

4.1.1 WindSim Software

In this master thesis project, the WindSim software program was applied for wind field simulations. The WindSim package is a software program developed by the WindSim AS Company located at Tonsberg, Norway. The software package is designed based on the PHOENICS code for solving nonlinear transport equations of mass, momentum, and energy to provide complete solutions to the RANS equations of motion [39]. The PHOENICS code is a general-purpose computational fluid dynamics (CFD) model technology that enables the WindSim software to be used as a wind park design tool for simulating wind fields and to

optimize wind turbines' placement in order to maximize energy production in any area of interest.

The very first commercially available WindSim software, version 4.2, was launched in 2003. Since then, there has been a gradual growth in the development of new versions that came with remarkable improvements that enables the users to navigate the challenges of wind farm design and wind resource assessment. Table 4-1 shows the chronology of events in developing the improved versions of WindSim. In this project, specifically WindSim version 10.0 and WindSim Express were used for modelling the wind fields.

WindSim Version	Year Commercially Released
WindSim 4.2	2003
WindSim 5.0	2010
WindSim 5.1	2012
WindSim 6.2	2013
WindSim Express	2013
WindSim 7.0	2015
WindSim 8.0	2016
WindSim 9.0	2018
WindSim 10.0	2019

Table 4-1: *The chronology of the commercial release of the WindSim versions* [56]

4.1.2 Functionality of WindSim Express

WindSim Express was launched in 2013 alongside WindSim version 6.2 with the sole purpose of making CFD-based micro-siting accessible for everyone. It is applied in tandem with the other WindSim versions to ensure complete modelling of the wind fields. The WindSim Express conducts the CFD based micro- siting in three steps that include:

4.1.2.1 Project Setup

This step involves defining the project. It includes naming the project, defining project layout, as well as revealing the customer to whom the project is intended to satisfy. Figure 4-1 shows the WindSim express outline of the project setup stage.

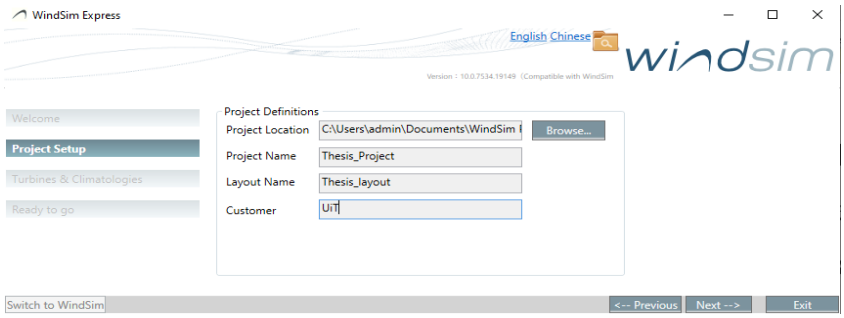

Figure 4-1: *Showing the project setup outline in WindSim Express.*

4.1.2.2 Loading the Turbine Positions and Measurement Data

In this step, a few sub-steps are followed sequentially to ensure that everything is in order; otherwise, WindSim will generate an error code to indicate that there is mismatch in some settings. The first section is to load the layout information, which incorporates defining the type of turbine to use, turbine height, and the selected turbine's rotor diameter. Subsequently, the turbine locations are defined based on the coordinate system of choice. In this project, the preferred coordinate system applied was the Geographic latitude and longitude coordinates, datum 33 system of WGS84. In addition, the planar units selected were the Arc Degrees, as shown in figure 4-2 (a). The geographic coordinate system is like the Cartesian XY-coordinate system, whereby the x-axis represents the eastings which are basically the longitudinal locations. At the same time, the y-axis is the northings that translate to latitude locations of the wind turbines. The datum system WGS84 is capable of defining and translating the geographic coordinate system so that the wind turbines' exact locations are defined in the WindSim.

It must be noted that in the event that a new wind turbine model is required for the simulation and it is not amongst the pre-installed default turbines in the WindSim Express, there is an option of creating a new power curve whereby the information of the new wind turbine is manually entered into the system as shown in figure 4-2 (b).

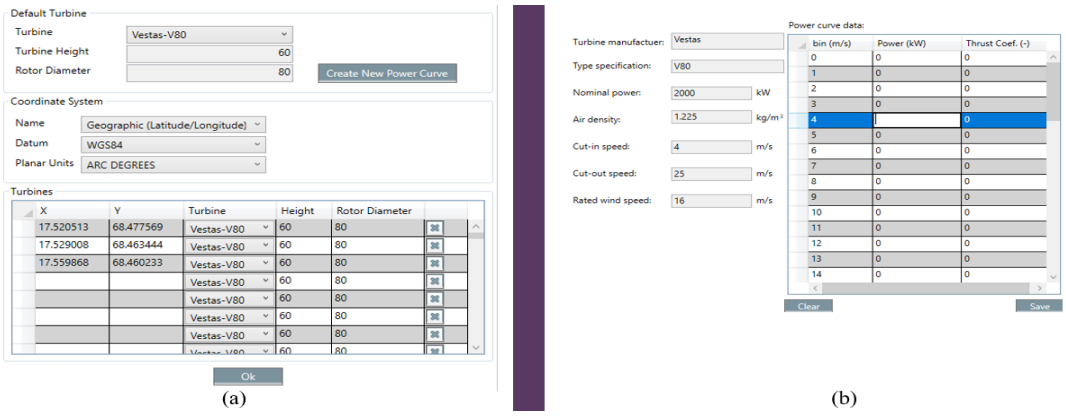

Figure 4-2: *(a) Wind Turbines location setup and (b) setting up a new turbine into WindSim express.*

After all the above procedures, the next substep in this section is to load the measurement data in the WindSim Express. This is done by selecting on the **"<Import Time series>"** and this will lead to the location of the files where all the files that were earlier imported from the Windographer 4.0 are stored. The preferred file will be selected and loaded into the system. WindSim Express can open the file extensions (.TWS) or the (.WWS) files. Since the data generated from the Windographer are in TWS format files, the WindSim Express will open and load it automatically, as shown in figure 4-3.

Thereafter, it behooves one to check the information entered and confirm the correct units, then proceed with the process of climatology conversion whereby you confirm and specify the climatology location as shown in figure 4-4. In this project, the chosen climatology location was the coordinates of the Djupvik site in Narvik since the wind flow data was collected in reference to the site. The program takes a short-while to convert the fed data into the format that is recognizable by the system. Given that WindSim uses the UTM coordinates system, the entered geographical coordinate format will be converted to the UTM system. The final procedure in this substep is to specify the sectors and the bins. All the simulations on this project were run on the default sectors and bins of 12 and 50 respectively.

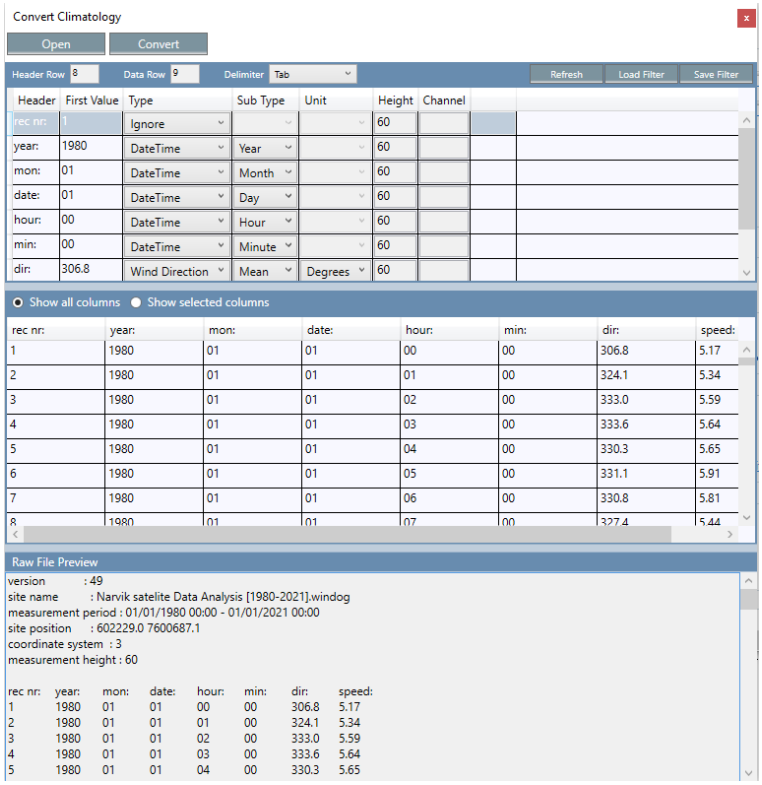

Figure 4-3: *Showing the loaded climatology data into WindSim express*

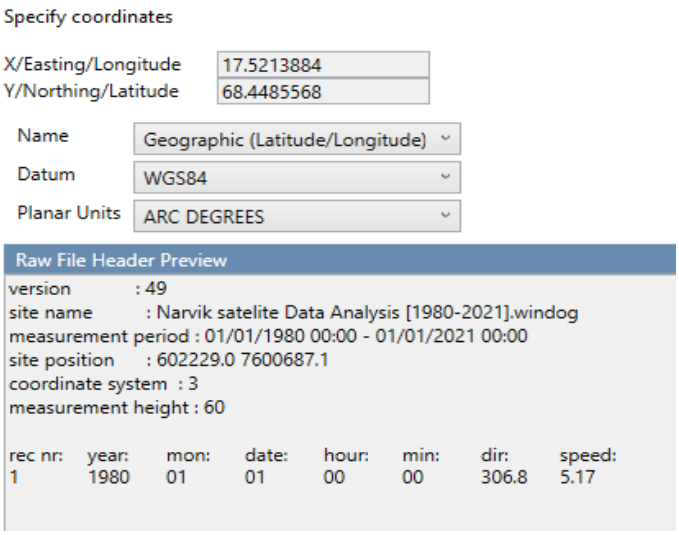

Figure 4-4: *Showing the loaded climatology data with specified site coordinates.*

4.1.2.3 Setting the Resolution to the Numerical Model

It is the very last procedure in WindSim Express software, and it involves selecting the appropriate elevation data set, roughness data set, and roughness table. Eventually, the WindSim Express will download the terrain module of the area of interest and also run the object module simulation.

In this project, the elevation dataset of choice was ASTER GDEM v2 Worldwide Elevation Data (1 arc-second resolution), the roughness data set used was the CORINE Land Cover Europe 2006 (100m resolution), the roughness table chosen was CORINE Land Cover (summer roughness or winter roughness), and the Map Image dataset selected was World Imagery as shown in figure 4-5.

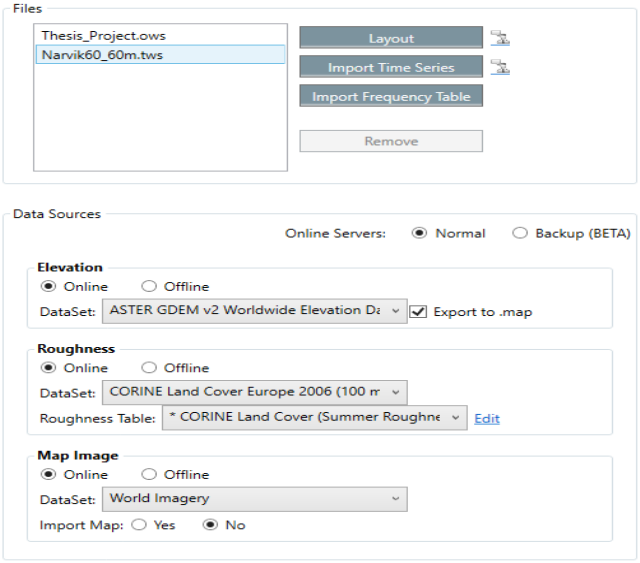

Figure 4-5: *Showing the Data Sources settings for WindSim Express simulation.*

After the simulation runs in WindSim Express, it is possible to select **"<Switch to WindSim>"** to open WindSim 10.0 modules for continued simulation of the rest of the modules. The WindSim Express will close down after simulating the terrain and object modules, while WindSim 10.0 will open for continued simulation of the remaining four modules.

4.1.3 Modules of WindSim 10.0 version

In WindSim 10.0, six modules must be wholly simulated in the correct order to fulfill the wind farm micro-siting. The six modules include terrain, wind fields, objects, results, wind resources, and energy modules, as illustrated in figure 4-6.

Figure 4-6: *Illustration of the different modules in WindSim10.0.*

After completion of the six modules simulation in WindSim, the resultant outcomes include the wind direction display in wind rose, wind turbine maps, wind resource maps showing wind speed variations, terrain and roughness index maps, and the annual energy production (AEP) that can possibly generated in the area. All these information are contained in a WindSim word report document which can be downloaded from the program.

4.1.3.1 Terrain Module

The module establishes 3D numerical models based on height and roughness data of a particular area of interest. This is possible by loading the data set containing the elevation and roughness data of the given location in WindSim Express, which generates the 2D fields, 3D models, and extensions. The terrain module is simulated in WindSim Express, where a grid file (.gws) is generated. Figure 4-7 shows the setup in the terrain module.

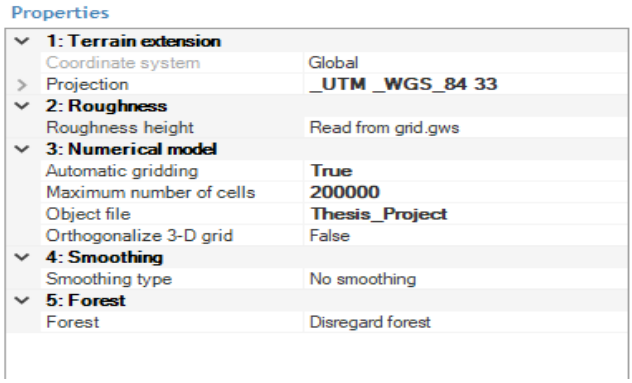

Figure 4-7: *Set up in Terrain Module.*

4.1.3.2 Wind Fields Module

This module involves the calculation of the numerical wind fields as a result of solving the Reynold Averaged Navier- Stokes (RANS) equations [56]. The simulation of the wind fields' module starts immediately after completion of the Terrain module. However, it is proper to set up the required boundaries and initial conditions before running the module. The number of sectors selected in all the simulations in this project was 12 uniformly distributed. The height of the boundary layer was set to 500 m while the turbulence model under the physical models was set to **"Standard k- epsilon."** In the calculation parameters, the number of Iterations for this project was set at 500, while 0.001 was set as the convergence criteria. Figure 4-8 shows an illustration of wind fields' module setup.

Properties

1: Boundary and initial conditions	
Do Nesting	Disregard nesting
Sector input type	Uniform distribution of the sector angles
Number of sectors	12
Sectors for next run	0;30;60;90;120;150;180;210;240;270;300;330
Height of boundary layer	500
Speed above boundary layer height	10
Use previous run as input	False
Boundary condition at top	Fixed pressure
2: Physical models	
Potential temperature	Disregard temperature
Air density	1.225
Turbulence model	Standard k-epsilon
3: Calculation parameters	
Solver	GCV
Number of simultaneous sectors	1
Number of iterations	**500**
Convergence wizard	False
Convergence criteria	**0.001**
4: Convergence monitoring	
Coordinate system	**Global**
Spot value X position	**604042**
Spot value Y position	**7597300**
Spot value Z position	**80**
Field value to monitor	Speed scalar XYZ
5: Output	
Height of reduced wind database	300
Run in batch mode	**True**

Figure 4-8: *Illustration of wind field module in WindSim 10.0*

4.1.3.3 Objects Module

The module incorporates the setting and positioning of the wind turbines as well as processing of the climatology data. The object module is pre-simulated in the WindSim Express after loading the desired wind turbines' locations in the given area. Figure 4-9 shows entry information of 3 different wind turbines as it appears in the object module. This module also provides room for improving the wind turbines' locations and adjustments of the wind turbine hub heights and rotor diameters. In this entire project simulation process, different hub heights were experimented while trying to get the optimal height, translating to maximum AEP yield. The most tested heights were 50m, 60m, 70, 80m, 90m, and 100m.

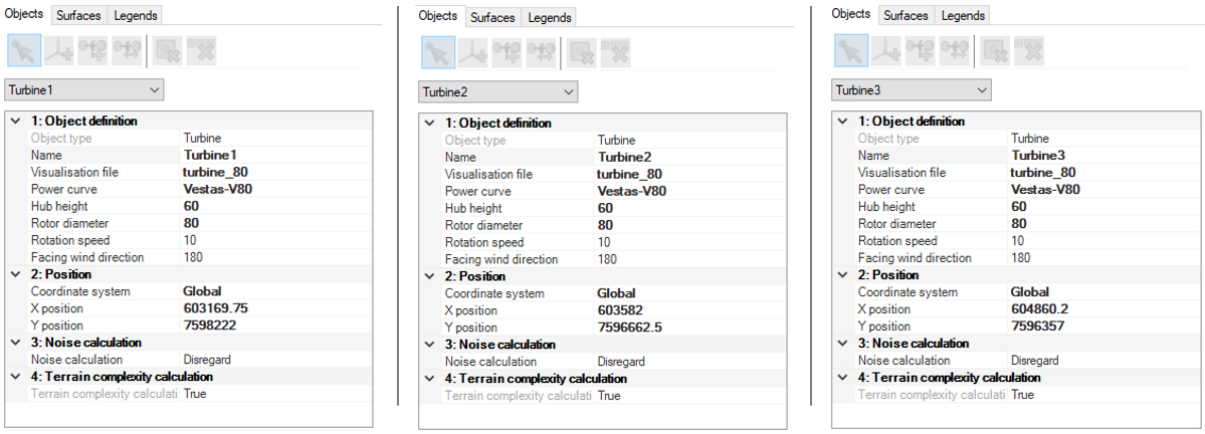

Figure 4-9: *Showing entry information of wind turbines as it appears in the object module.*

4.1.3.4 Results Module

The results module analyzes the numerical wind fields. The results of the wind field simulations are stored in a reduced database that occupies the vertical extension from the ground up to the "height of reduced wind database" [56].

In order to run the result module simulation, one must select on "***New***" under the properties function, then adjust the normalization variable to "***Speed scalar XYZ,"*** as illustrated in figure 4-10. Equally, it is also possible to change the heights, and entry of multiple heights is permitted.

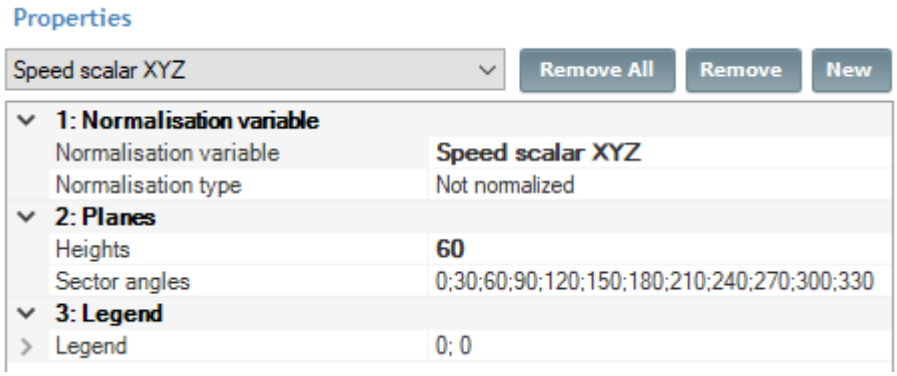

Figure 4-10: *Illustration of Results Module in WindSim 10.0.*

4.1.3.5 Wind Resource Module

In this module, wind resource maps are generated by statistically comparing the numerical wind fields' database against the climatology. The wind resource module contains a tool for area classification capable of finding high wind speed connected areas by simply grouping areas according to the wind speed and size [56]. As a result, it is possible to estimate power production in the given site.

Before running the Wind Resource module, at least one climatology must exist. All sectors defined in the climatology must exist in the wind database; otherwise, WindSim will generate an error code. In addition, one is expected to select or disregard the wake models. There are three different wake models to choose from, and in this project, "***Wake Model 1***" was predominantly used, as shown in figure 4-11. However, the other wake models were also tried in a few simulations to test if there was any significant variation in power output. Furthermore, adjustments of heights above ground level are possible before running the module, as illustrated in figure 4-11.

Properties

1: Wind resource map	
Heights	**60**
Sector interpolation	True
Wake model	**Wake Model 1**
Wake Decay Factor	Automatic
Roughness	Read from grid.gws
Number of sub-sectors	30
Influence range	1; 50
Multiple wakes model	Based on sum of squares
Air density correction	No correction
Distance weighting	1
2: Legend	
Legend	0; 0
3: Export	
Export to ASCII format	False
Export to WAsP format	False
4. Cross-checking	
Wind Speed	False
Wind Speed st.dev	False

Figure 4-11: *Illustration of Wind Resource Module in WindSim 10.0*

4.1.3.6 Energy Module

It is the last module to complete the WindSim simulation cycle. Annual energy production (AEP) is calculated statistically through the numerical wind fields and climatology data for all visible wind turbine objects. Before running this module, it is essential to adjust the "***wake model"*** and "***height of reference productions***" in conformity with the choices made in the preceding module, as indicated in figure 4-12.

Properties

1: Calculations	
Air density correction	No correction
Method for density correction	Pitch-regulated WECS
Sector interpolation	True
Wake model	**Wake Model 1**
Wake Decay Factor	Automatic
Roughness	Read from grid.gws
Number of sub-sectors	30
Influence range	1; 50
Multiple wakes model	Based on sum of squares
Heights of reference productions	**60**
Activate REWS calculation	False
Distance weighting	1
Manual weighting	False
2: Export	
Export power history	False
Export rotor profiles	False
Export turbine assessment	False
Export vertical profiles	False
3: IEC Classification	
IEC classification	False

Figure 4-12: *Illustration of Energy Module in WindSim 10.0*

4.2 Wind Turbines Selection

In this master thesis execution plan, WindSim software was used to simulate wind energy production, as earlier mentioned in section 4.1. The simulation was conducted to help determine the suitable location(s) where wind turbine(s) could be sited for the overall goal of generating electrical power for use in the Djupvik site for the electrolysis process of hydrogen production. The simulation modelling equally assisted in choosing the appropriate wind turbine for installation and in this project three different wind turbine models were used to bring different aspects of energy production. Thereafter, a suitable wind turbine in an appropriate location was recommended. As a result, this section will look into the specifications of the wind turbine models used and their brief descriptions.

The three wind turbine models used in this project for the simulation process were; the Vesta V80 model, Gamesa G52 model, and Gamesa G58 model. These models were chosen based on their widespread availability and long-standing reputation in the wind energy sector. The Vestas V80 model was the mainly used turbine in the simulations, while Gamesa G52 and G58 were used as control experiments and analysis comparisons. The following subsections show the details of the various wind turbines that were applied in the simulation modelling of wind energy production around Djupvik and its environs.

4.2.1 Wind Turbine Vestas V80-2.0MW model Specifications

The Vestas V80-2.0MW model was manufactured by the Danish company called Vestas Wind System AS. Tables 4-2 and 4-3 illustrate the wind turbine datasheet and the turbine characteristics with power and thrust coefficient at every wind speed.

Turbine type	Vestas V80 model
Manufacturer	Vestas Wind system
Rated power (kW)	2000
Rated wind speed (m/s)	16
Cut-in wind speed (m/s)	4
Cut-off wind speed (m/s)	25
Rotor Diameter (m)	80
Hub heights (m)	60, 67, 78, 100
air density (kg/m3)	1.225

Table 4-2: *Vestas V80 model wind turbine datasheet*

Wind Speed (m/s)	Power (kW)	Thrust coefficient
0	0	0.05
1	0	0.05
2	0	0.05
3	0	0.05
4	58	0.818
5	149	0.806
6	277	0.804
7	461	0.805
8	698	0.806
9	996	0.78
10	1331	0.737
11	1645	0.649
12	1854	0.571
13	1955	0.41
14	1988	0.314
15	1996	0.249
16	1998	0.202
17	2000	0.167
18	2000	0.14
19	2000	0.118
20	2000	0.101
21	2000	0.088
22	2000	0.076
23	2000	0.067
24	2000	0.059
25	2000	0.052

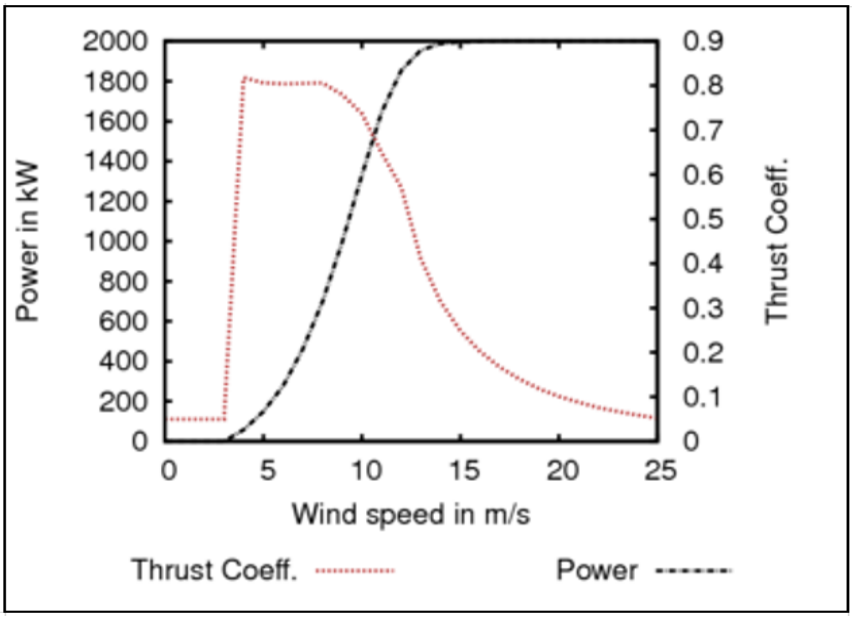

Table 4-3: *Vestas V80 Wind turbine characteristics with power and thrust coefficient at every wind speed.*

4.2.2 Wind Turbine Gamesa G52-850kW model Specifications

These wind turbines were manufactured by Siemens Gamesa Renewable Energy and commissioned in 2001 for onshore installations. Tables 4-4 and 4-5 are a brief description of the specification data sheet and power curve and thrust coefficient characteristics.

Turbine type	G52
Manufacturer	Siemens Gamesa
Rated power (kW)	850
Rated wind speed (m/s)	13
Cut-in wind speed (m/s)	4
Cut-off wind speed (m/s)	25
Rotor Diameter (m)	52
Hub Heights (m)	44, 55, 65
air density (kg/m3)	1.225

Table 4-4: *Gamesa G52 model Datasheet*

Wind Speed (m/s)	Power (kW)	Thrust coefficient
0	0	0
1	0	0
2	0	0
3	0	0
4	25.5	0.808
5	67.4	0.784
6	124	0.78
7	201	0.779
8	297	0.776
9	408	0.758
10	525	0.712
11	638	0.637
12	730	0.536
13	792	0.43
14	826	0.34
15	842	0.272
16	848	0.222
17	849	0.185
18	850	0.156
19	850	0.134
20	850	0.116
21	850	0.101
22	850	0.089
23	850	0.079
24	850	0.071
25	850	0.064

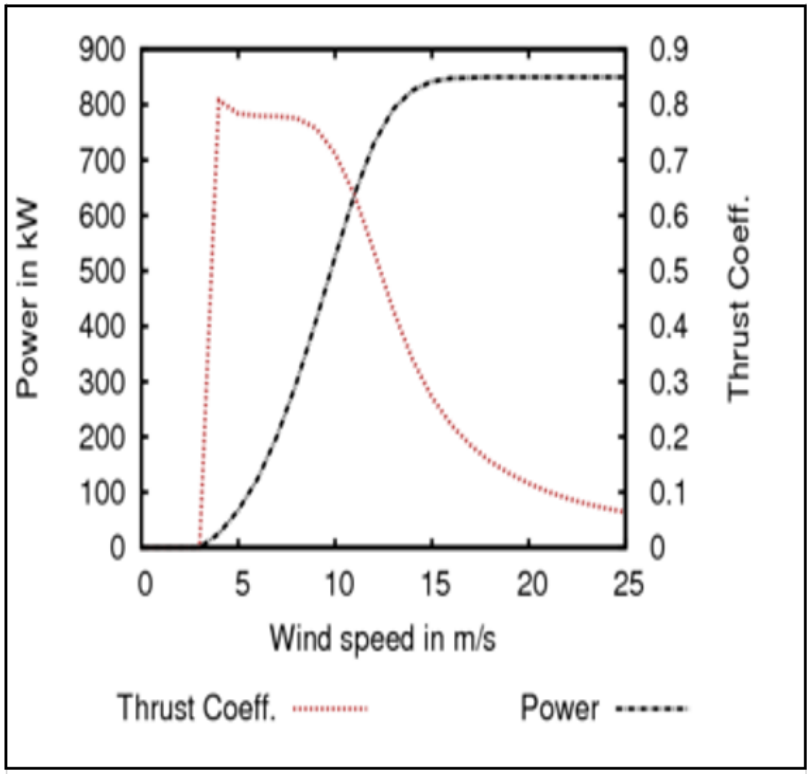

Table 4-5: *Gamesa G52 Wind Turbine characteristics with power and thrust coefficient.*

4.2.3 Wind Turbine Gamesa G58/850 model Specifications

These turbines, just like G52, came from the same manufacturer and was designed and commissioned for onshore installations in 2001. Tables 4-6 and 4-7 describe the specification datasheet and power curve and thrust coefficient characteristics.

Turbine type	G58
Manufacturer	Siemens Gamesa
Rated Power (kW)	850
Rated wind speed (m/s)	12.5
Cut-in wind speed (m/s)	3
Cut-off wind speed (m/s)	20
Rotor Diameter (m)	58
Hub heights (m)	44, 55, 65, 74
air density (kg/m3)	1.225

Table 4-6: *Gamesa G58 model Datasheet.*

Wind Speed (m/s)	Power (kW)	Thrust coefficient
0	0	0
1	0	0
2	0	0
3	9.7	0.879
4	31.2	0.844
5	78.4	0.828
6	148.2	0.822
7	242.7	0.82
8	368.8	0.819
9	525.3	0.795
10	695	0.703
11	796.6	0.561
12	835.9	0.427
13	846.8	0.326
14	849.3	0.256
15	849.9	0.205
16	850	0.168
17	850	0.14
18	850	0.119
19	850	0.102
20	850	0.089
21	850	0.079

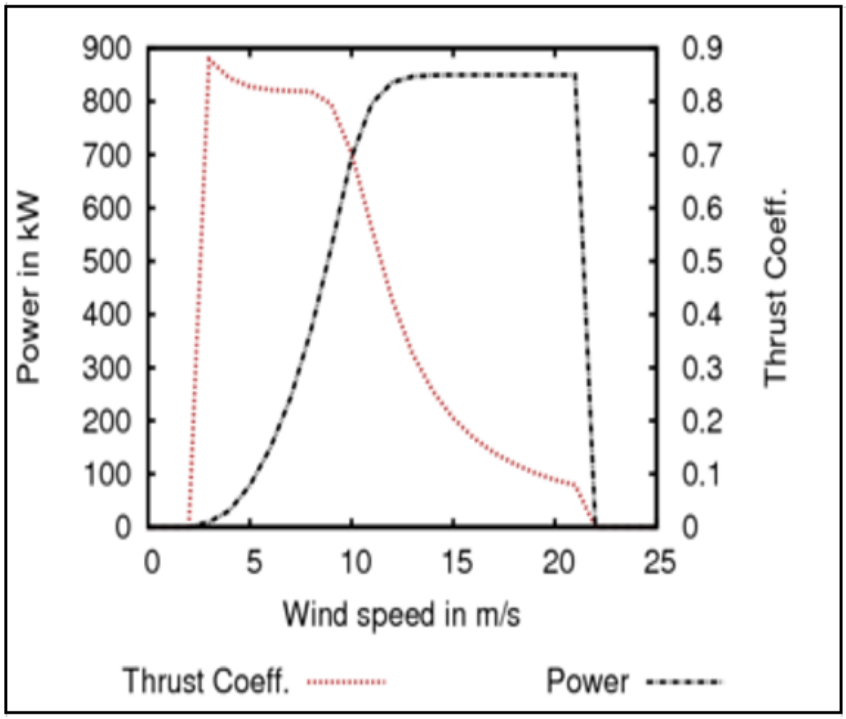

Table 4-7: *Gamesa G58 Turbine characteristics with power and thrust coefficient.*

4.3 Site Selection CFD Simulation

Given that the hydrogen production site had been predetermined and established at a geographical coordinate of **68.4485568˚N, 17.5213884˚E** in Djupvik near Narvik, the wind turbine(s) location should be as close as possible to the site to minimise additional costs of connectivity from far-flung areas. Therefore, the process of site selection considered the distance from the hydrogen site. Other factors considered include wind speed and direction, the elevation of the terrain, obstacles, government policies, and non-interference to other agencies. The fundamental objective of the site selection process was to find a location nearest to the hydrogen refueling site in Djupvik, with optimal wind speed and stable direction, minimal interference to other agencies, and optimal hours of wind turbine operation at full potential.

The first step in this process was to study the wind maps of Narvik and its environs at different heights to predict the probable average wind speed in the area, as indicated in figures 4-13 and 4-14. After studying the available wind maps, a brief visit to the Djupvik site and its surrounding was conducted for familiarity and to gather first-hand experience of the geographical terrain of the area. This assisted in making quick observations on possible factors that might affect the wind turbine siting around the area. In addition, such excursions were of immense significance as they helped in unearthing the possible bottlenecks and other underlying issues that might influence the wind field simulation of the nearby areas.

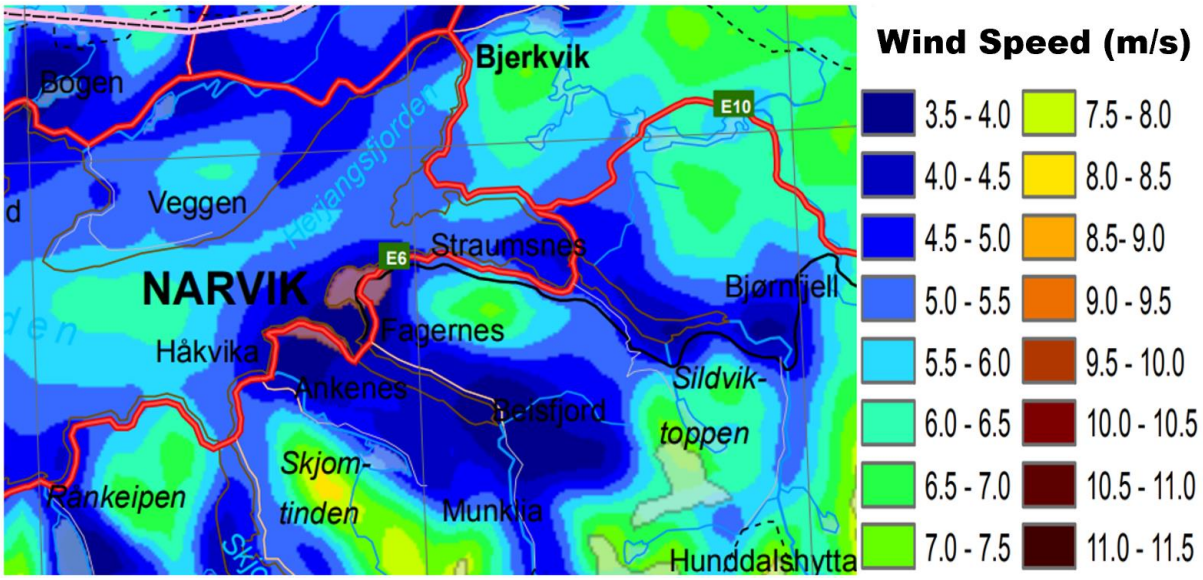

Figure 4-13: *Wind map of Narvik and environs showing wind speed at 50m height.*

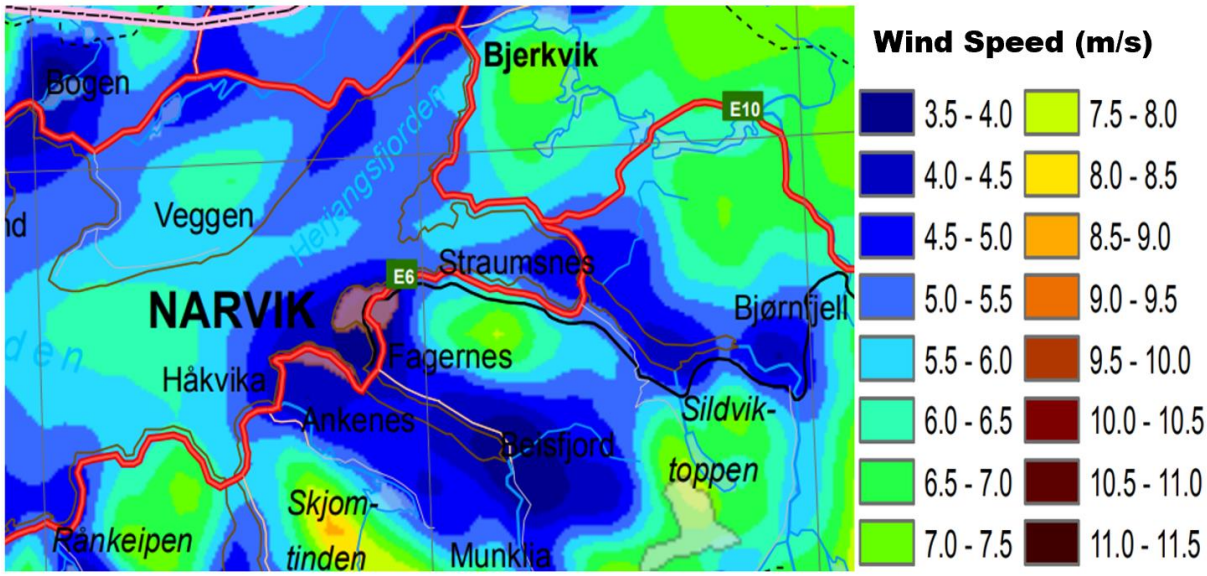

Figure 4-14: *Wind map of Narvik and its environs showing wind speed at 80m height.*

4.3.1 Site Location modelling

This process began by randomly selecting a considerable number of locations around Djupvik and its environs, then feeding the data into the WindSim software for modelling. Thereafter, analysis of the results was conducted to choose the appropriate locations. Several rounds of simulations were carried out with the same wind turbine model at constant hub height until four different areas were identified for further analysis on wind turbine siting. The choice of the wind turbine model applied on this process was only based on simulation, and no unique factor was considered.

Turbine Type	Hub Height (m)	No. of turbines	Capacity (MW)	Gross AEP (GWh/y)	Average wind speed (m/s)	Wake losses (%)	Full load hours (hours)	Capacity factor (%)
Vestas V80 model	60.0	31	62.0	83.4	**5.1**	n.a.	1345.9	15.4

Table 4-8: *Key wind farm and production characteristics*

Turbine name	Turbine type	Hub height	Easting	Northing	z
Turbine1	Vestas V80 model	60.0	596974.6	7597095.5	0.0
Turbine2	Vestas V80 model	60.0	596474.8	7599123.5	0.0
Turbine3	Vestas V80 model	60.0	602133.1	7597573.5	37.8
Turbine4	Vestas V80 model	60.0	602336.6	7597886.0	43.8
Turbine5	Vestas V80 model	60.0	602977.2	7597635.5	39.9
Turbine6	Vestas V80 model	60.0	604911.6	7599721.0	231.0
Turbine7	Vestas V80 model	60.0	604893.0	7599407.5	212.1
Turbine8	Vestas V80 model	60.0	605190.3	7599191.5	246.4
Turbine9	Vestas V80 model	60.0	605512.8	7599552.5	280.1
Turbine10	Vestas V80 model	60.0	605185.6	7599556.5	248.7
Turbine11	Vestas V80 model	60.0	603077.7	7597880.0	67.6
Turbine12	Vestas V80 model	60.0	602857.6	7597601.0	29.6
Turbine13	Vestas V80 model	60.0	607605.4	7599660.5	395.5
Turbine14	Vestas V80 model	60.0	605634.8	7601654.5	385.3
Turbine15	Vestas V80 model	60.0	606077.6	7604479.5	249.5
Turbine16	Vestas V80 model	60.0	609142.9	7604358.5	474.3
Turbine17	Vestas V80 model	60.0	608839.6	7601960.0	517.3
Turbine18	Vestas V80 model	60.0	608601.4	7599013.5	458.2
Turbine19	Vestas V80 model	60.0	602175.0	7597444.0	32.3
Turbine20	Vestas V80 model	60.0	602992.1	7597559.5	32.4
Turbine21	Vestas V80 model	60.0	603919.9	7597684.5	27.4
Turbine22	Vestas V80 model	60.0	603004.2	7598195.0	68.6
Turbine23	Vestas V80 model	60.0	603080.2	7597744.0	55.1
Turbine24	Vestas V80 model	60.0	603125.8	7597162.5	0.0
Turbine25	Vestas V80 model	60.0	603133.9	7596698.0	0.0
Turbine26	Vestas V80 model	60.0	602948.8	7596371.0	0.0
Turbine27	Vestas V80 model	60.0	603688.1	7596454.0	0.0
Turbine28	Vestas V80 model	60.0	603176.9	7595662.0	1.4
Turbine29	Vestas V80 model	60.0	603673.4	7595827.0	5.9
Turbine30	Vestas V80 model	60.0	602831.1	7597631.5	30.0
Turbine31	Vestas V80 model	60.0	603613.2	7597687.0	25.4

Table 4-9: *Turbine names, types, and positions*

The first simulation process in identifying suitable sites was conducted in 31 different locations using a wind turbine Vestas V80 model with a rotor diameter of 80m and a hub height of 60m, as shown in table 4-8. Table 4-9 displays the location of each wind turbine as generated from the WindSim word report. The geographical coordinates of the locations were chosen using

google maps and google earth with wind resource maps as the guide to finding the grounds with higher wind speeds.

The actual ground locations of the wind turbines are as shown in figure 4-15 as generated in the satellite google maps display of the object module.

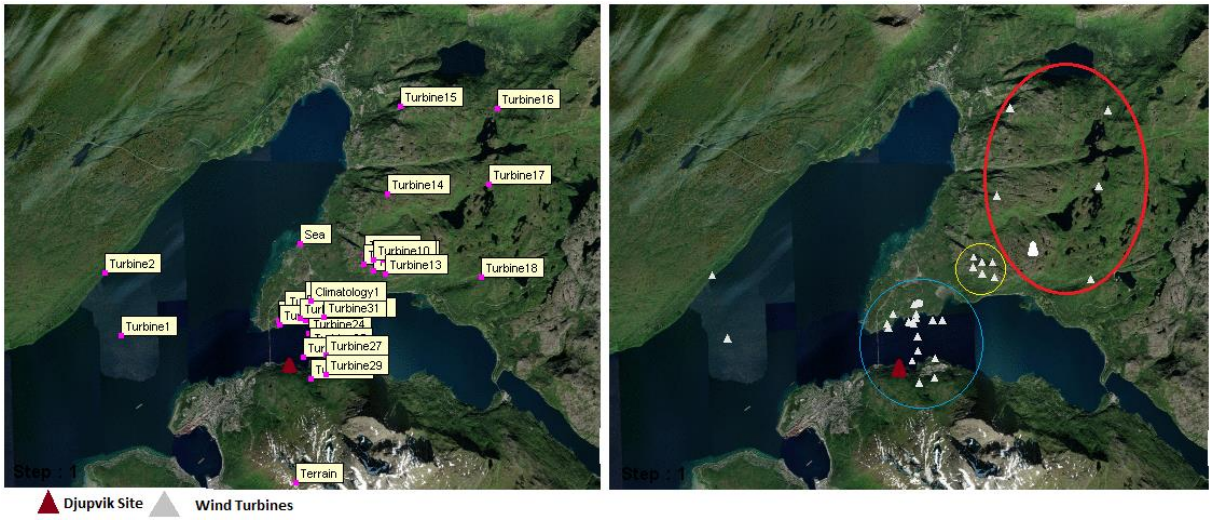

Figure 4-15: *Showing the digital wind turbines locations on a satellite map around Narvik.*

The very first simulation was on a trial-and-error basis punctuated with a lot of errors. In contrast, the succeeding simulations showed elements of improvement. Given the hydrogen site in Djupvik is at the foot of a mountainous area with thick vegetation cover, wind resource simulation of any location nearest to the site encountered unsolvable errors, which hindered complete simulation of the six modules.

To continue with the subsequent simulations in order to find the final suitable location for wind turbine siting, a wind resource map in figure 4-16 was studied to assist in making decisions of the areas with relatively higher wind speed and omitting the areas with lower wind speed. The wind resource maps were generated from the WindSim program modelling report. As can be observed, wind speed around the area where the hydrogen site is situated is deficient. This prompted an investigation into the surrounding areas with relatively promising wind speeds for further experimentation until an appropriate location was selected.

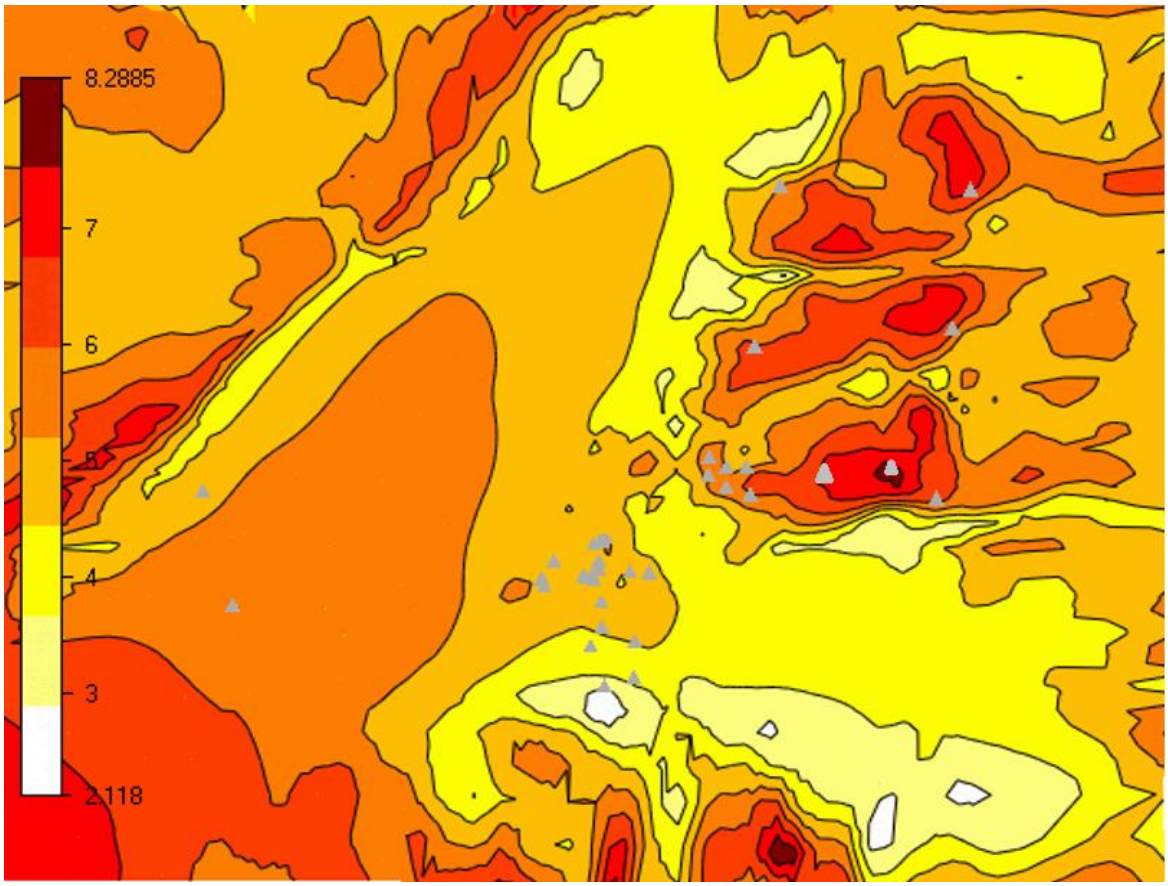

Figure 4-16: *Showing the wind resource map generated from the WindSim report for Djupvik.*

After completing the simulation with disregarded wake losses, every wind turbine's resultant average wind speed outcome was generated as summarised in table 4-10. Disregarding wake losses was on the assumption that every wind turbine would experience optimum wind speed at their points of simulation, and the location with a higher wind speed would be suitable for selection.

The findings of the first simulation showed that even though wake loss effects were disregarded, it was possible to conclude that wind turbines that were suitably spaced in location modelling experienced more incredible average wind speed than those closely packed. This could explain why turbines 1, 14, 16, 17, and 18 had much higher wind speeds than the rest based on figures 4-15, 4-16, and table 4-10 results. The demerit of those locations is that they are far much away from the specified Djupvik site. It is worth noting that turbines 6, 7, 8, 10, 11, and 13 had above average wind speed results despite being closely packed. This prompted further investigation on such locations since they are much closer to the site and they showed promising results in term of average wind speed.

Turbine name	Turbine type	Air density (kg/m^3)	Average wind speed (m/s)	Wake Losses (%)	Total load hours (hours)
Turbine1	Vestas V80 model	1.225	**5.650**	n.a	1710.650
Turbine2	Vestas V80 model	1.225	**5.020**	n.a	1311.900
Turbine3	Vestas V80 model	1.225	**4.900**	n.a	1207.400
Turbine4	Vestas V80 model	1.225	**4.790**	n.a	1130.000
Turbine5	Vestas V80 model	1.225	**4.820**	n.a	1167.800
Turbine6	Vestas V80 model	1.225	**5.460**	n.a	1546.100
Turbine7	Vestas V80 model	1.225	**5.280**	n.a	1433.350
Turbine8	Vestas V80 model	1.225	**5.570**	n.a	1652.300
Turbine9	Vestas V80 model	1.225	**4.960**	n.a	1230.900
Turbine10	Vestas V80 model	1.225	**5.160**	n.a	1352.300
Turbine11	Vestas V80 model	1.225	**5.100**	n.a	1326.250
Turbine12	Vestas V80 model	1.225	**4.630**	n.a	1046.800
Turbine13	Vestas V80 model	1.225	**5.960**	n.a	1926.450
Turbine14	Vestas V80 model	1.225	**6.070**	n.a	1970.000
Turbine15	Vestas V80 model	1.225	**5.210**	n.a	1390.550
Turbine16	Vestas V80 model	1.225	**6.820**	n.a	2532.700
Turbine17	Vestas V80 model	1.225	**6.500**	n.a	2303.100
Turbine18	Vestas V80 model	1.225	**6.380**	n.a	2207.050
Turbine19	Vestas V80 model	1.225	**4.880**	n.a	1187.600
Turbine20	Vestas V80 model	1.225	**4.780**	n.a	1142.450
Turbine21	Vestas V80 model	1.225	**4.720**	n.a	1092.250
Turbine22	Vestas V80 model	1.225	**4.920**	n.a	1201.050
Turbine23	Vestas V80 model	1.225	**5.000**	n.a	1268.000
Turbine24	Vestas V80 model	1.225	**4.530**	n.a	1016.850
Turbine25	Vestas V80 model	1.225	**4.500**	n.a	1007.850
Turbine26	Vestas V80 model	1.225	**4.310**	n.a	955.700
Turbine27	Vestas V80 model	1.225	**4.480**	n.a	1000.300
Turbine28	Vestas V80 model	1.225	**3.390**	n.a	592.450
Turbine29	Vestas V80 model	1.225	**3.950**	n.a	788.950
Turbine30	Vestas V80 model	1.225	**4.590**	n.a	1017.600
Turbine31	Vestas V80 model	1.225	**4.560**	n.a	1005.800

Table 4-10: *Annual energy production based on average wind speed per wind turbine*

The second simulation was conducted using the exact wind turbine specifications as above but with a reduced number of wind turbine location experimentation. This time around, the selected locations were much closer to the site, and the turbine spacing was more expansive than in the first modelling experiment. Tables 4-11 and 4-12 show the results of average wind speed and full load operational capacity of the turbines obtained at constant air density with wake losses disregarded in this particular stage.

Turbine Type	Hub Height (m)	No. of turbines	Capacity (MW)	Gross AEP (GWh/y)	Average wind speed (m/s)	Wake losses (%)	Full load hours (hours)	Capacity factor (%)
Vestas V80 model	60.0	15	30.0	87.3	**9.1**	n.a.	2911.0	33.2

Table 4-11: *Illustration of wind farm and production characteristics*

Turbine name	Turbine type	Air density (kg/m3)	Average wind speed (m/s)	Gross AEP (GWh/y)	Wake Losses (%)	Full load hours (hours)	Easting Location	Northing location	Z
Turbine1	Vestas V80	1.225	**8.460**	6.226	n.a	3113.0	602133.1	7597573.5	38.2
Turbine2	Vestas V80	1.225	**8.860**	6.880	n.a	3440.2	603169.8	7596222.0	82.3
Turbine3	Vestas V80	1.225	**8.300**	6.209	n.a	3104.75	602336.6	7597886.0	41.2
Turbine4	Vestas V80	1.225	**7.510**	5.697	n.a	2848.35	602977.2	7597635.5	34.4
Turbine5	Vestas V80	1.225	**10.640**	6.840	n.a	3454.25	607605.4	7599660.5	548
Turbine6	Vestas V80	1.225	**6.280**	4.280	n.a	2139.75	603582.0	7596662.5	0.0
Turbine7	Vestas V80	1.225	**5.080**	2.604	n.a	1301.85	604860.2	7596357.0	0.0
Turbine8	Vestas V80	1.225	**10.590**	6.232	n.a	3115.90	597742.1	7597306.5	0.0
Turbine9	Vestas V80	1.225	**10.020**	5.675	n.a	2837.50	594278.1	7597308.5	0.0
Turbine10	Vestas V80	1.225	**9.980**	5.639	n.a	2819.35	595224.1	7598422.5	0.0
Turbine11	Vestas V80	1.225	**10.840**	6.454	n.a	3227.00	596034.4	7597330.5	0.0
Turbine12	Vestas V80	1.225	**10.630**	6.185	n.a	3092.65	598320.8	7596588.0	0.0
Turbine13	Vestas V80	1.225	**10.930**	6.453	n.a	3226.60	597985.2	7595688.5	0.0
Turbine14	Vestas V80	1.225	**10.160**	5.822	n.a	2910.95	600178.9	7598176.0	0.0
Turbine15	Vestas V80	1.225	**10.420**	6.095	n.a	3047.50	597705.6	7598457.0	0.0

Table 4-12: *Analysis of average wind speed, gross AEP, and operational capacity per turbine*

The eastings and northings locations information contained in table 4-12 describe the exact siting locations on which the turbines should be fixed if the choice was made to fix them, which is well captured in figure 4-17. The Z coordinates are the elevation above ground level. From the information generated, it is observable that only Turbine numbers 1 to 5 are located onshore, and the rest are either on the sea or a few metres from the sea.

The information in figure 4-17 indicate that turbines were uniformly distributed on either side of the production site with eight turbines located to the west, i.e., turbine numbers 8, 9, 10, 11, 12, 13, 14, and 15, while seven turbines situated on the eastern side, i.e., turbines 1, 2, 3, 4, 5, 6, and 7. It can be observed that turbines located on the western side may operate on much higher average wind speed compared to those on the eastern side as indicated in table 4-12. All turbines from number 8 to 15 each operate on an average wind speed of more than 10m/s with the exception of turbine number 10 that had 9.98m/s operational wind speed. On the other hand, turbines 1 to 7 operate on lower wind speed with the highest average wind speed experienced by turbines 2 and 5. This could be summarised that the western side of the Djupvik site experiences much higher wind speed than the eastern part.

If a decision was to be made only based on the average wind speed, then the suitable site location would have been on the western side. However, other factors came into play. For instance, all the turbines on the west side were distant from the Djupvik site despite experiencing higher wind speeds. Another factor that was keenly observed was the operational full load hours. Turbines 2 and 5, despite operating at much lower average wind speed than

their counterparts on the western side, they had much higher operational full load hours making over 39.27% capacity factor compared to the average of 33.2%. This indicated that if a wind turbine was located at 2 or 5, then despite lower wind speed, the turbine would operate for a much more extended period at full capacity in a year, translating to higher gross AEP. Therefore, basing the argument on the full load hour operation and the resultant gross AEP output, locating turbines on the eastern side of the site would be a suitable venture.

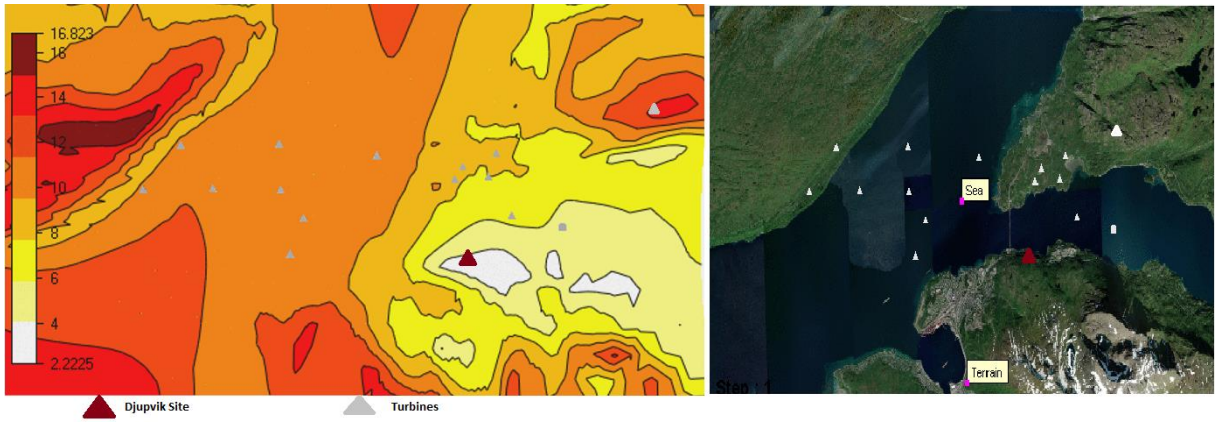

Figure 4-17: *Wind resource map (left) and wind turbines location information (right)*

Because of the two antagonistic sides, further probes would be a better option. A narrower approach with reduced number of turbine locations selected, and wake effects were considered. In the subsequent trials, turbines 1 to 5 on the eastern side of Djupvik site were further modelled separately, and those on the western side, i.e., turbine locations 8 to 15, were modelled separately.

The ensuing modelling process considered the best locations in the preceding simulation process where the best three turbines locations in the eastern part and the best four turbines' locations on the western side were subjected to further analysis. The outcome is as shown in tables 4-14 and 4-16. The wind turbine specifications and models remained unchanged, and wake model 1 was selected. Modelling of eastern locations took turbine locations ***1, 2, 3*** in that order while western locations took locations ***8, 11, 12***, and ***13*** in the same order.

Turbine name	Turbine type	Hub height	Easting	Northing	z
Turbine 1	Vestas V80 model	60.0	602133.1	7597573.5	38.9
Turbine 2	Vestas V80 model	60.0	**603169.8**	**7598222.0**	87.7
Turbine 3	Vestas V80 model	60.0	**607605.4**	**7599660.5**	542.3

Table 4-13: *showing virtual wind turbine locations (eastern side of Djupvik site)*

Turbine name	Turbine type	Air density (kg/m3)	Average wind speed (m/s)	Gross AEP (GWh/y)	Wake Losses (%)	AEP with wake losses (GWh/y)	Full load hours (hours)
Turbine1	Vestas V80 model	1.225	7.150	5.207	0.159	5.199	2599.400
Turbine2	Vestas V80 model	1.225	**8.620**	**6.883**	0.484	**6.850**	**3425.050**
Turbine3	Vestas V80 model	1.225	**10.290**	**7.414**	1.837	**7.312**	**3506.250**

Table 4-14: *Modelled outcomes of the turbines' locations on the Eastern side of the Djupvik site*

Table 4-14 shows that turbine locations ***2*** and ***3*** maintained relatively similar outcomes in the new simulation model as compared to the outcome of the immediate preceding trial. Equally, in table 4-16 below, the turbines ***2*** and ***4*** locations maintained higher average wind speed with lower percentage wake losses as well as relatively stable operational full load hour capacity. As a result, the four locations were subjected to a joint final simulation run.

Turbine name	Turbine type	Hub height	Easting	Northing	z
Turbine1	Vestas V80 model	60.0	597742.1	7597306.0	0.0
Turbine2	Vestas V80 model	60.0	**596034.4**	**7597330.5**	0.0
Turbine3	Vestas V80 model	60.0	598320.8	7596588.0	0.0
Turbine4	Vestas V80 model	60.0	**597985.2**	**7595688.5**	0.0

Table 4-15: *Showing virtual wind turbines' locations on the Western side of Djupvik site*

Turbine name	Turbine type	Air density (kg/m3)	Average wind speed (m/s)	Gross AEP (GWh/y)	Wake Losses (%)	AEP with wake losses (GWh/y)	Full load hours (hours)
Turbine 1	Vestas V80 model	1.225	9.830	6.380	1.368	6.293	3146.60
Turbine 2	Vestas V80 model	1.225	**10.060**	**6.566**	**0.184**	**6.554**	**3277.05**
Turbine 3	Vestas V80 model	1.225	9.910	6.387	0.396	6.362	3180.95
Turbine 4	Vestas V80 model	1.225	**10.210**	**6.731**	0.201	**6.718**	**3358.90**

Table 4-16: *Modelled outcomes of the turbines' locations on the western side of the Djupvik site*

The final modelling process in this section involved selecting turbine location **2** and **3** in table 4-13 and locations **2** and **4** in table 4-15 then conducting a series of simulation experiments with three different wind turbine types at different hub heights to find the overall best location choice, suitable wind turbine type and optimal production hub height. Table 4-17 shows the exact locations of the proposed turbine locations for further WindSim modelling experiments.

Proposed Turbines locations	Easting	Northing	Longitude (°E)	Latitude (°N)
Turbine 1	597985.2	7595688.5	17.391589	68.456721
Turbine 2	603169.8	7598222.0	17.520513	68.477569
Turbine 3	596034.4	7597330.5	17.345550	68.472108
Turbine 4	607605.4	7599660.5	17.630238	68.488794

Table 4-17: *Shows the geographical coordinates of the proposed wind turbines locations.*

The proposed turbine locations **1** and **3** are offshore, while locations **2** and **4** are onshore, as can be seen in figure 4-18, showing the geographical map with the exact proposed locations of the wind turbines. The proposed location 2 is much nearer to the Djupvik site based on the geographical distance than the rest. Table 4-18 shows the approximate distances of the four locations in reference to the Djupvik site and the elevation above sea levels.

Figure 4-18: *Shows the proposed wind turbines geographical locations*

Proposed Wind Turbine Location	ApproximateDistance to Djupvik Site (m)	Height above sea level, z (m)
1	5400.18	0.0
2	3245.36	84.3
3	7671.83	0.0
4	6326.76	597.6

Table 4-18: *Distances of proposed wind turbine locations from the hydrogen production site.*

Further analysis and simulations were conducted to find the most suitable location of all and the appropriate wind turbine model that could give an optimal yield of annual energy production. As a result, the four locations were taken into several rounds of WindSim modelling

experiments using three kinds of wind turbines described in section 4.2 above and at different hub heights, and thereafter results were analysed. For a start, three different hub heights were used for experimentation and comparison, i.e., 50m, 60m, and 80m.

4.4 Local wind climatology CFD Simulation

The average wind condition of Narvik and its environs was used to calibrate the wind resources and in the Annual Energy Production estimation. A wind climatology is presented as a wind rose, showing the average wind speed distribution velocity intervals called bins and wind directions called sectors [57]. The simulation was preset at 50 bins and 12 sectors. The 12 sectors are divisions of the incoming wind directions where the first sector is centered on the geographical north as the reference point of measurement. The original wind speed data is divided into one meter per second bins, and the frequency distribution is fitted to a Weibull distribution.

According to wind climatology characteristics of Narvik city and its surrounding, the average wind speed is about 5.07m/s at the height of 50m as can be seen in table 4-19 and counter confirmed by the wind rose in figure 4-19. The average wind speed at every sector for all the sectors used in every simulation process of CFD modelling is summarized in table 4-20.

Climatology: Narvik_50m

Filename	Narvik_50m		
Period, # records	01/01/1980 00:00 - 22/03/2014 23:00	300000	
Position: easting, northing, z (agl)	604860.2	7596357.0	50.0
Average wind speed, Weibull k, A	5.07	1.65	5.45

Table 4-19: *Climatology characteristics including average wind speed (m/s) for all sectors, Weibull shape (k), and scale (A) parameters for all sectors.*

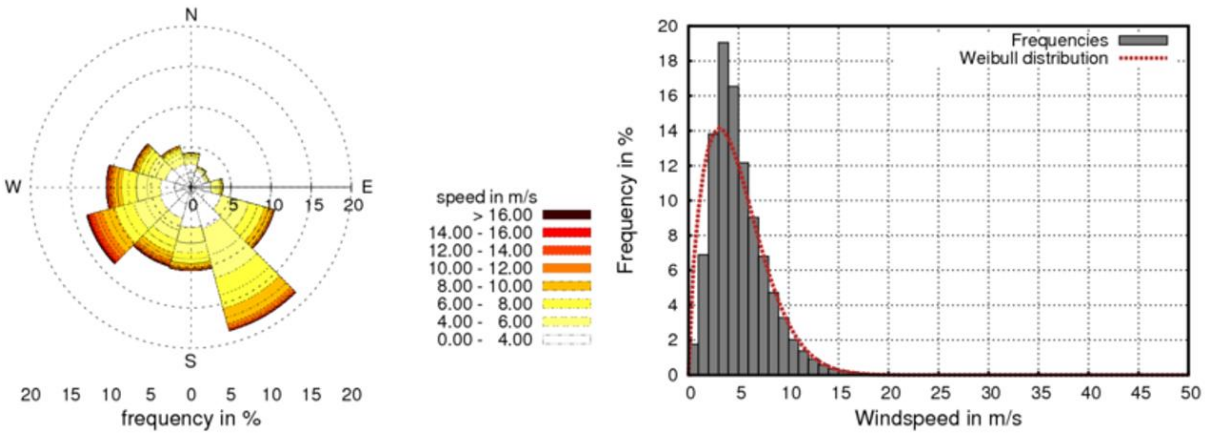

Figure 4-19: *Wind rose (left) and frequency distribution with Weibull fitting (right) for all sectors.*

Sectors	1	2	3	4	5	6	7	8	9	10	11	12
Average wind speed (m/s)	3.61	3.00	3.01	3.75	5.12	5.56	4.59	5.36	6.28	5.52	4.84	4.14
Frequency (%)	4.25	2.69	2.39	3.97	10.79	18.46	10.37	10.18	13.45	10.55	7.60	5.30
Weibull shape, k	1.79	1.92	1.84	1.98	1.98	2.04	1.70	1.66	1.72	1.68	1.82	1.70
Weibull scale, A	3.99	3.37	3.34	4.16	5.60	6.11	4.90	5.79	6.86	5.98	5.34	4.48

Table 4-20: *Average wind speed, frequency, and Weibull shape (k) and scale (A) parameters versus sectors*

A numerical wind database is established by CFD simulations for areas under study using the WindSim program. The numerical wind database is used to transfer the wind conditions from the measurement point to the wind turbine hub height positions. Three different turbines were selected for use in this project as earlier mentioned, and at different hub heights of 50m, 60m, and 80m to help in establishing a single suitable location for siting the wind turbine for power generation. A digital terrain model containing elevation and roughness data was generated for the area, as shown in figure 4-20. However, it was noted that the underlying datasets for elevation and roughness had different resolutions.

The coordinate system applied was UTM, Zone: 33, Datum: WGS84 and this is the coordinate system referred to whenever coordinates are used in WindSim reporting. The following online sources were used for elevation: ASTER GDEM v2 Worldwide Elevation Data (1 arc-second Resolution) and for roughness: CORINE Land Cover Europe 2006 (100 m Resolution).

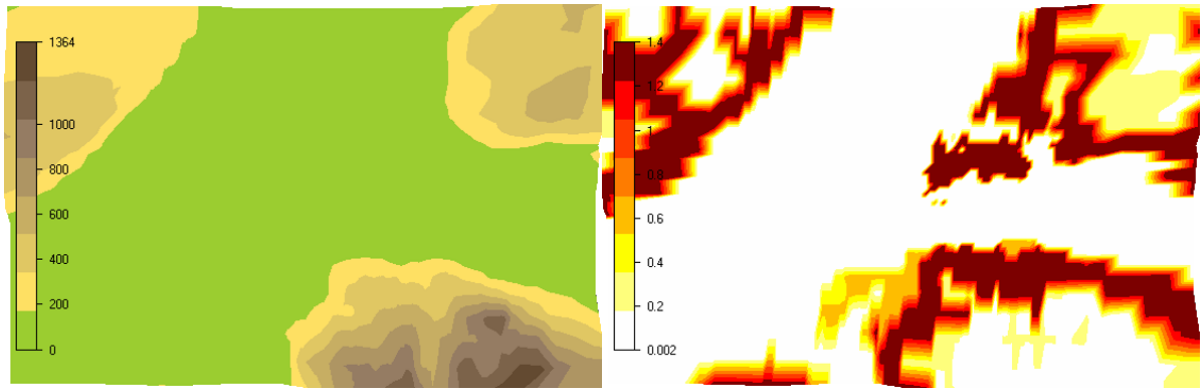

Figure 4-20: *Terrain elevation (m) (left) and roughness (m) (right)*

The complexity at the site depends on the changes in elevation and roughness. The complexity in elevation is visualized by the inclination angles, which is a derived quantity expressing the first-order derivatives of the elevation. Figure 4-21 shows the terrain inclination of the area. Caution was taken not to establish turbines at complex terrains with high roughness factors.

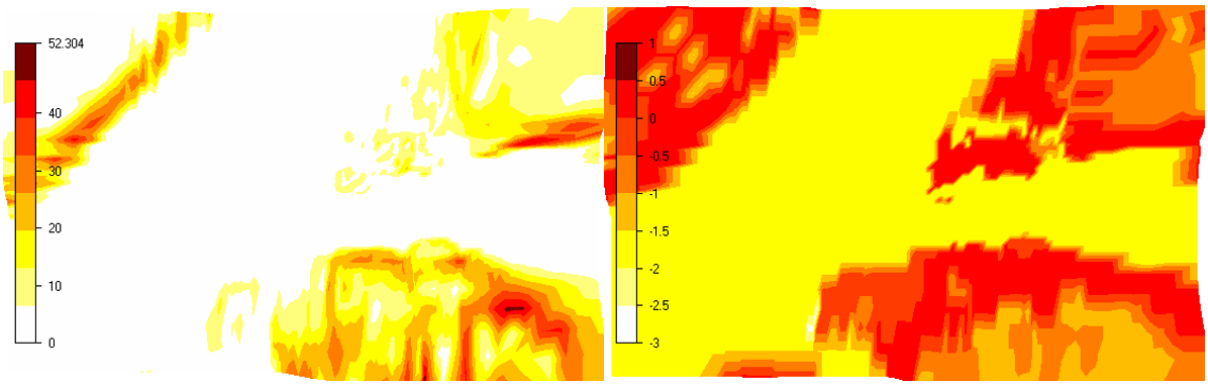

Figure 4-21: *Terrain inclination (deg) (left) and logarithmic roughness (m) (right)*

The digital simulation model represents the computational domain where the Reynolds averaged Navier – Stoke equations have been numerically solved. A total of 12 simulations were performed to have a 3D wind field for every 30-degree sector. The simulation solver setting used is as given in table 4-21.

Height of boundary layer (m)	500.0
Speed above the boundary layer (m/s)	10.0
The boundary condition at the top	fix pres.
Potential temperature	No
Turbulence model	Standard
Solver	GCV
Maximum iterations	500

Table 4-21: *Solver settings for simulation*

4.5 CFD Simulation Findings and Results

Having looked at the local wind climatology of Narvik area and identified the solver settings of the CFD simulation, the step that followed was a joint wind flow modelling of the four sites identified in section 4.3 for further analysis. Three different wind turbine models were applied at varying hub heights and the results were generated in a WindSim word report. The results generated were wind resource maps, and Annual Energy Production (AEP) table.

The wind resource maps, and AEP are usually generated in WindSim based on the long-term on-site wind conditions and CFD simulation results [57]. The wind resource map is used to identify the high wind speed area based on the average wind speed. The wind resource maps are established by comparing the CFD results against the expected average input conditions. If several climatologies are available, the wind resource maps are developed based on them all by comparing the inverse radial distance to each climatology.

Therefore, figures 4-22, 4-23, and 4-24 show the wind resource maps that were generated after CFD simulations of the four identified sites using wind turbines V80, G52, and G58 models at hub heights of 50m, 60m, and 80m, respectively. The wind resource maps indicate wind flow patterns of the surrounding area with variations in average wind speeds.

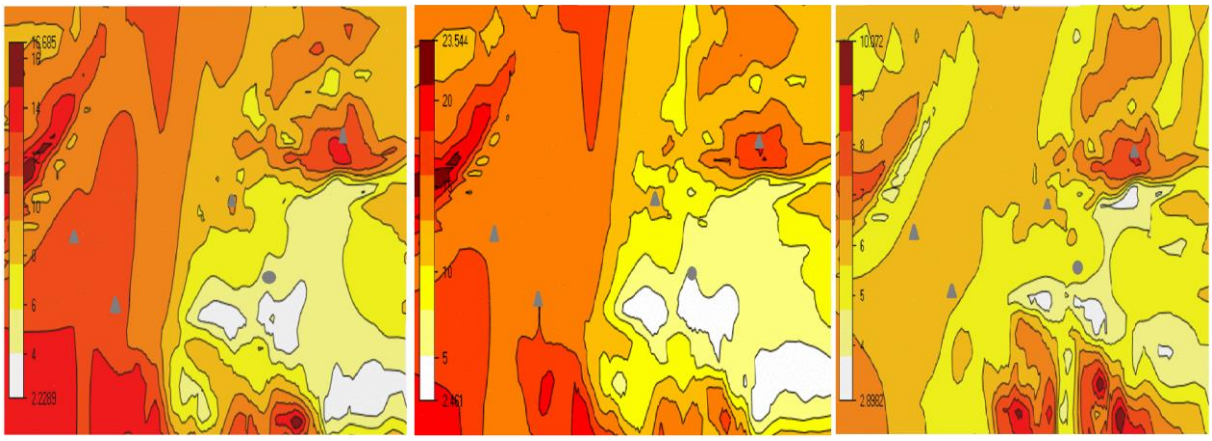

Figure 4-22: *The generated wind resource maps with average wind speed (m/s) using Vestas V80 model at hub heights of 50, 60, and 80 meters. Triangle: wind turbines, Dot: climatology.*

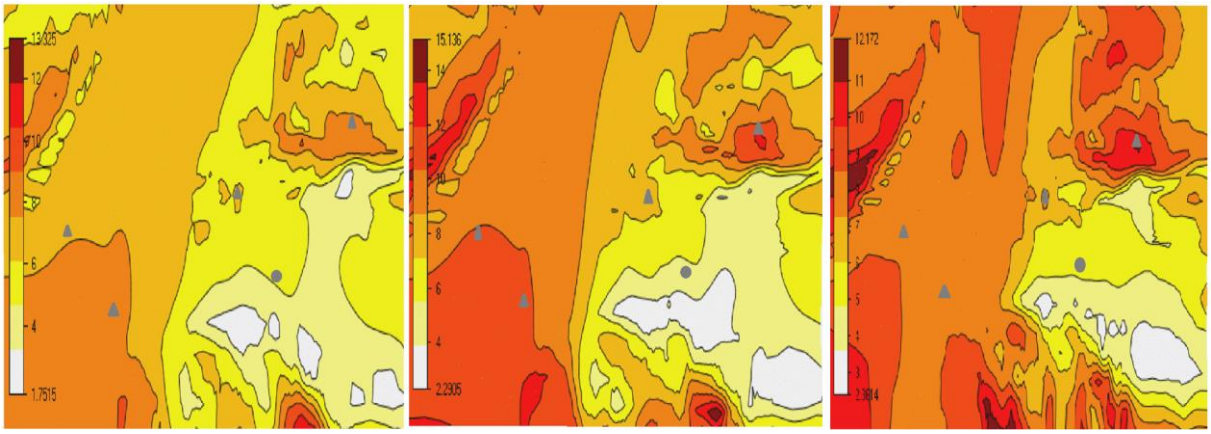

Figure 4-23: *The generated wind resource maps with average wind speed using Gamesa G52 model at hub heights of 50, 60, and 80 meters. Triangle: wind turbines, Dot: climatology.*

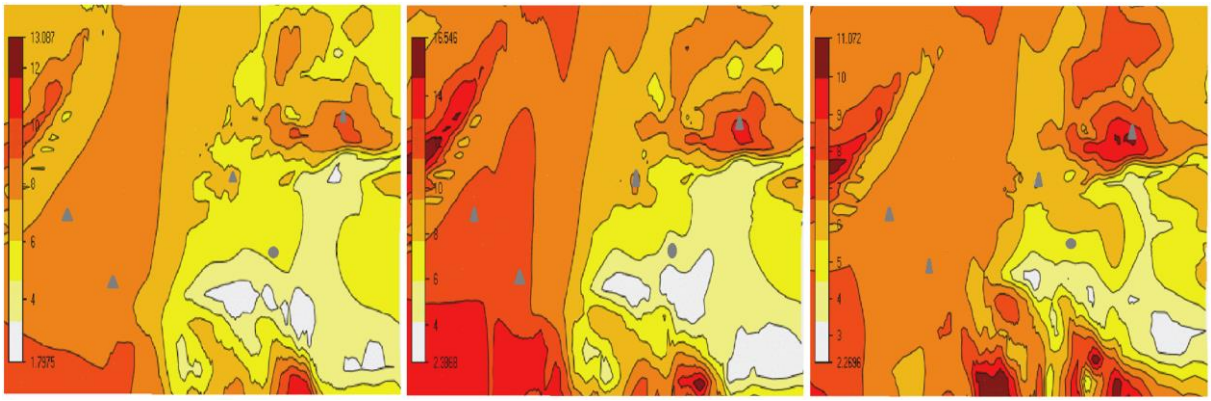

Figure 4-24: *The generated wind resource maps with average wind speeds using Gamesa G58 model at hub heights of 50, 60, and 80 meters. Triangle: wind turbines, Dot: climatology.*

The analysis of wind resource maps in figures 4-22, 4-23, and 4-24 show one significant observation that the average wind speed was lowest around the site where the hydrogen refueling unit is located and therefore siting a wind turbine nearest to the area would experience lowest wind speed thus minimal AEP output. Therefore, a search for a suitable wind turbine location considered areas with higher wind speeds and nearest to the hydrogen refueling site.

Another resultant outcome of the CFD simulation was the gross and net AEP results. The gross AEP is the wind farm's energy production calculated by predicting free stream wind speed distribution at the hub height of each turbine location and the turbine's power curve information provided by the manufacturers [31]. The free stream wind speed distribution is obtained by the WindSim flow model and the long-term on-site wind conditions.

Given that wind turbines extract energy from the wind, as a result, wind speed downstream from the wind turbine is therefore reduced. This is called the wake effect and as the flow proceeds further, the wake is spread in a descending pattern until normal free stream conditions are recovered [30]. The potential net AEP is obtained by taking into account the wake losses. The WindSim wake models calculate the wake effect of every wind turbine and eventually the net AEP is generated.

Tables 4-22, 4-23, and 4-24, shows the CFD simulation findings of gross AEP, net AEP, and wind turbine's operational hours at the four identified sites with three different turbine models hoisted at varying heights. The results were for vestas V80, gamesa G58, and G52, respectively.

VESTAS V80-2.0MW MODEL							
Hub Heights (m)	Turbine Locations	Average wind speed (m/s)	Gross AEP (GWh/y)	Wake Losses (%)	Net AEP (with wake losses) (GWh/y)	Full load hours (hours)	Capacity Factor (%)
50	1	12.210	7.265	0.023	7.263	3631.500	41.46
	2	9.780	7.442	0.000	7.442	3721.150	**42.48**
	3	12.070	7.204	0.099	7.197	3598.650	41.08
	4	12.070	8.691	0.000	8.691	4345.450	**49.61**
60	1	15.550	5.526	0.033	5.525	2762.300	31.53
	2	11.680	6.587	0.000	6.587	3293.550	**37.60**
	3	15.090	5.504	0.120	5.498	2748.900	31.38
	4	17.640	7.166	0.000	7.166	3583.100	**40.90**
80	1	5.750	3.457	0.006	3.457	1728.650	19.73
	2	6.430	4.431	0.000	4.431	2215.300	**25.29**
	3	5.810	3.530	0.108	3.526	1763.000	20.13
	4	8.230	6.681	0.000	6.681	3340.550	**38.13**

Table 4-22: *Simulation results of proposed locations using Vestas V80 wind turbine model.*

GAMESA G58-850KW MODEL							
Hub Heights (m)	Turbine Locations	Average wind speed (m/s)	Gross AEP (GWh/y)	Wake Losses (%)	Net AEP (with wake losses) (GWh/y)	Full load hours (hours)	Capacity Factor (%)
50	1	8.290	2.801	0.025	2.800	3294.000	**37.60**
	2	6.770	2.127	0.000	2.127	2502.471	28.57
	3	7.920	2.646	0.038	2.645	3111.647	35.52
	4	9.170	3.421	0.000	3.421	4024.588	**45.94**
60	1	12.130	3.084	0.016	3.083	3627.529	41.41
	2	9.760	3.337	0.000	3.337	3925.765	**44.82**
	3	11.950	3.001	0.047	2.999	3528.470	40.28
	4	13.330	3.774	0.000	3.774	4439.529	**50.68**
80	1	7.100	2.561	0.020	2.561	3012.823	**34.39**
	2	6.680	2.312	0.000	2.312	2720.000	31.06
	3	7.100	2.516	0.099	2.514	2957.294	33.76
	4	9.930	3.826	0.000	3.826	4500.824	**51.38**

Table 4-23: *Simulation results of proposed locations using Gamesa G58 turbine model.*

GAMESA G52-850KW MODEL							
Hub Heights (m)	Turbine Locations	Average wind speed (m/s)	Gross AEP (GWh/y)	Wake Losses (%)	Net AEP (with wake losses) (GWh/y)	Full load hours (hours)	Capacity Factor (%)
50	1	7.850	2.305	0.017	2.305	2711.177	**30.95**
	2	6.410	1.681	0.000	1.681	1977.176	22.57
	3	7.440	2.099	0.019	2.099	2469.177	28.19
	4	8.510	2.765	0.000	2.765	3252.706	**37.13**
60	1	10.720	3.212	0.009	3.212	3778.588	43.13
	2	8.620	2.886	0.000	2.886	3395.765	38.76
	3	10.380	3.241	0.037	3.240	3812.000	**43.55**
	4	10.930	3.711	0.000	3.711	4365.529	**49.83**
80	1	8.280	2.687	0.015	2.686	3160.118	36.07
	2	7.580	2.502	0.000	2.502	2943.294	33.60
	3	8.280	2.707	0.074	2.705	3181.882	**36.32**
	4	10.720	3.674	0.000	3.674	4322.824	**49.35**

Table 4-24: *Simulation results of proposed locations using Gamesa G58 turbine model.*

4.6 Discussion of CFD Simulation Results

From the results obtained in tables 4-22, 4-23, and 4-24 above, the average wind speed, the gross AEP and the net AEP analysis at different hub heights for all the four locations is summarised in the form of comparative bar graphs as displayed in the figures 4-25 all the way to figure 4-30. Based on the findings above and subsequent analysis in figures 4-25, 4-26, and 4-27, the proposed location 4 depicted a region of relatively higher wind speed at varying heights. The region experienced the highest wind speed at a hub height of 60m, as shown by the results from all the three wind turbines used for modelling. Equally, locations 1, 2, and 3

had their best average wind speeds at a hub height of 60m, as shown by the results from all the three wind turbines used in the simulation experiments.

Average Wind Speeds Generated in Vestas V80 Wind Turbine Model			
Turbine Locations	Average Wind speed at 50m (m/s)	Average Wind speed at 60m (m/s)	Average Wind speed at 80m (m/s)
Location 1	12.21	15.55	5.75
Location 2	9.78	11.68	6.43
Location 3	12.07	15.09	5.81
Location 4	12.07	17.64	8.23
TOTAL	46.13	59.96	26.22

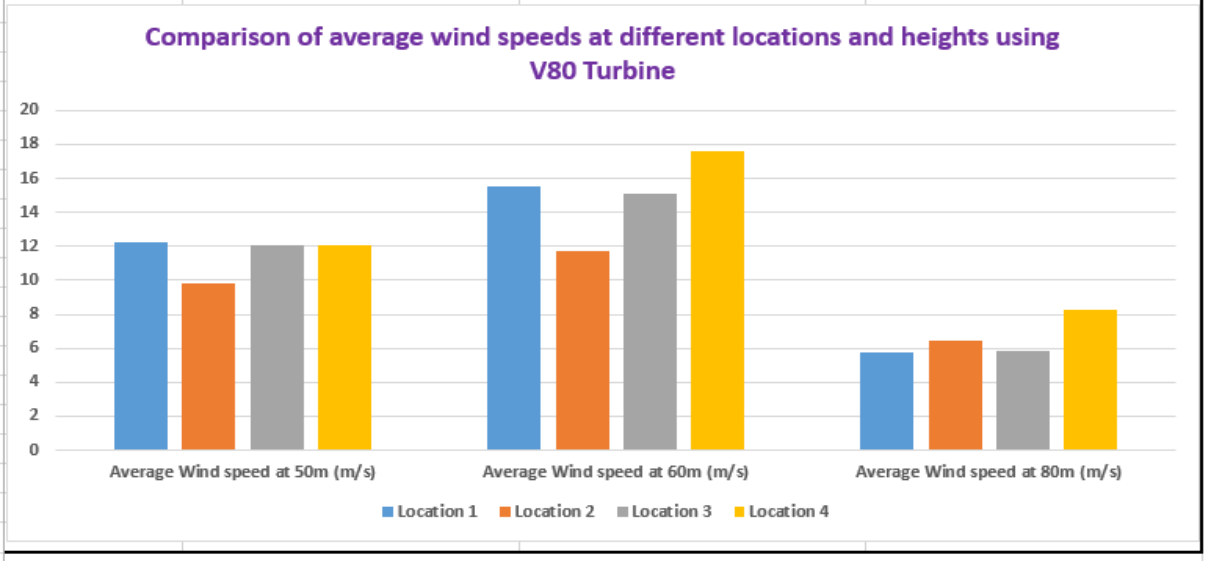

Figure 4-25: *Comparative graphs showing the simulated average wind speed of the proposed locations at varying heights using V80 model wind turbine.*

Average Wind speeds Generated in Gamesa G58 Wind Turbine Model			
Turbine Locations	Average Wind speed at 50m (m/s)	Average Wind speed at 60m (m/s)	Average Wind speed at 80m (m/s)
Location 1	8.29	12.13	7.1
Location 2	6.77	9.76	6.68
Location 3	7.92	11.95	7.1
Location 4	9.17	13.33	9.93
TOTAL	32.15	47.17	30.81

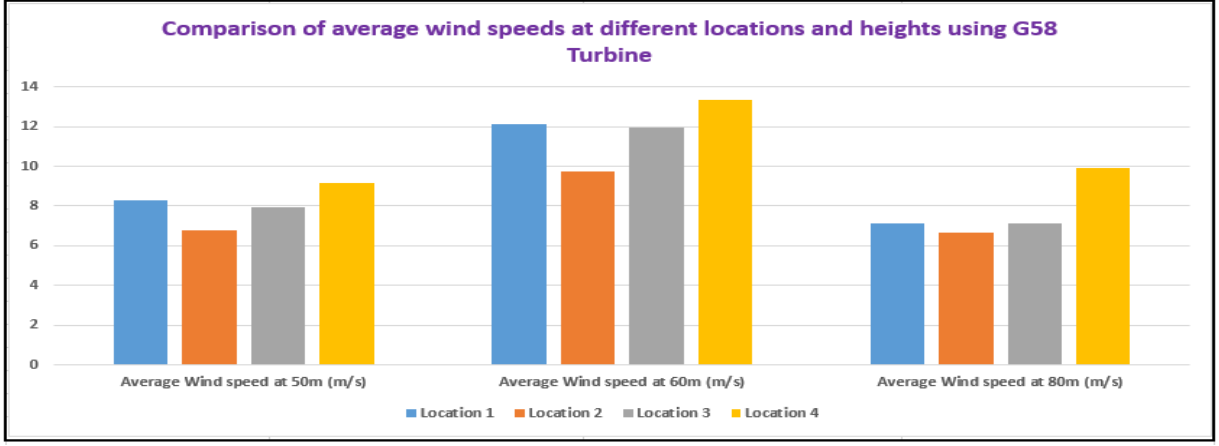

Figure 4-26: *Comparative graphs showing the simulated average wind speed of the proposed locations at varying heights using G58 model wind turbine.*

Average Wind speeds Generated in Gamesa G52 Wind Turbine Model			
Turbine Locations	Average Wind speed at 50m (m/s)	Average Wind speed at 60m (m/s)	Average Wind speed at 80m (m/s)
Location 1	7.85	10.72	8.28
Location 2	6.41	8.62	7.58
Location 3	7.44	10.38	8.28
Location 4	8.51	10.93	10.72
TOTAL	30.21	40.65	34.86

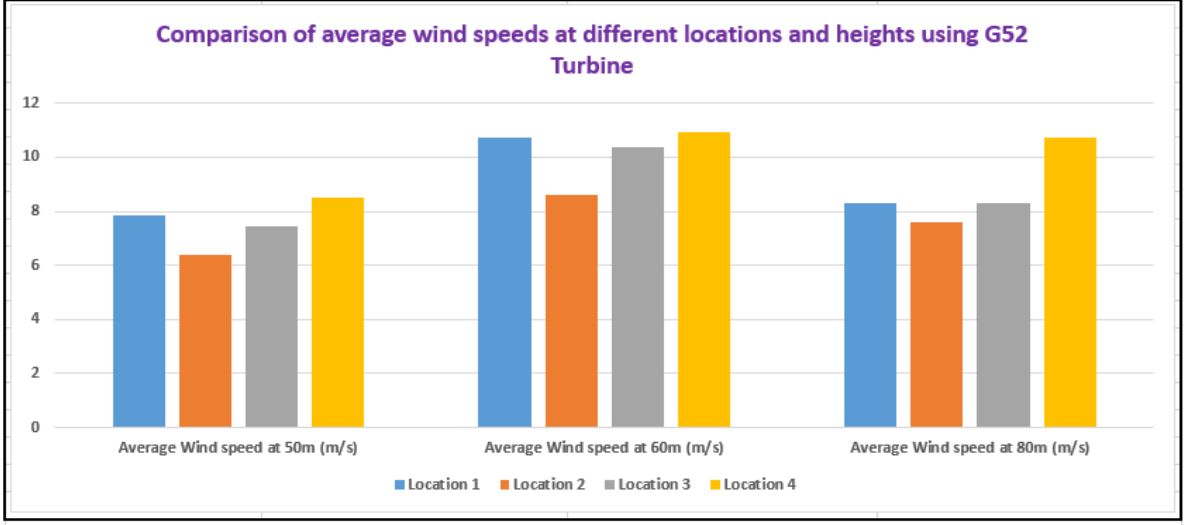

Figure 4-27: *Comparative graphs showing the simulated average wind speed of the proposed locations at varying heights using G52 model wind turbine.*

Similarly, the performance of the wind turbines in terms of full load hour capacity is also discussed. From the results, it can be observed that the wind turbine Vestas V80 model performance reduces with an increase in hub height whereby in all the proposed locations, the full load hours are highest at 50m height followed by 60m and then 80m. A further simulation of wind flow at 40m hub height of Vestas V80 turbine showed results much lower than those in 50m and 60m hub height for all the locations. However, the performance at 40m height was slightly higher than that of 80m height in all the proposed locations under investigation. An extended simulation analysis on hub height 70m showed an increasing trend in capacity factor. As a result, in choosing vestas V80 model, considerations were made into selecting the suitable height that would have optimal capacity factor. However, one could possibly conclude that vestas V80 model wind turbine would perform better at hub heights between 50m and 80m in the region based on the results from all the proposed locations. A further investigation on a broader range of hub heights relative to the net AEP performance is discussed in section 4.8.

Basing an argument on the results, the optimal average wind speeds in the region under study would be at hub heights of between 50m and 60m when Vestas V80 model turbine is sited, and any similar wind turbine sited at any particular height within that range will experience higher average wind speeds. However, this is not absolute since only three hub heights were selected for the purposes of finding the suitable location and wind turbine.

A similar trend is also showcased by the Gamesa models G58 and G52 wind turbines in CFD simulation whereby higher average wind speed was experienced at hub height 60m, and the difference was encountered in the analysis check of 50m and 80m heights. While G58 forecasted higher average wind speed at hub height 50m in all the proposed locations under investigation, G52 models exhibited contrary results. The G58 model set out almost similar results of average wind speed for all the proposed sites at hub heights 50m and 80m with some slight discrepancy in both results from every proposed location. The G52 model's average wind speed results showed that wind speed at 80m was relatively higher than at 50m hub height for all the proposed locations. Further probe of results at 40m and 70m suggested that both the wind turbine models G52 and G58 would operate optimally at any hub height between 50m and 75m in the region for which this study was performed with peak average wind speeds recorded at 60m height.

When the study changed gear to focus on net AEP analysis, the same trend experienced in the average wind speed analysis was detected. Figures 4-28, 4-29, and 4-30 illustrate some comparison of the net AEP values from the three wind turbine models virtually sited at the proposed locations at varying hub heights. Comparing the net AEP against the hub heights and wind turbine models in all the locations, the wind turbine Vestas V80 model displayed the best performance in terms of net AEP in all the locations and in all the hub heights as compared to the Gamesa models. In particular, it showed the highest net AEP at hub height of 50m, followed by 60m and then 80m with the optimal turbine site at locations 4 then 2, 1, and 3.

The Gamesa turbines G52 and G58 showcased relatively lower AEP values as compared to the vestas V80 model. The net AEP of Gamesa turbine models was about three times lower than that of the Vestas V80 model. This was assumed to mean that vestas V80 model wind turbines would perform in these locations far much greater than the Gamesa counterparts. In comparing the Gamesa models, the G58 model exhibited higher values of average net AEP and capacity factors in all the four proposed locations and varying hub heights compared to the G52 model.

Net AEP as Generated in Vestas V80 Wind Turbine Model Simulation			
Turbine Locations	Net AEP at 50m (GWh/y)	Net AEP at 60m (GWh/y)	Net AEP at 80m (GWh/y)
Location 1	7.263	5.525	3.457
Location 2	7.442	6.587	4.431
Location 3	7.197	5.498	3.526
Location 4	8.691	7.166	6.681
TOTAL	30.593	24.776	18.095

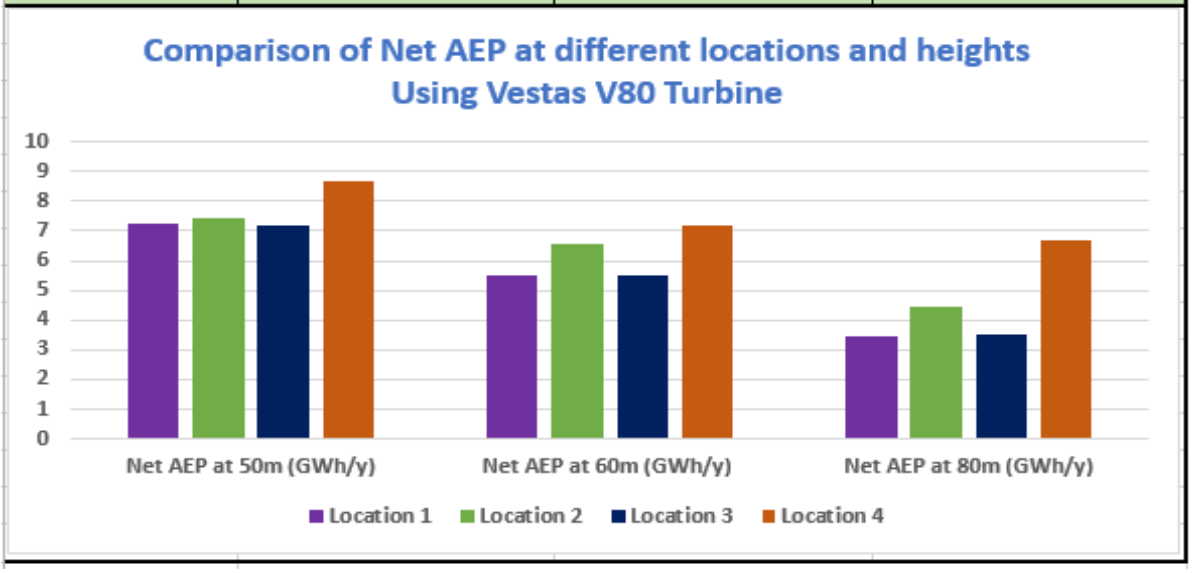

Figure 4-28: *Comparative graphs showing the simulated net AEP of the proposed locations at varying heights using V80 model wind turbine.*

Gamesa-G58 Wind Turbine Model			
Turbine Locations	Net AEP at 50m (GWh/y)	Net AEP at 60m (GWh/y)	Net AEP at 80m (GWh/y)
Location 1	2.8	3.084	2.561
Location 2	2.127	3.337	2.312
Location 3	2.646	2.999	2.514
Location 4	3.421	3.774	3.826
TOTAL	10.994	13.194	11.213

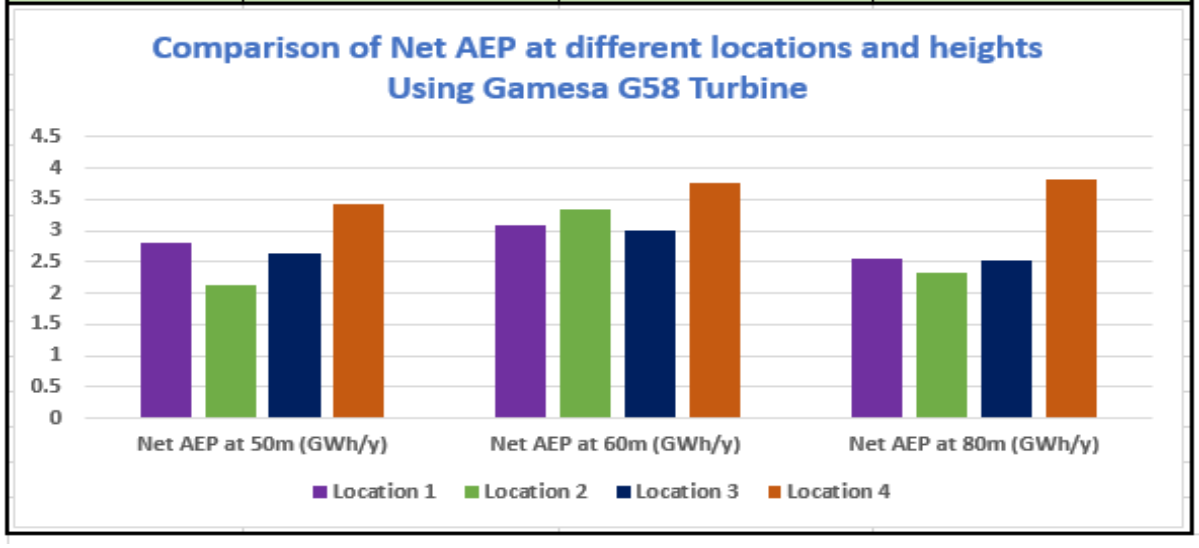

Figure 4-29: *Comparative graphs showing the simulated average wind speed of the proposed locations at varying heights using G58 model wind turbine.*

Net AEP as Generated in Gamesa-G52 Wind Turbine Model Simulation			
Turbine Locations	Net AEP at 50m (GWh/y)	Net AEP at 60m (GWh/y)	Net AEP at 80m (GWh/y)
Location 1	2.305	3.212	2.686
Location 2	1.681	2.886	2.502
Location 3	2.099	3.24	2.705
Location 4	2.765	3.711	3.674
TOTAL	8.85	13.049	11.567

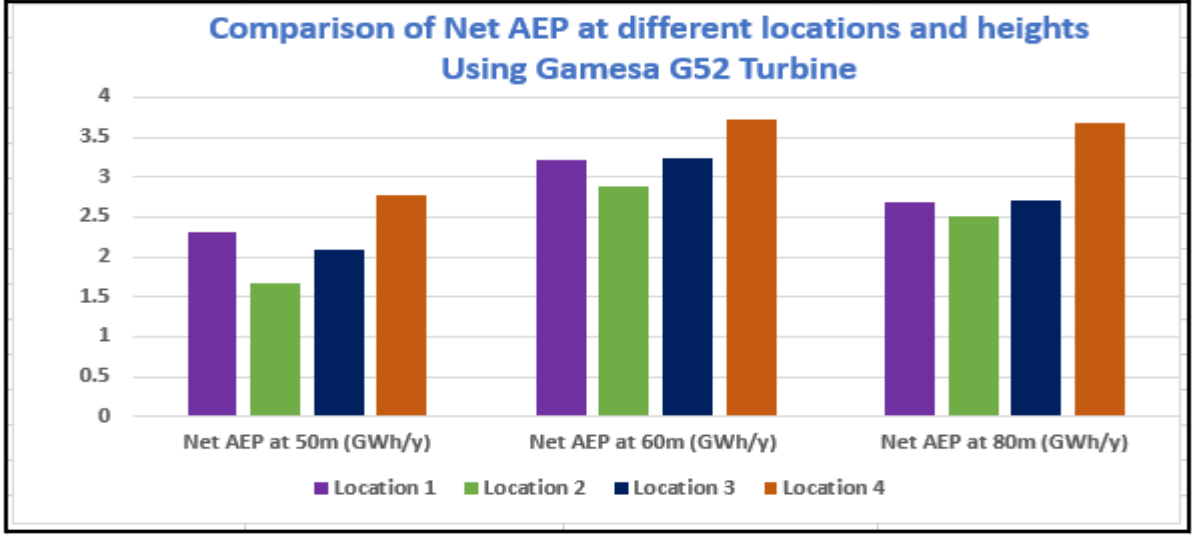

Figure 4-30: *Comparative graphs showing the simulated average wind speed of the proposed locations at varying heights using G52 model wind turbine.*

4.7 Proposal of Suitable Wind Turbine Siting Location

Based on the findings above and looking into all parameters of this project like the average wind speed, net AEP, the capacity factors as well as the distance from the hydrogen site, this study suggest that the most suitable spot for locating the wind turbine is location 2. Furthermore, this research recommends that the appropriate wind turbine model for the location is the Vestas V80 model hoisted at hub heights between 50m and 80m. Table 4-25 outlines the conclusive proposals for the wind turbine location site, wind turbine model, and operational hub heights.

The proposed wind turbine location	*Location **2** (68.477569°N, 17.520513°E)*
The proposed wind turbine model	*Vestas V80-2.0M model*
The Proposed hub height	*Between 50m-80m*

Table 4-25: *Proposals of the wind turbine siting location, type, and hub height range.*

The location was selected based on its nearness to the hydrogen refueling site, and also because it was onshore thereby wind turbine installation would be much cheaper and more accessible than the offshore locations. Location 2 also showed better net AEP potential with Vestas V80

model turbine at 50m and 60m hub heights only second to location 4. Location 4 would have been the most ideal for wind turbine siting based on findings above and given that it is onshore, but it was discovered that it is over 6.3km away from the proposed hydrogen production site compared to location 2, which was only 3.2km away. As a result, electrical power connectivity to the site would incur extra costs unnecessarily given that location 2 has the potential of producing more than enough net AEP for the hydrogen production. Consequently, in the event that power demand increases in future, this study suggests that an additional wind turbine be installed in location 4. So far, the power requirement for the hydrogen production site can be well served by production from a single vestas V80 model turbine at proposed location 2.

Proposed locations 1 and 3 were dropped on technical grounds that the locations are offshore. A lot of socio-economic activities like fishing and transport are taking place within the sea near Narvik hence installation of any turbine on the sea would cause unnecessary and unacceptable interferences. This is based on the site seeing field excursions taken around the proposed locations where the wind turbines were to be sited. Equally, the process of setting up the wind turbines offshore is much more tedious and costly than onshore installations, as elaborated by Stehly and Beiter of the US National Renewable Energy Laboratory (NREL) in their review article about the cost of wind energy in 2018 [58]. Besides, the factor of the newly built bridge connecting Bjerkvik and Narvik was considered in that connecting overhead power cables from the wind turbines located offshore would be much tedious and expensive across the bridge to the hydrogen site.

The choice of vestas V80 model wind turbine was purely on the net AEP output, operational full load hours, as well as the average wind speed, found from the simulation results of proposed location 2 as can be seen in figure 4-31. The figure 4-31 is a comparative analysis of simulation results using different wind turbine models compared on basis of the average wind speed and net AEP for the purpose of choosing appropriate turbine type for use in the proposed location. Moreover, the Vestas wind turbine models have a history of application in several wind farms around the arctic region more so in Scandinavia and, more specifically, Norway. Therefore, their performance in the area would be beyond reproach.

Wind Energy Generation Characteristics at Proposed location 2 at height 60m			
Parameters	Vestas V80 wind turbine Model	Gamesa G58 wind turbine Model	Gamesa G52 Wind turbine Model
Average Wind Speed (m/s)	11.68	9.76	8.62
Net AEP (GWh/y)	6.587	3.337	2.886

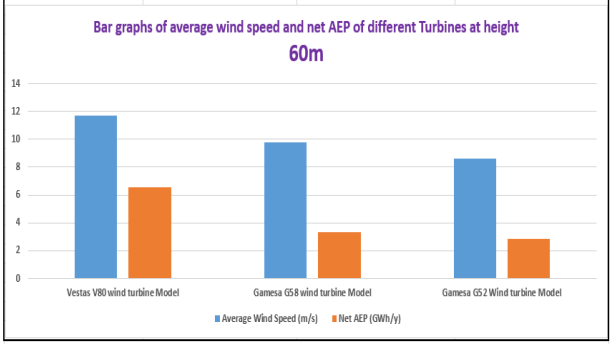

Wind Energy Generation Characteristics at Proposed location 2 at height 50m			
Parameters	Vestas V80 wind turbine Model	Gamesa G58 wind turbine Model	Gamesa G52 Wind turbine Model
Average Wind Speed (m/s)	9.78	6.77	6.41
Net AEP (GWh/y)	7.442	2.127	1.681

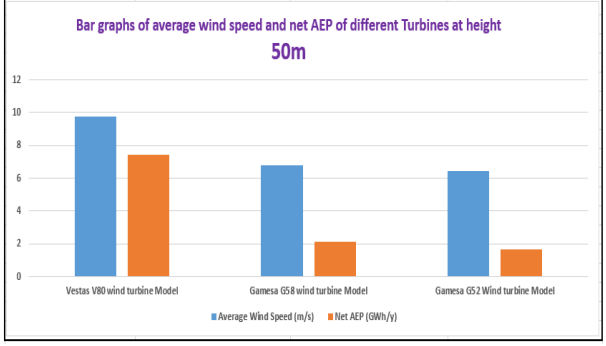

Figure 4-31: *Comparison of different wind turbine model performance at hub height 50m (right) and 60m (left) virtually sited at the proposed location of choice.*

4.8 Further CFD Simulation Analysis on the Proposed Site

Based on the above proposals, the anticipated estimated results are shown in table 4-26 as derived from the simulation experiments above in consideration of the information adapted from table 4-25. Using the wind turbine of choice in table 4-25, advanced CFD simulations were conducted at varying hub heights at the particular proposed location to determine the hub height that would provide optimal net AEP yield. The findings are shown in figure 4-32.

Turbine Type	Average wind speed (m/s)	Gross AEP (GWh/y)	Wake Losses (%)	Net AEP with wake losses (GWh/y)	Full load hours (hours)	capacity factor (%)
Vestas V80 model	9.780- 11.680	6.50- 7.50	0.000	6.50-7.50	3200- 3800	36.5- 43.5

Table 4-26: *Summary of anticipated results estimates*.

WIND TURBINE VESTAS V80-2.0MW MODEL											
Turbine Hub Heights (m)	45	50	55	60	65	70	75	80	90	100	AVERAGE
Net AEP (GWh/y)	4.058	4.943	6.748	6.587	6.698	7.487	6.937	6.752	4.779	4.900	5.9889
Average Wind Speed (m/s)	6.30	7.00	8.50	8.08	8.4	10.3	10.91	12.79	6.68	6.77	8.57
Full Load Hours (hrs)	2028.90	2471.60	3374.20	3210.85	3348.90	3743.50	3468.60	3376.1	2389.35	2449.85	2986.19
Capacity Factor (%)	23.16	28.21	38.52	36.65	38.23	42.73	39.60	38.54	27.28	27.97	34.09

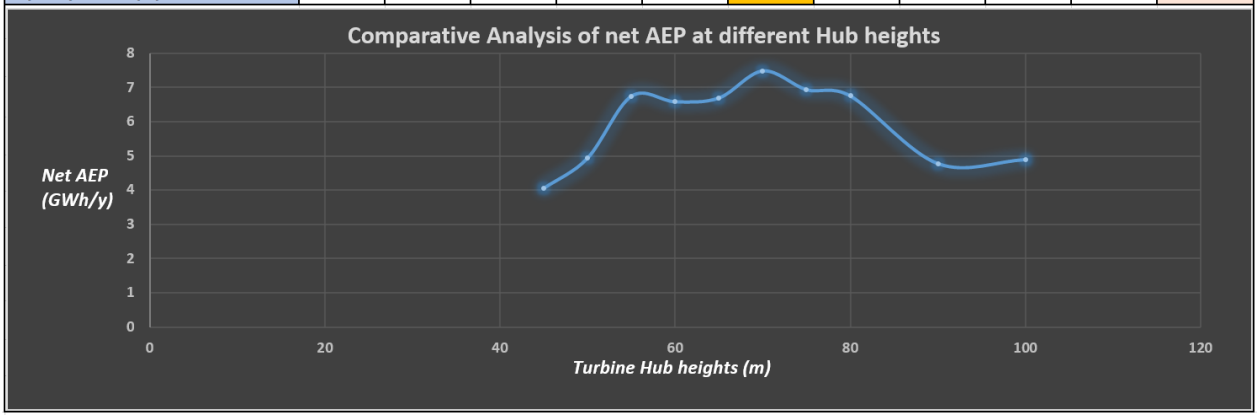

Figure 4-32: *Analysis of net AEP at different hub heights*

When further simulations at varying hub heights were performed as displayed in figure 4-32 above, totally different findings were generated which could not be revealed by only three

sampled heights as was the case in the preceding sections of this topic. This is a testimony that sampling three different hub heights is not good enough to dictate the optimal height for use in wind turbine micrositing. From the above findings, which was anchored on a comparison of 10 different heights ranging from 45m to 100m, the optimal operational hub heights for the Vestas V80 wind turbine model ranged from 55m to 80m. The peak average wind speed and net annual energy production was found when the wind turbine hub height was at 70m in the proposed location under study. Therefore, this dispelled the earlier observation that the peak height was at 60m since it was a comparison of only three sampled heights. Within the height range of 55m to 80m, the net AEP values remained promising as earlier observed, with peak annual energy production of **7.487 GWh/y**, the average wind speed of **10.3m/s**, and the capacity factor above 42%. The results in figure 4-32 were exported for hydrogen production and analysis in the succeeding chapter five.

4.9 Electrical Power Stabilization

The power generated from the wind turbines is volatile due to the fluctuation in the amount of wind speed during the hours of the day. As a result, such power cannot be connected directly to the electrolysis system for hydrogen generation. Therefore, an electrical voltage stabilizer must be used to connect the wind turbine generation and the electrolysis system setup.

A voltage stabilizer, also called Automatic Voltage Regulator (AVR), is an electronic device used to provide stable and constant input voltage to the various electrical systems and appliances such as the electrolysis setup system regardless of the fluctuations in its input supply [59]. The fluctuating voltage from the AC mains supply is connected to the voltage stabiliser for correction. Thereafter, the constant voltage output is passed through to the electrical appliances as input voltage. The entire concept is to maintain the same voltage output as shown in figure 4-33, the outline of the power correction flow.

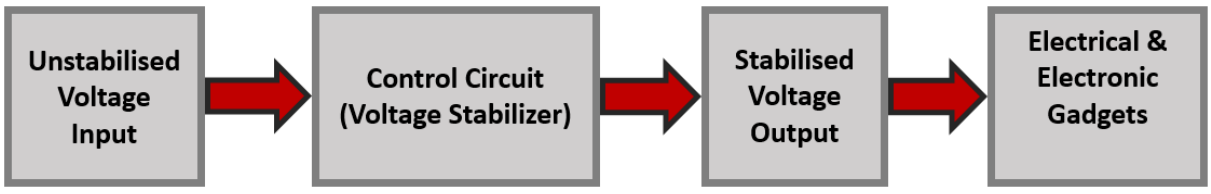

Figure 4-33: *Block diagram showing the function of Voltage stabiliser.*

The justification for voltage stabiliser usage is to protect electrical and electronic gadgets from possible damage in cases of voltage surge/ fluctuations, over-voltage, and under-voltage conditions. Figure 4-34 is a display of some of the problems associated with voltage fluctuations.

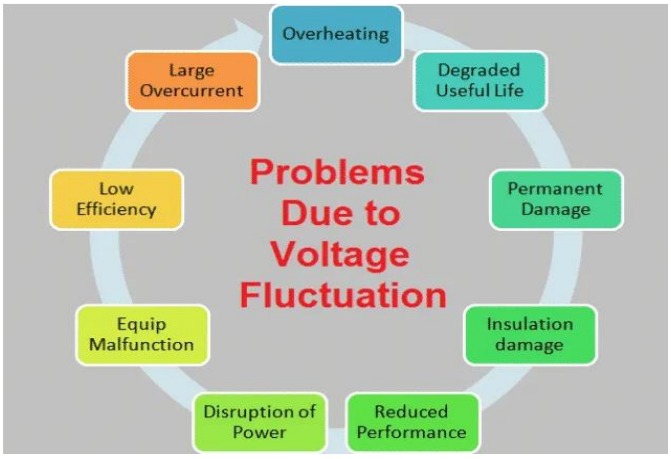

Figure 4-34: *Problems associated with voltage fluctuation* [59]

There are different types of voltage stabilisers, both analog and digital, which are either single-phase (Output of 220-230 volt) or three-phase (Output of 380-400 volt) depending on the applications [60]. Some of them include:

4.9.1 Relay Type Voltage Stabilizers:

They stabilise the voltage through relay switching, whereby the number of tapings of the transformer connected to the load to perform buck and boost operations [59]. They are majorly used in low-power rating appliances, and they are less costly. However, they are slow in responding to voltage fluctuation due to low fluctuation tolerance limits; hence they can't withstand high voltage surges [61]. This makes them very unreliable.

4.9.2 Electronic Servo Controlled Voltage Stabilizers:

These stabilisers work on the principle of servomechanism, where the servo motor is the main component that is used for the voltage correction [61]. Other features include a buck-boost transformer, autotransformers, motor driver, and control circuitry. These voltage stabilizers are found in three different categories: Single Phase Servo Based Voltage Stabilizers, Three Phase Balanced Type Servo Based Voltage Stabilizers, and Three Phase Unbalanced type Servo Based Voltage Stabilizers. They quickly respond to voltage fluctuations, making them have high voltage stabilization accuracy, hence being very reliable [59]. Equally, they can withstand high voltage surges, but they need periodic maintenance in alignment with Servo motor, which requires the services of highly skilled personnel.

4.9.3 Static Voltage Stabilizers:

They use Power Electronic Converter Circuit to provide stabilized voltage for various electronic devices [60]. This type of stabiliser is the most popular and produces the highest accuracy of

all. Its components include buck-boost transformer, microcontroller, microprocessor, Insulated Gate Bipolar Transistor (IGBT) power converter, and DSP-based controller. They have an extremely fast response to the voltage fluctuation, making them have a very high accuracy of voltage stabilization hence highly reliable [60]. Since they do not have any moving parts, they are highly efficient with meager maintenance costs. However, it is very costly to acquire them. There are various models of voltage stabilisers from different manufacturers in the market. Acquisition of the stabiliser depends on the usage, which will dictate the capacity of the stabiliser to purchase. Figure 4-35 is a pictorial view of different models of voltage stabilisers.

Figure 4-35: *Examples of Different models and types of Voltage stabilisers [61].*

The anticipated electrical power generation in this project would be highly unstable due to voltage fluctuation as a result of variations in average wind speed and direction. Such kind of power output cannot be directly connected to any electrical appliance such as electrolyser system. Therefore, a need to install voltage stabilisers and power converters to ensure constant and stable voltage output into the electrolyser systems is highly recommended.

4.10 General Issues

While trying to find the most appropriate location for wind turbine siting, a number of issues came into play for consideration. First, the terrain of the hydrogen site in Djupvik made it very difficult to find a suitable place for wind turbine location within the hydrogen site locality. The site is on the slopes of a mountain, and any attempt to simulate any particular area around the site developed some error codes 1999 and 2999 from the WindSim program; and as a result, finding a suitable place within the locality was impossible.

Secondly, there is a helicopter station a few miles from the hydrogen site, and therefore this would have affected the siting of the wind turbine in the unlikely event that the suitable site was found right at the site. The third issue that affected the choice of an appropriate wind turbine location was the socioeconomic activities around the area. Several locations with promising average wind speed and net AEP were found offshore but because of the socio-economic

activities like fishing, recreation, and transportation taking place within the ocean and the ecological life inside the sea influenced the decision since the installation of a wind turbine in such territories would have led to interferences which could result into civil strife from the community. In the same line of thought, the chosen location for the wind turbine micrositing is subject to approval from the Narvik kommune, given that they are the custodians of all construction locations and clearances.

The connectivity of the power cables across the ocean from the location of choice would be a factor that must be considered. Since the selected area is the nearest point to the site where higher average wind speed is found, connecting overhead power cables would be required for power transmission purposes. The design of the power lines from the wind turbine location to the site would be of essence, and other physical system parameters would have to be seriously considered. This was also a significant factor put into consideration while selecting the site. All the offshore locations that were put into scrutiny were far west of the site, and hence power cables would have been used past the newly launched bridge. This would have affected the design of the power transmission lines.

Finally, the process of public participation must be considered necessary in this massive project since the local community must give their views on the proposal to install the wind turbine around their locality as this may be accepted or rejected in equal measure.

5 HYDROGEN PRODUCTION ANALYSIS.

Once the power generated from the wind turbine(s) is transmitted from the wind park to the hydrogen production site and thereafter the connection is passed through the electrical power stabilisers for constant voltage flow, the output voltage from the stabiliser is passed through the rectifiers then connected to the water electrolysis system setup for the commencement of hydrogen production process as shown in the flow chart in figure 5-1.

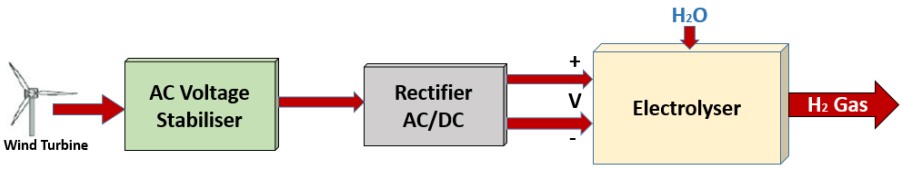

Figure 5-1: *Electrical power transmission for electrolytic hydrogen production*

The net AEP values obtained in chapter four were the critical determinants of hydrogen production. By the end of this topic, the rate of hydrogen production is forecasted by way of analytical calculations. Thereafter, a possible conclusion is drawn as to whether it would be viable to produce hydrogen from electrical energy generated from wind power around the site based on the analytical values obtained.

5.1 Electrolysers Specifications

The hydrogen production takes place in electrolyser systems. There are several commercial electrolyzers in the market from renowned manufacturers such as Nel Hydrogen (Norway), Hydrogenics Corporation (Canada), Teledyne Technologies (USA), De Nora (Italy), and Airox Nigen Equipments Pvt. Ltd (India), among others. Figure 5-2 is a flow chart that illustrates the major processes in the water electrolysis system during hydrogen production. The flow processes are similar in all the water electrolyser types currently available, but the only difference is in the electrolyser's stack design and the electrolyte supply, depending on the kind of electrolyser selected for use. As earlier observed, the type of electrolyte used in the stack system dictates the name of the electrolyser type.

There are different types of water electrolysers, but the most commonly available low temperature commercial electrolysers are the alkaline electrolysers (AE), and the Proton Exchange Membrane (PEM) electrolysers. The most developed and low cost water electrolysis technology is alkaline electrolysers. This is why they are readily available and widely spread for the production of hydrogen.

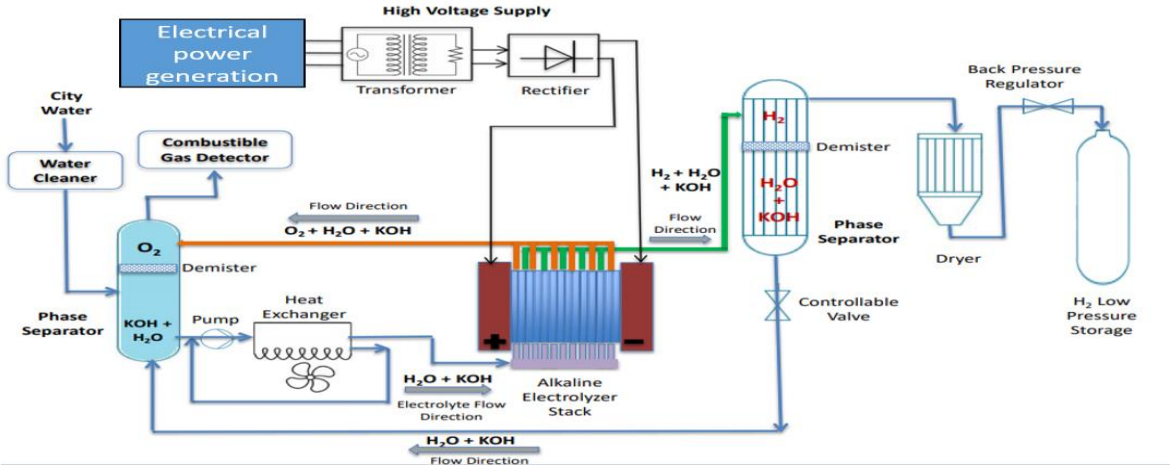

Figure 5-2: *Flow processes in water alkaline electrolysis system* [29]

The PEM electrolysers are in development stages, and they have similar applications compared to water alkaline electrolyzers. However, their higher prices is the main handicap for their dwindling demand. Therefore, alkaline water electrolysis is the leading industrial electrolysis method used for large-scale hydrogen production. In this project, more attention was given to alkaline electrolyser systems. Table 5-1 is a comparative analysis of the alkaline electrolysers and PEM electrolysers in terms of specifications and parameters of the operating conditions.

Specifications	*Alkaline Electrolysers*	*PEM Electrolysers*
Electrolyte	Caustic solution	Polymer electrolyte
Cell area (m^2)	<4	<30
Cell Temperature (°C)	60 – 80	50 – 84
Current Density (A/cm^2)	0.2 – 1.0	1.0 – 2.5
Cell Voltage (V)	1.8 – 2.4	1.8 – 2.2
Specific Energy Consumption (kWh/Nm^3)	4.1 – 5.0	4.1 – 5.5
Maximum current density (A/cm^2)	1.6	10.0
H_2 delivery pressure from stack (bar)	<30 bar	<300
H_2 purity (dry basis) (%)	99.98	99.999
Stack Lifetime (hrs.)	< 60,000	< 25,000
System Lifetime (yr.)	20 – 30	10 – 20
Partial Load Range (%)	20 – 40	0 –10
System Efficiency (%)	59 – 70	65 – 82

Table 5-1: *The operation parameters of Alkaline and PEM electrolysers* [18, 22, 26, 29].

The main electrolyser parameters for hydrogen production are the cell voltage and appropriate specific energy consumption. A well-established and effective electrolyser operating at 100%

efficiency requires 39 kilowatt-hours (kWh) of electricity and 8.9 liters of water to produce a unit kilogram (kg) of hydrogen at 25°C and 1 atmosphere pressure [12]. However, studies have shown that at varying efficiencies, the specific energy consumption for hydrogen production in most commercially available electrolysers is between 4.1 and 4.8 kWh/Nm^3 for alkaline electrolysers operating at current densities of 0.3–1.0 A/cm^2 and PEM electrolysers operating at current densities between 1.0 and 1.8 A/cm^2 [18, 22, 26, 29]. The alkaline electrolysers operating at nominal current densities of 0.45 A/cm^2 have a specific energy consumption of 4.35 kWh/Nm^3. In comparison, the PEM electrolysers have similar specific energy consumption for hydrogen production when operating at a nominal current density of 1.0 A/cm^2 [22]. In summary, both alkaline electrolyser and PEM electrolyser have a specific energy consumption of 4.35 kWh/Nm^3 at a nominal current density of 0.45 A/cm^2 and 1.0A/cm^2, respectively. Therefore, in the subsequent sections of this topic, the calculations are anchored on 4.35kWh/Nm^3 as the baseline assumption of the specific energy consumption of hydrogen production.

5.2 Parameters of Hydrogen production

The amount of hydrogen produced is directly proportional to the amount of electric power generated from the wind turbines, as discussed in chapter four. It, therefore, means that the amount of electrical energy produced from wind power would be utilised in electrolysers to produce hydrogen. From the net AEP values in figure 4-32 in chapter four, it was possible to determine the hourly and daily power production and, thereafter, the values were used to estimate the possible amount of hydrogen that would be produced. The energy consumption per unit mass (with units in kWh/kg) was used in this project to compare productivity rates of different electrolysers as well as power generation from the Vestas V80 wind turbine at varying hub heights.

According to ideal gas laws, the measure of hydrogen gas flow rate of 1.0Nm^3/hr is equivalent to 0.088kg/hr as demonstrated by the gas law analysis below:

The ideal gas law indicate that: $PV = nRT$ in which $n = \frac{m}{M}$; whereby

$n = mole\ number; m = mass\ flow\ rate$ (kg/hr); $V = volumetric\ flow\ rate$ (m^3/hr); and $M = molecular\ weight\ of\ hydrogen\ gas; P = gas\ pressure;\ \ and\ \ T = gas\ temperature(K)$

In Normal conditions and according to the SI units definitions, $P = 100kPa$ and $T = 273.15K$ and $R = gas\ constant = 8.314$Pa.$m^3$/mol.K.

Therefore; $PV = \frac{m}{M}RT \; or \; m = \frac{PVM}{RT}$

At normal conditions; m(kg/hr)= $\frac{100MV}{8.314 \times 273.15}$ (Nm^3/hr) = $0.044MV$(Nm^3/hr)

Given that the molecular weight of hydrogen gas is 2.0 and the hydrogen gas volume flow rate is taken to be 1.0Nm^3/hr, the mass flow rate, $m = 0.044 \times 2.0 \times 1.0 = \mathbf{0.088\ kg/hr}$

Subsequently, the mass flow rate of hydrogen gas of ***1.0kg/hr*** is equivalent to ***11.364Nm^3/hr.*** These conversions were necessary because, in the next section of calculating the hydrogen production, the values would be presented in kilograms per hour and not in normal cubic meters per hour for easy understanding and interpretation.

5.3 Hydrogen Production Calculations and Analysis

In the foregoing section 5.1 of this chapter, it was divulged that the specific energy consumption of hydrogen production for alkaline electrolyser operating at a nominal current density of 0.45A/cm^2 is similar to that of PEM electrolyser operating at the nominal current density of 1.0 A/cm^2, which is taken as 4.35kWh/Nm^3. This can be interpreted based on the above conversion values to mean that the specific energy consumption of hydrogen is 49.43kWh/kg. This means that, in an electrolyser system operating at 100% efficiency with all other factors remaining constant, the amount of electrical power required to produce one kilogram of hydrogen gas is 49.43kWh. This value is within the limits of the electrical consumption rate of the modern electrolysers as per the opinion of [27], who states that contemporary devices consume 48kWh of electricity for a unit kilogram of H_2. Given this information together with the net AEP results found in chapter four, it was possible to mathematically calculate the amount of hydrogen that would be produced from the wind energy harnessed from the proposed wind turbine location.

Assuming 100% electrolyser efficiency and 100% electrical energy consumption, i.e. no power losses during transmission and in the electrolysis system, the following results on hourly and daily hydrogen production were calculated as in table 5-2, where electrical power was generated from a wind turbine Vestas V80 model installed at varying hub heights for comparison.

From table 5-2, it can be observed that the hourly hydrogen production at 100% system efficiency at a nominal current density of 0.45A/cm^2 for alkaline electrolysers and 1.0 A/cm^2 for PEM electrolysers range between **9.3717kg/hr** to about **17.29kg/hr** based on the power generation from vestas V80 model wind turbine hoisted at varying hub heights between 45m to 100m. The amount of hydrogen produced per hour or per day is proportional to the amount of

Net AEP earlier obtained in chapter four. The highest hydrogen production rate was recorded at the hub height with the highest net AEP and vice versa for the lowest production rate.

Producing 1kg of Hydrogen requires 49.43kWh										
Turbine Hub Heights	45	50	55	60	65	70	75	80	90	100
Net AEP (GWh/y)	4.058	4.943	6.748	6.587	6.698	7.487	6.937	6.752	4.779	4.900
Diurnal Energy Production (MWh/day)	11.1178	13.5425	18.4877	18.04658	18.3507	20.5123	19.0055	18.4986	13.0932	13.4247
Hourly Energy Production (kWh/hr)	463.242	564.269	770.320	751.941	764.612	854.680	791.895	770.776	545.548	559.361
Hourly Hydrogen Production (kg/hr)	9.3717	11.4155	15.5841	15.2122	15.4686	17.2907	16.0205	15.5933	11.0368	11.3162
Daily Hydrogen Production (kg/day)	224.920	273.973	374.017	365.094	371.246	414.977	384.493	374.239	264.883	271.589

Table 5-2: *Daily and hourly findings of hydrogen production based on Net AEP results for a wind turbine at varying hub heights.*

It must be noted that the calculated results obtained in table 5-2 are ideal since no system can ever operate at optimal efficiency of 100% without any elements of a system malfunction, failures, or leakages. Besides, there are possibilities of power losses at every stage from the point of power generation to the final point of power consumption, and such losses must be accounted for. For instance, in the process of converting alternating current (AC) to direct current (DC), some portion of electrical power is lost. In addition, part of the electrical energy is used to support systems operations such as lighting, heating, and other miscellaneous operations. Such amount of energy is not supplied for direct use in the electrolysis process and therefore is counted as energy wasted since it is not consumed for the purpose of producing hydrogen.

Given that the operational system efficiency based on hydrogen yield for alkaline electrolyser is estimated to be between 59 to 70% while that of PEM electrolyser is estimated between 65 to 82%, as shown in table 5-1, it would be of essence to determine the amount of hydrogen produced when efficiency factors are considered. It must be noted that efficiency values are not absolute since they vary from one manufacturer to another. Due to improvements in technology, changes are prone to occur in efforts to improve electrolysis systems. Table 5-3 shows the hydrogen production calculated results for both alkaline and PEM electrolysers at their estimated minimum and maximum efficiency values.

Producing 1kg of Hydrogen requires 49.43kWh											
Turbine Hub Heights (Vestas V80) (m)		45	50	55	60	65	70	75	80	90	100
Net AEP (GWh/y)		4.058	4.943	6.748	6.587	6.698	7.487	6.937	6.752	4.779	4.900
Diurnal Energy Production (MWh/day)		11.1178	13.5425	18.4877	18.04658	18.3507	20.5123	19.0055	18.4986	13.0932	13.4247
Hourly Energy Production (kWh/hr)		463.242	564.269	770.320	751.941	764.612	854.680	791.895	770.776	545.548	559.361
Hourly Hydrogen Production (kg/hr)	Alkaline @ 59% Eff.	5.5293	6.7352	9.1946	8.9752	9.1265	10.2015	9.4521	9.2000	6.5117	6.6766
	alkaline @ 70% Eff.	6.5602	7.9909	10.9088	10.6486	10.8280	12.1035	11.2144	10.9153	7.7257	7.9214
	PEM @ 65% Efficiency	6.0916	7.4201	10.1296	9.8880	10.0546	11.2390	10.4133	10.1356	7.1739	7.3555
	PEM @ 82% Efficiency	7.6848	9.3607	12.7789	12.4740	12.6842	14.1784	13.1368	12.7865	9.0502	9.2793
Daily Hydrogen Production (kg/day)	Alkaline @ 59% Eff.	132.7030	161.6438	220.6702	215.4052	219.0351	244.8366	226.8508	220.8010	156.2808	160.2377
	alkaline @ 70% Eff.	157.4442	191.7808	261.8121	255.5655	259.8721	290.4841	269.1450	261.9672	185.4179	190.1125
	PEM @ 65% Efficiency	146.1982	178.0822	243.1112	237.3108	241.3098	269.7353	249.9203	243.2553	172.1737	176.5330
	PEM @ 82% Efficiency	184.4346	224.6575	306.6941	299.3767	304.4216	340.2814	315.2841	306.8759	217.2038	222.7032

Table 5-3: *Results of hydrogen production based minimum and maximum efficiency values for alkaline and PEM electrolysers.*

Turbine Hub Heights (m)	45	50	55	60	65	70	75	80	90	100
Alkaline @ 59% Eff.	5.5293	6.7352	9.1946	8.9752	9.1265	10.2015	9.4521	9.2000	6.5117	6.6766
alkaline @ 70% Eff.	6.5602	7.9909	10.9088	10.6486	10.8280	12.1035	11.2144	10.9153	7.7257	7.9214
PEM @ 65% Efficiency	6.0916	7.4201	10.1296	9.8880	10.0546	11.2390	10.4133	10.1356	7.1739	7.3555
PEM @ 82% Efficiency	7.6848	9.3607	12.7789	12.4740	12.6842	14.1784	13.1368	12.7865	9.0502	9.2793

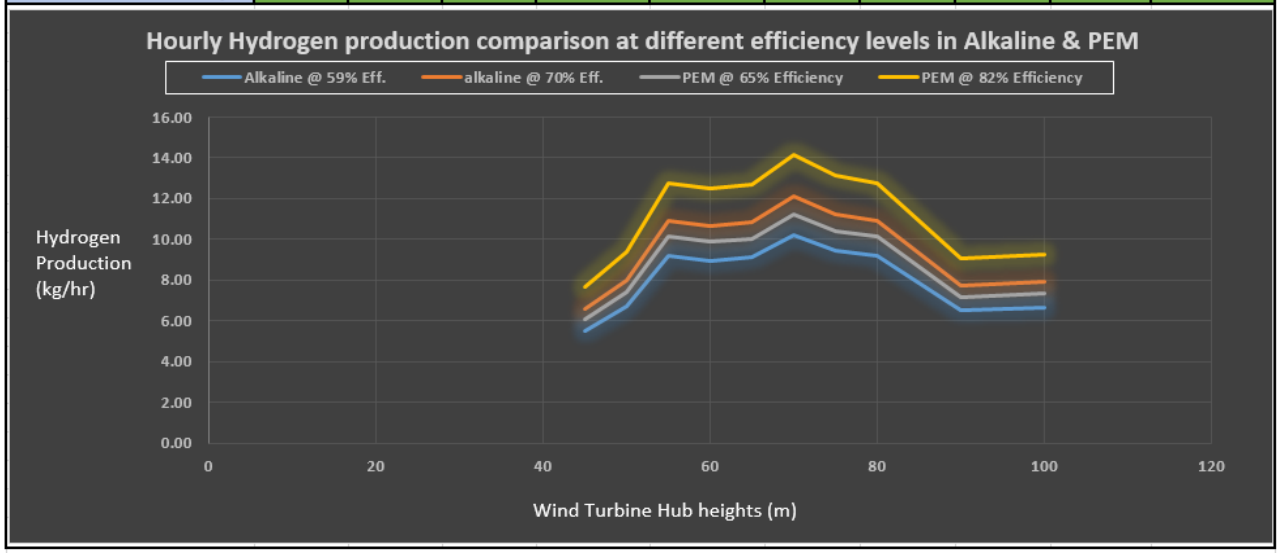

Figure 5-3: *Comparison of hourly hydrogen production at Min. and Max. Efficiencies in alkaline and PEM electrolysers*

From table 5-3 and figure 5-3, it can be deduced that when an alkaline electrolyser system is used at 0.45A/cm^2 nominal current density, the minimum amount of hydrogen that can be produced is 5.5293kg/hr, which translates to 132.703kg/day and the possible maximum amount is 12.1035kg/hr which transforms to 290.4841kg/day. This result is based on the estimated minimum possible system efficiency of 59% and estimated maximum efficiency of 70% respectively, and on the assumption that there are no power losses and that all power generated is utilised in the electrolysis process.

Looking into the PEM electrolyser results at 1.0A/cm^2 nominal current density, the possible minimum amount of hydrogen that can be obtained is 6.0916kg/hr translating to 146.1982kg/day and the possible maximum production rate is 14.1784kg/hr, which culminate into 340.2814kg/day. The results are based on 65% and 82% estimated efficiencies respectively, and the power loss assumptions are like those in the alkaline electrolyser.

In reality, the amount of power generated cannot be transmitted 100% for use in the electrolysis process. As earlier mentioned, there are elements of energy losses between the point of generation at the wind turbine location to the point of consumption such as electrical faults, turbine performances, transmission losses, and environmental effects. These and many more have an impact on the overall amount of energy that is consumed in the electrolyser systems for producing hydrogen.

The calculation of the overall process efficiency of an electrolyzer system should take into consideration the efficiency of the electrical power source. According to Yaramasu and Bin [14], the net electrical energy output from wind turbines reduces by 17.9% at the point of a user's meter. In a similar train of thought, Zhang [31] suggests that the total wind power production losses range between 10-20% exclusive of the wake losses. Similarly, Mehmet and Demirci [22], in their publication about advances in hydrogen production technologies, reveal that the efficiency of electrical power stations is in a range lower than 50%, and as a result, the overall efficiency of hydrogen production processes is approximately 40%. The US National Renewable Energy Laboratory (NREL) report of 2020 also indicate that the wind power losses from the point of generation to point of interconnection such as array wake losses, electric collection and transmission losses and blade soiling losses total to 15-20% [58]. These revelations provide very fertile grounds in factoring the electrical power generation and transmission losses into the overall power consumption by the electrolyser systems.

Therefore, assuming 30% of power production and transmission losses, and 15% energy conversion losses and miscellaneous operations power supply, the overall net AEP from the wind power plant would reduce by 45% for direct consumption in the electrolysis process, which will trickle down to affect the overall hydrogen production rate as can be seen in results table 5-4 and figures 5-4 and 5-5.

Producing 1kg of Hydrogen requires 49.43kWh											
Turbine Hub Heights (Vestas V80) (m)		45	50	55	60	65	70	75	80	90	100
Net AEP (GWh/y)		4.058	4.943	6.748	6.587	6.698	7.487	6.937	6.752	4.779	4.900
Net AEP (Excluding 45% Power Losses)		2.2319	2.71865	3.7114	3.62285	3.6839	4.11785	3.81535	3.7136	2.62845	2.695
Diurnal Energy Production (MWh/day)		6.11479	7.44836	10.1682	9.925616	10.0929	11.2818	10.453	10.1742	7.2012	7.3836
Hourly Energy Production (kWh/hr)		254.783	310.348	423.676	413.567	420.537	470.074	435.542	423.927	300.051	307.648
Hourly Hydrogen Production (kg/hr)	Alkaline @ 59% Eff.	3.0411	3.7043	5.0570	4.9364	5.0196	5.6108	5.1987	5.0600	3.5814	3.6721
	alkaline @ 70% Eff.	3.6081	4.3950	5.9999	5.8567	5.9554	6.6569	6.16791	6.00342	4.2492	4.3567
	PEM @ 65% Efficiency	3.3504	4.0811	5.5713	5.4384	5.5300	6.1814	5.72734	5.5746	3.9456	4.0455
	PEM @ 82% Efficiency	4.2266	5.1484	7.0284	6.8607	6.9763	7.7981	7.2253	7.0326	4.9776	5.1036
Daily Hydrogen Production (kg/day)	Alkaline @ 59% Eff.	72.9866	88.90411	121.3686	118.4729	120.4693	134.6601	124.7679	121.4405	85.9544	88.1307
	alkaline @ 70% Eff.	86.5943	105.4795	143.9966	140.5610	142.9297	159.7663	148.0297	144.0820	101.9798	104.5619
	PEM @ 65% Efficiency	80.4090	97.94521	133.7112	130.5210	132.7204	148.3544	137.4562	133.7904	94.6956	97.0932
	PEM @ 82% Efficiency	101.4390	123.5616	168.6818	164.6572	167.4319	187.1548	173.4063	168.7818	119.4621	122.4868

Table 5-4: *Results of hydrogen production Calculations based on net AEP exclusive of all the possible power losses.*

Turbine Hub Heights (m)	45	50	55	60	65	70	75	80	90	100
Alkaline @ 59% Eff.	3.0411	3.7043	5.0570	4.9364	5.0196	5.6108	5.1987	5.0600	3.5814	3.6721
alkaline @ 70% Eff.	3.6081	4.3950	5.9999	5.8567	5.9554	6.6569	6.16791	6.00342	4.2492	4.3567
PEM @ 65% Efficiency	3.3504	4.0811	5.5713	5.4384	5.5300	6.1814	5.72734	5.5746	3.9456	4.0455
PEM @ 82% Efficiency	4.2266	5.1484	7.0284	6.8607	6.9763	7.7981	7.2253	7.0326	4.9776	5.1036

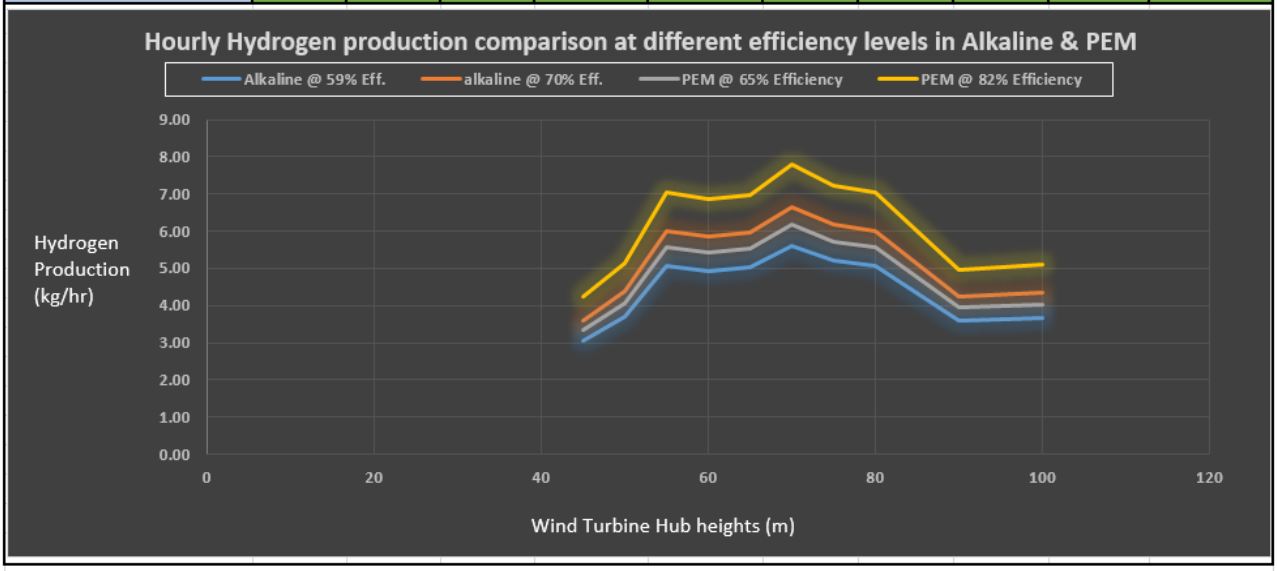

Figure 5-4: *Comparative hourly hydrogen production rate in Alkaline and PEM electrolysers at different efficiencies against varying power production hub heights.*

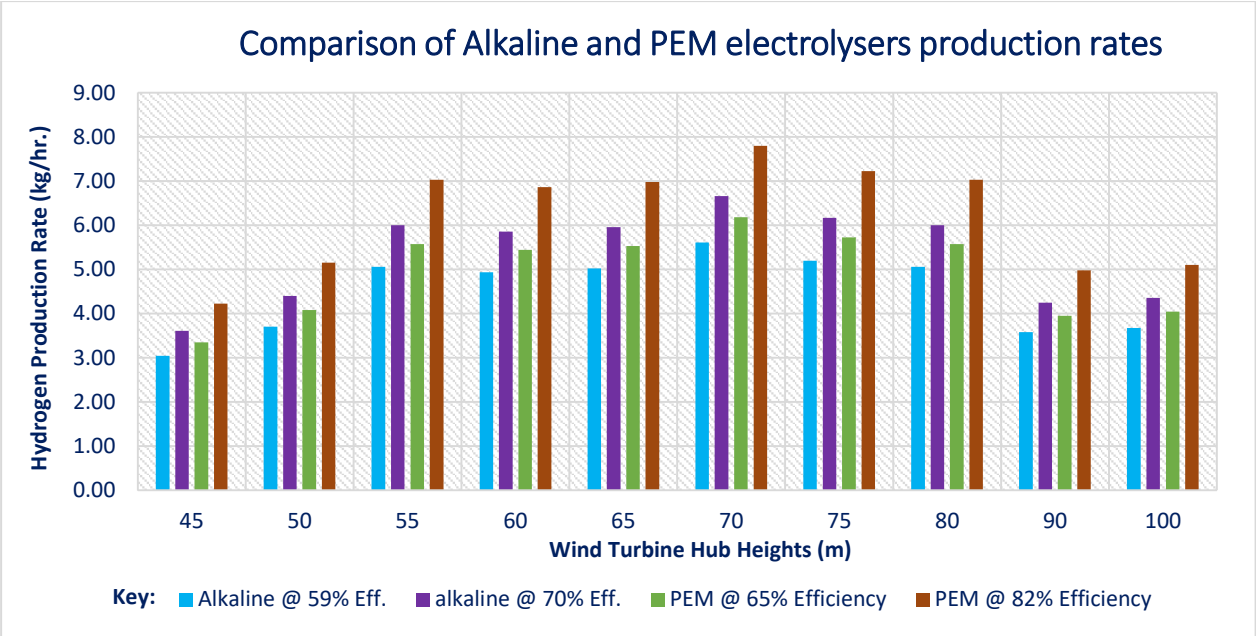

Figure 5-5: *Levels of hydrogen production rates of alkaline and PEM electrolysers at different efficiencies.*

As a result of factoring in the power losses in the hydrogen production calculations, it is observable that the hydrogen production rate reduced drastically in all the options of wind turbine elevation heights. For instance, the highest possible production from an alkaline electrolyser at 59% efficiency using electrical power generated from a wind turbine erected at 70m hub height will reduce to 5.6108kg/hr from initial value of 10.2015kg/hr and the same electrolyser at 70% efficiency and same power source will have reduced hydrogen production rate from 12.1035kg/hr to 6.6569kg/hr. A similar trend is also observed in the PEM electrolyser whereby the highest possible production rate, at the lowest efficiency of 65%, reduces from 11.239kg/hr to 6.1814kg/hr, and maximum production rate at 82% electrolyser efficiency declines from 14.1784kg/hr to 7.7981kg/hr. Figure 5-5 is a clear show of the trends in the hydrogen production rates of alkaline and PEM electrolysers at their lowest and highest efficiency levels with power generations from wind turbines at varying heights.

It must be noted that 45% electrical power loss is an estimation that can fluctuate upwards or downwards depending on the systems used and technologies applied to minimise power losses. However, with technological advancements in modern times, it is possible to say that 45% power loss is on the higher side for the purposes of gauging the probable amount of hydrogen that can be produced in the worst-case scenario during electrical power generation. In that regard, drastic measures must be employed to ensure that the electrical power losses are stagnated to the minimum so that maximized power is utilised in the electrolysis processes.

Generally, with all the considerations factored into the calculations, the lowest possible hydrogen production using alkaline electrolyser under this study was ***3.0411kg/hr*** translating to ***72.9866 kg/day*** with electrical power supply from wind energy generated using Vestas V80 wind turbine at the selected site and installed at hub heights ranging from 45m to 100m. The highest possible amount that can be generated from the same electrolyser under the same conditions was ***6.6569kg/hr*** conforming to the daily production of ***159.7663kg/day*** as shown in table 5-4 and confirmed by figures 5-4 and 5-5. For PEM electrolyser operating under similar conditions as the alkaline electrolyser described above, its lowest possible hydrogen production rate would be ***3.3504kg/hr,*** which fulfills the daily production rate of ***80.4096kg/day,*** while the highest production rate was recorded as ***7.7981kg/hr*** which converts to ***187.1544kg/day***. These values are within the limits of industrial systems production capacity that usual oscillate in the range of ***0.44kg/hr*** to ***44kg/hr*** of Hydrogen production rate [26].

Given that alkaline water electrolysis is the best developed and low cost technology at present and that several industrial alkaline electrolyzers are used in the large-scale production of hydrogen, this project looked into the features of two industrial alkaline electrolysers as a way of using the specifications and the net AEP values, obtained from the windSim modelling, to forecast the probable amount of hydrogen that can be produced in an event that any of the electrolysers is acquired. Therefore, the next section is the analysis of two case studies of Atmospheric alkaline electrolysers from Nel Hydrogen, Norway and HySTAT™ hydrogen generator alkaline electrolyser from the Hydrogenics Corporation, Canada.

5.4 CASE STUDY 1: - Atmospheric Nel Hydrogen Alkaline Electrolyser.

Nel Hydrogen Company is one of the gurus in manufacturing electrolyser systems. The atmospheric alkaline electrolyser (A-series) is considered the most energy-efficient electrolyser from Nel Hydrogen Company [18]. Table 5-5 shows specifications of the atmospheric alkaline water electrolyser system manufactured by the Norwegian company, while figure 5-6 shows the structural design of the electrolyser.

From the parametric table 5-5 provided, the specific energy consumption of electrolyser at the ambient temperature of between 5 and 35°C and at standard pressure of 1bar is 3.8 – 4.4 kWh/Nm^3 at a current density of up to $0.3A/cm^2$. Assuming average specific energy consumption of 4.1 kWh/Nm^3, which translates to 46.59kWh/kg of hydrogen production together with pre-defined system efficiency assumptions, it was possible to calculate the rate of hydrogen production of this electrolyser using the electrical energy values obtained from the

simulation experiments in the previous chapter which had also been used in earlier sections of this topic. The possible amount of hydrogen that can be produced is as shown in results table 5-6.

Specific Parameters	Values
Cell type	B-FP
Electrolyte	25% solution of KOH
Current density (A/cm^2)	0.3
Energy consumption (kWh/Nm^3)	3.8 – 4.4
Delivery Pressure (bar)	1
Temperature (°C)	5– 35
Cell Efficiency (%)	65 – 75
Hydrogen purity (%)	99.9
Electrolyser Area (m^2)	150

Table 5-5: *Operating conditions of A-series Alkaline Electrolyser from Nel Hydrogen* [22, 62].

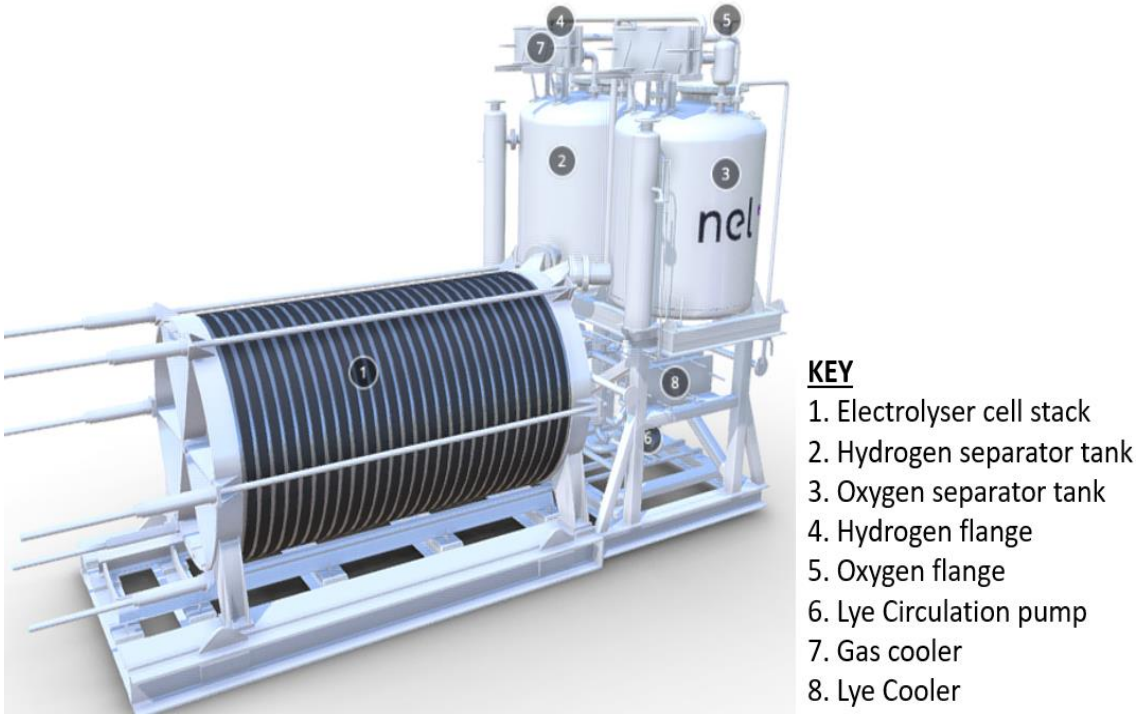

Figure 5-6: *Structural design of A150-series Alkaline Electrolyser from Nel Hydrogen* [62].

Nel Hydrogen Atmospheric Alkaline electrolyser - Hydrogen Production Rate is 46.59kWh/kg											
Turbine Hub Heights (Vestas V80) (m)		45	50	55	60	65	70	75	80	90	100
Net AEP (GWh/y)		4.058	4.943	6.748	6.587	6.698	7.487	6.937	6.752	4.779	4.900
Net AEP (Excluding 45% Power Losses)		2.2319	2.71865	3.7114	3.62285	3.6839	4.11785	3.81535	3.7136	2.62845	2.695
Diurnal Energy Production (MWh/day)		6.11479	7.44836	10.1682	9.92562	10.0929	11.2818	10.453	10.1742	7.2012	7.3836
Hourly Energy Production (kWh/hr)		254.783	310.348	423.676	413.567	420.537	470.074	435.542	423.927	300.051	307.648
Hourly Hydrogen Production (kg/hr.)	Nel Electrolyser @ 65% Efficiency	3.5546	4.3298	5.9109	5.7699	5.8671	6.5582	6.07646	5.91441	4.1862	4.2922
	Nel Electrolyser @ 75% Efficiency	4.1015	4.9959	6.8203	6.6576	6.7697	7.5672	7.0113	6.8243	4.8302	4.9525
Daily Hydrogen Production (kg/day)	Nel Electrolyser @ 65% Efficiency	85.3105	103.916	141.862	138.4772	140.8107	157.3977	145.8351	141.9459	100.4679	103.0117
	Nel Electrolyser @ 75% Efficiency	98.4352	119.903	163.687	159.7813	162.4739	181.6127	168.2713	163.7838	115.9245	118.8597

Table 5-6: *Hydrogen productivity Results using Atmospheric alkaline electrolyser from Nel Hydrogen*

From the tabulated results above, it can be highlighted that the hydrogen productivity using the Atmospheric alkaline electrolyser with efficiency between 65-75% is between ***3.5kg/hr*** to about ***7.5kg/hr*** based on the electrical power productivity from wind energy using the Vestas V80 wind turbine at varying hub heights between 45m to 100m and on the assumption that only 55% of the power generated would be directly utilised in the electrolysis system. The findings equally suggest that the maximum hydrogen production will correspond to the highest power output tapped when the wind turbine is installed at the 70m hub height and the lower hydrogen productivity estimates correspond to the low power production, as shown in the comparative bar graphs in figure 5-7. This is a continuous confirmation that the maximum hydrogen production output would be possible if and only if the Vestas V80 wind turbine is installed at 70m hub height.

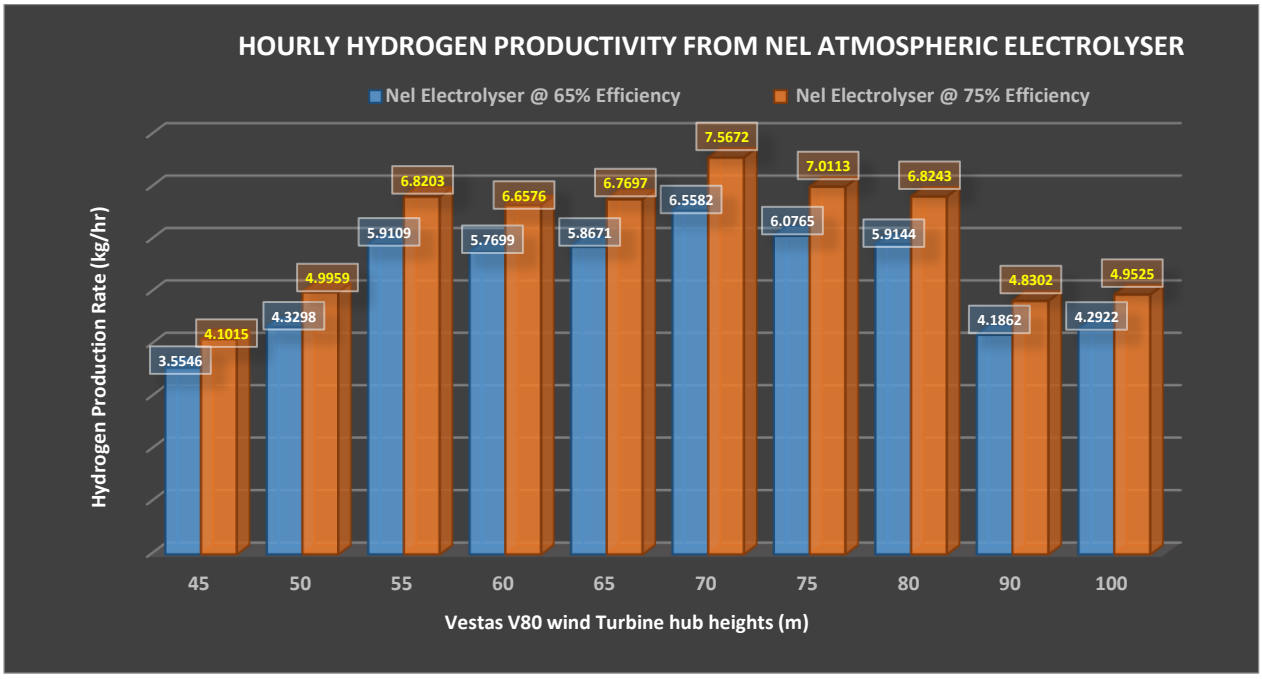

Figure 5-7: *Comparison of hydrogen production rates using Nel hydrogen alkaline electrolyser using electrical power from vestas V80 wind turbine at different hub heights.*

The hydrogen production at different efficiency levels of minimum 65% and maximum 75% for the atmospheric Nel Alkaline electrolyser depicted some element of trend similarity whereby despite variation in values, the maximum hydrogen productivity would be experienced at 70m wind turbine hub height and lowest hydrogen productivity will be at 45m wind turbine hub height for the different efficiencies as shown in figure 5-8.

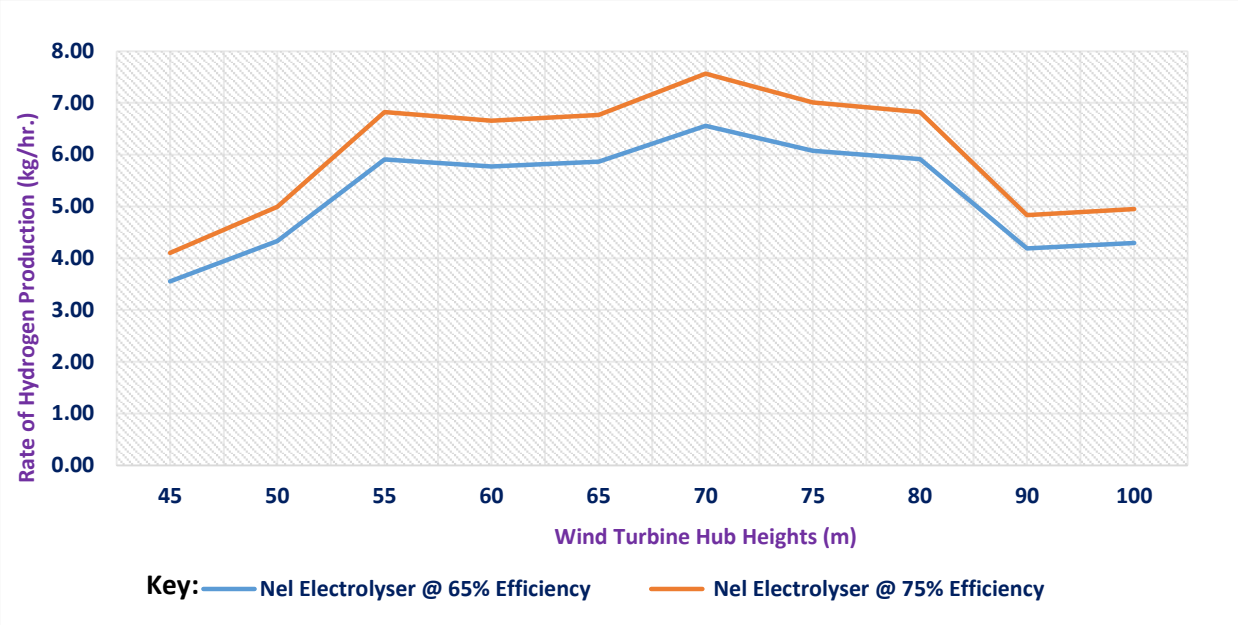

Figure 5-8: *Comparison of hydrogen production rate at a minimum and maximum operational efficiency of Atmospheric Nel hydrogen electrolyser.*

From the results table 5-6, the lowest approximate amount of hydrogen that can be obtained from this system when all the above conditions are observed is ***3.5546kg/hr,*** while the highest approximate amount is ***7.5672kg/hr,*** with most of the values within that range are above 5kg/hr of hydrogen production as displayed in figures 5-7 and 5-8.

There are five different Nel Hydrogen electrolyser system models depending on their rated production capacity. They include the A150 series, A300 series, A485series, A1000 series, and A3880 series. The Atmospheric Nel Hydrogen electrolyser system models operating at one-atmosphere pressure, the A150 series has a net hydrogen production rate between 4.5kg/hr and 13.5kg/hr; the A300 series has a productivity rating of 13.5kg/hr to 27.0kg/hr, the A485 series has its production capacity rate of 27kg/hr to 43.58kg/hr, the A1000 series has production capacity rating of between 54kg/hr and 87.25kg/hr and the biggest atmospheric electrolyser A3880 series has rated capacity of between 215.8kg/hr and 348.92kg/hr [62]. Comparing the experimental or practical average values with the theoretical values of the Atmospheric A150 series Nel Hydrogen electrolyser system shows that most of the values are within the rated production capacity limits of the electrolyser. Therefore, this is an exoneration that the electrical

power production from the site selected is capable of powering the electrolyser to produce hydrogen at its rated capacity after factoring in the cell efficiency and 45% overall electrical power losses.

5.5 CASE STUDY 2:- Alkaline HySTAT™ Hydrogen Generator.

This is a state-of-the-art alkaline electrolyser manufactured by the Hydrogenics Corporation. Hydrogenics Corporation came into life after the amalgamation of the Canadian Stuart Energy Systems Corporation with a Belgian Vandenborre Hydrogen Systems in 2005 [22]. The operational parameters of the electrolyser are as conveyed in table 5-7, while the structural setup of the HySTAT alkaline stack generator is as shown in figure 5-9.

Specific Parameters	Values
Electrolyte	30% solution of KOH
Current density (A/cm^2)	0.2–1.0
Energy consumption (kWh/Nm^3)	4.3 – 5.58
Delivery Pressure (bar)	10 – 25
Temperature (°C)	35 – 80
Cell efficiency (%)	56 –73
Hydrogen purity (%)	99.9

Table 5-7: *Operating conditions of Alkaline HySTATTM hydrogen generators [18, 22, 63].*

The system is fully automated with a delivery pressure of between 10 and 25 bars without an external compressor. The specific electrical energy consumption is 4.3–5.58 kWh/Nm^3 of hydrogen, taking into account the energy required for the operation of supporting systems [63]. They apply a pressurized electrolysis process to generate high hydrogen purity of 99.9%.

At output pressure of between 10 and 25bars, the Hydrogenics HySTAT^{TM} alkaline electrolyser operating at an ambient temperature of 70°C and nominal current density of $0.25A/cm^2$ has a specific energy consumption of $4.3kwh/Nm^3$ with a stack energy efficiency of between 56 to 73% [29]. With this information and taking energy consumption as 4.3 kWh/Nm^3 translating to 48.86kwh/kg, it was possible to calculate the hydrogen productivity based on the electrical power generation from the net AEP results obtained in figure 4-32 of chapter 4. The findings are as shown in tables 5-8, and 5-9 and figures 5-10 and 5-11.

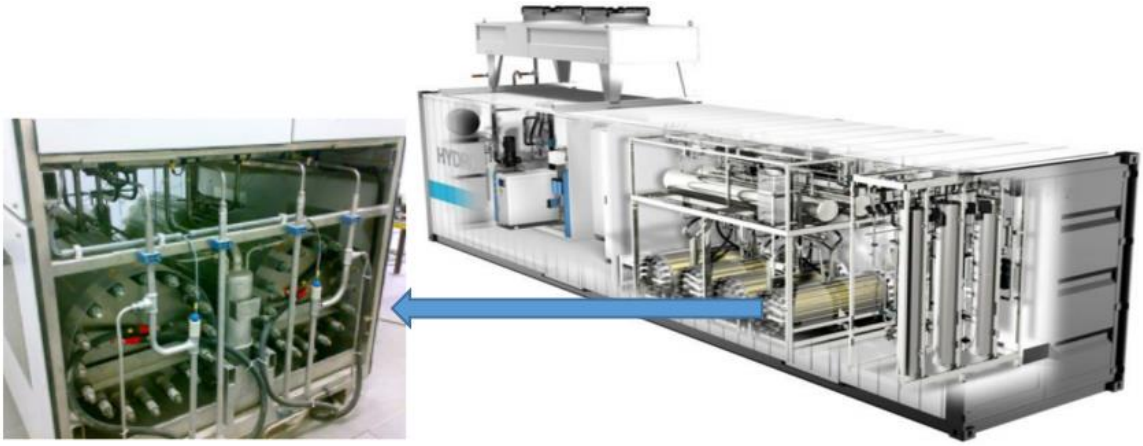

Figure 5-9: *Hydrogenics HySTAT™ Alkaline Stack Electrolysis system* [21, 22, 63].

Hydrogenics HySTAT Alkaline electrolyser - Hydrogen Production Rate is 48.86kWh/kg.											
Turbine Hub Heights (Vestas V80) (m)		45	50	55	60	65	70	75	80	90	100
Net AEP (GWh/y)		4.058	4.943	6.748	6.587	6.698	7.487	6.937	6.752	4.779	4.900
Net AEP (Excluding 45% Power Losses)		2.2319	2.7187	3.7114	3.6229	3.6839	4.1179	3.8154	3.7136	2.6285	2.695
Diurnal Energy Production (MWh/day)		6.1148	7.4484	10.168	9.9256	10.0929	11.282	10.453	10.174	7.2012	7.3836
Hourly Energy Production (kWh/hr)		254.78	310.35	423.676	413.567	420.537	470.074	435.54	423.93	300.051	307.648
Hourly Hydrogen Production (kg/hr.)	HySTAT Electrolyser @ 56% Efficiency	2.9202	3.5570	4.8559	4.7400	4.8199	5.3877	4.9919	4.8588	3.4390	3.5261
	HySTAT Electrolyser @ 73% Efficiency	3.8066	4.6368	6.3300	6.1790	6.2831	7.0232	6.5073	6.3337	4.4830	4.5965
Daily Hydrogen Production (kg/day)	HySTAT Electrolyser @ 56% Efficiency	70.0836	85.368	116.541	113.7606	115.6777	129.3041	119.8053	116.6103	82.5356	84.6253
	HySTAT Electrolyser @ 73% Efficiency	91.3590	111.283	151.92	148.2951	150.7941	168.5571	156.1748	152.0098	107.5911	110.3152

Table 5-8: *Hydrogen productivity Results using Hydrogenics HySTAT™ alkaline electrolyser specifications.*

Turbine Hub Heights (Vestas V80) (m)		45	50	55	60	65	70	75	80	90	100
Hourly Hydrogen Production (kg/hr.)	HySTAT Electrolyser @ 56% Efficiency	2.9202	3.5570	4.8559	4.7400	4.8199	5.3877	4.9919	4.8588	3.4390	3.5261
	HySTAT Electrolyser @ 73% Efficiency	3.8066	4.6368	6.3300	6.1790	6.2831	7.0232	6.5073	6.3337	4.4830	4.5965

Table 5-9: *Results of the hourly rate of Hydrogen production using HySTAT™ alkaline electrolyser.*

The results show that the HySTAT™ alkaline electrolyser has productivity values ranging from ***2.9202kg/hr*** to ***7.0232kg/hr*** within the efficiency limits of between 56% and 73%. The productivity values have a relatively more comprehensive range between the approximate minimum value and the maximum value. This can be associated with wide limits of system efficiency spanning from 56%, which is just above the average, to 73%, which is below the fourth quartile, as can be seen in figure 5-11. It must be noted that the majority of the resultant approximate values are inclined above ***3.5kg/hr,*** with only two values appearing below the 3.5kg/hr productivity mark, as can be observed in table 5-9 and figure 5-10. The hydrogen productivity flow pattern remains similar to that of Nel electrolyser with a clear show that highest productivity can be tapped at site location when wind turbine generates electrical power at a hub height of 70m.

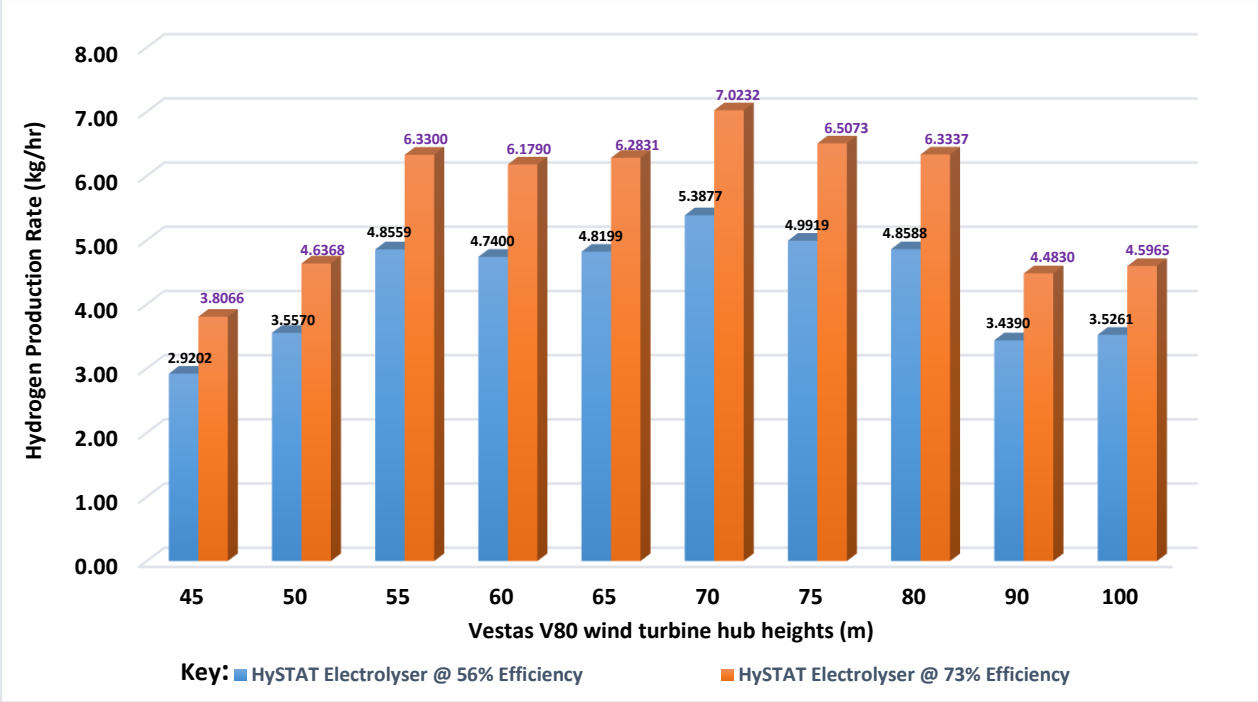

Figure 5-10: *Comparison of hydrogen production rates using Hydrogenics HySTAT™ alkaline electrolyser at varying electrical power generated through Vestas V80 wind turbine at different hub heights.*

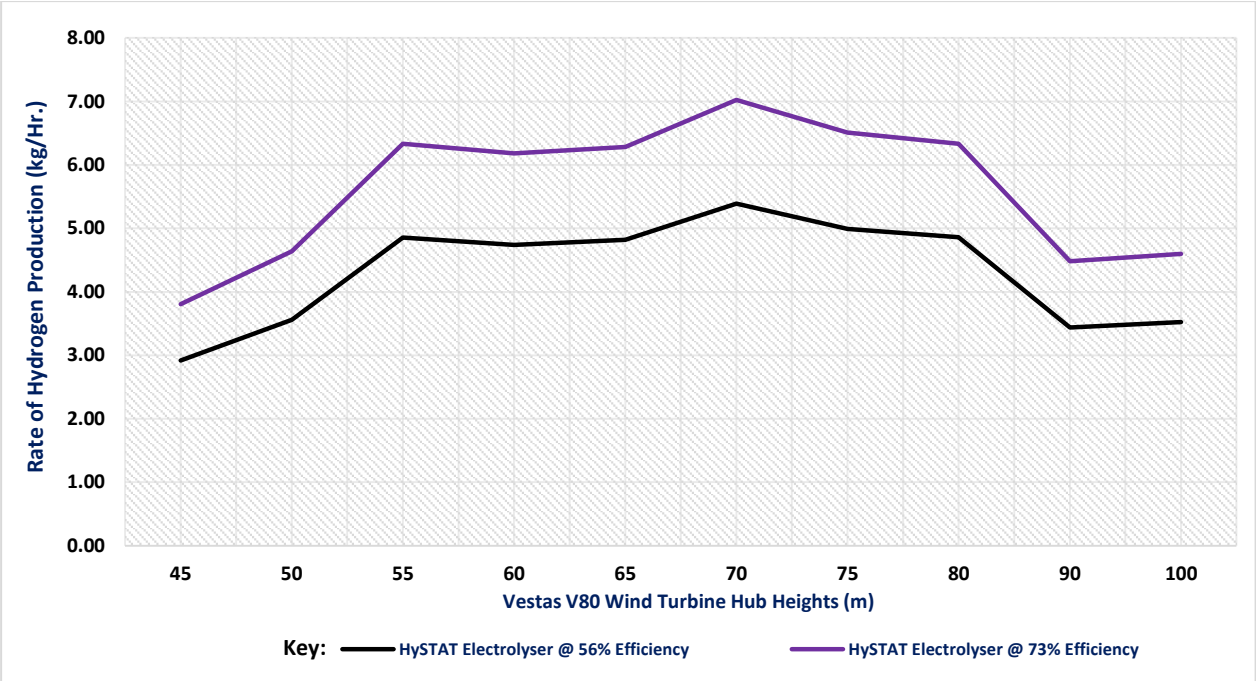

Figure 5-11: *Comparison of hydrogen production rate at a minimum and maximum operational efficiency of Hydrogenics HySTAT alkaline electrolyser.*

At the lowest possible efficiency of 56%, the electrolyser system has a hydrogen productivity rate ranging from ***2.9202kg/hr*** to ***5.3877kg/hr.*** ***A***t the highest possible efficiency of 73%, the HySTAT™ electrolyser has hydrogen productivity values ranging from ***3.8066kg/hr*** to ***7.0232kg/hr*** rate of hydrogen production in both minimum and maximum efficiency values.

The results are based on the calculated results in table 5-8 and 5-9 and displayed in the comparative bar graphs in figure 5-10. The results are based on the electrical power estimates from wind turbine power generation at different hub heights and incorporation of all possible power losses and systems efficiencies.

Depending on the operational efficiencies and hydrogen productivity rates, there are five different models of HySTAT™ alkaline electrolysers from the Hydrogenics Corporation. First is the HySTAT™ -10 model alkaline electrolyser with a maximum rated production capacity of 0.88kg/hr, second is the HySTAT™ -15 model alkaline electrolyser whose maximum rated production capacity is about 1.32kg/hr, third is the HySTAT™ -20 model alkaline electrolyser with hydrogen production capacity rates of between 0.704kg/hr to 1.76kg/hr [63]. The fourth model is the HySTAT™ -30 model alkaline electrolyser whose rated productivity is within limits from 1.056kg/hr to maximum rating of 2.64kg/hr and final model is the HySTAT™ -60 model alkaline electrolyser with minimum and maximum hydrogen production ratings of 2.112kg/hr and 5.28kg/hr respectively.

When the ratings of different models of HySTAT™ alkaline electrolysers are compared against the calculated values based on the general specifications in table 5-7, it is worth concluding that the experimental values are in tandem with the rated production capacity of the HySTAT™ alkaline generator models irrespective of the differences in the power generation. As a result, the daily demand can be attained when any of the models of HySTAT™ alkaline electrolyser models are acquired.

It must be noted that the hydrogen produced from alkaline electrolyzers must be subjected to proper purity control performance and 100% drying; otherwise, it cannot be directly applied in PEM fuel cells and other technological processes [27]. This is because hydrogen from the water alkaline electrolysis process contains a mixture of water vapor and traces of alkaline that renders it 0.1% impure.

Also, a water electrolyser operated at an increased pressure has an added advantage over those working at much lower pressure. This is because increasing the electrolyser's operating pressure impacts the energy consumption of the hydrogen purification unit by reducing the voltage of the electrolysis stack and reducing the energy required to produce hydrogen [18]. As a result, hydrogen produced at high pressure is far much easier to dry than the one produced at relatively lower pressure.

6 COST ESTIMATION

This topic involves the approximated economic cost of all the items that are likely to be procured in the event that the project is brought to life and the ecological benefits of the project. Some of the items that are likely to feature in economic cost estimations are equipment, labor, transport, and miscellaneous costs, which come by virtue of the factors under consideration in wind power generation costing, such as logistics, locations, transportation, accessibility, and weather patterns [64].

In determining the estimated cost of the wind power generation and electrolyzer system, two main parameters are considered i.e., capital expenditure (CapEx) and operational expenditure (OpEx). Capital expenditures are the one-time monetary investments in acquiring or upgrading the fixed assets such as wind turbines, electrical transmission cables, transformers, land leases, electrolyzers, fueling units, etc. On the other hand, operational expenditures are the monetary allocations that pertain to keeping the fixed assets in proper operational standards. They include appropriations for routine operation and maintenance (O&M) of the systems post-commissioning.

6.1 Wind Power Generation Cost Estimates

According to the NREL report [58], the measure of wind power generation cost is based on the levelised cost of energy (LCOE) equation (1) below. LCOE is a metric formulae used to evaluate the cost of generating electricity and the total power-plant-level impact from technology design changes [66]. It can be used to compare the costs of all types of power generations.

$$\mathrm{LCOE} = \frac{(\mathrm{CapEx} \times \mathrm{FCR}) + \mathrm{OpEx}}{(\mathrm{AEP_{net}}/1{,}000)} \qquad (1)$$

Where: LCOE = levelised cost of energy ($/MWh)

FCR = fixed charge rate (%)

CapEx = capital expenditures ($/kW)

AEP_{net} = net average annual energy production (MWh/yr.)

OpEx = operational expenditures ($/kW/yr.)

The total costs for installing commercial-scale wind turbines vary significantly depending on the location of the project, construction contracts, number of turbines ordered, cost of financing,

the period when the turbine purchase agreement was executed, and other factors, as shown in figure 6-1 [58]. The average cost for a commercial-scale wind turbine in the present time range from about $1.3 million to $2.2 million per Megawatt. The majority of such wind turbines available are the 2.0 MW capacity, whose costs are in the range of $3million to $4 million.

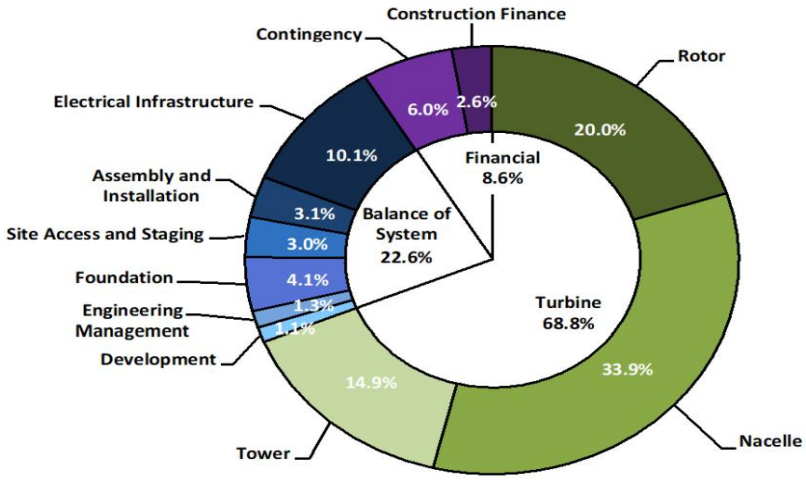

Figure 6-1: *The economic cost components of a wind turbine [58].*

The economic cost components that impact wind power projects other than the turbines include items such as wind resource assessment and site analysis expenses, construction expenses, permitting and interconnection studies, utility system upgrades, transformers, protection, and metering equipment, insurance, operations, warranty, repair and maintenance, legal and consultation fees and other factors like taxes and incentives [64]. Table 6-1 shows the approximate CapEx and LCOE breakdown of wind power projects for both onshore and offshore installations.

The operation and maintenance expenditure also form part of the wind power project costing to ensure that all the installed equipment are running optimally until they are replaced, and the consumables are periodically supplied for constant operation. According to [64], the O & M constitute a portion of variable costs, including the land rental, insurance, taxes, etc., and can take up to 20% of the total investment costs. OpEx cost estimates for wind projects are between 1.5% and 3.5% of the CapEx cost, translating to an average of $48/kW/year for onshore and $133/kW/year for offshore projects in the EU [58].

Given that site selected in this project is an onshore location and using the results in figure 68, it was possible to determine the levelised cost of energy (LCOE) for this particular wind project using equation (1) when a Vestas V80-2MW model wind turbine is set for installation.

Assuming a fixed charge rate of 7.5% and working with the CapEx values in table 6-1, the LCOE findings would be as shown in table 6-2.

Variables	Onshore Project ($/kW)	Offshore Project ($/kW)
Rotor Module	323	323
Rotor blades	201	201
Pitch assembly	68	68
Hub assembly	54	54
Nacelle Module	533	533
Nacelle electrical assembly	175	175
Drivetrain assembly	205	205
Nacelle structural assembly	110	110
Yaw assembly	43	43
Tower module	259	518
Turbine Capital Cost	**1,115**	**1,374**
Development cost	16	138
Engineering and management	19	92
Substructure and Foundation	60	676
Site access and staging	45	124
Assembly and Installation	45	338
Electrical infrastructure	148	1,150
Balance of system	**332**	**2,518**
Construction financing cost	49	183
Contingency fund	95	462
Financial Costs	**144**	**645**
TOTAL CAPITAL EXPENDITURES	**1,591**	**4,537**

Table 6-1: *The estimates of CapEx for onshore and offshore wind power projects* [58].

Parameters	Djupvik Project (Vestas V80-2MW Turbine)
CapEx ($/kW)	1591
OpEx ($/kW/yr.)	48
Fixed Charge rate (%)	7.5
Average AEP_{net} (MWh/yr.)	5988.9
Net Capacity factor (%)	42.73
LCOE ($/MWh)	**27.94**

Table 6-2: *Summary estimates of the LCOE for Djupvik wind power project*

6.2 Cost Estimates of Electrolysers

In hydrogen production through the electrolysis processes, electrolysers are the main components that are used in such projects, and therefore the cost estimates of electrolysers are very pivotal. The overall cost of electrolysis comprises the cost of electrolyzer, including maintenance and replacement of worn-out membranes, the cost of the electricity used for the process, and any subsequent costs for drying, cleaning, and compression of the gas, as well as transport [65]. Therefore, the costing parameters include electrolyzer CapEx and OpEx costs, Compressor CapEx and OpEx costs, Balance of System costs, which include piping, water, etc., electrolyzer lifetime that dictates when electrolyzer will need to be replaced, and conversion efficiency showing how efficiently water can be converted to H_2 gas. The electrolyser and compressor OpEx costs constitute 2-4% of the CapEx costs, which are estimated at $40/kW in the US and $50/kW in the EU [66]

Over the years, the investment cost of the electrolysers has remained high, but the manufacturers are putting every possibility in trying to lower the costs. According to [65], the investment cost of a PEM electrolyser that can produce a unit standard cubic meter of hydrogen per hour was around $7,600 as of 2018, and this has since reduced to between $4,900 and $6,000 as of April 2020. Equally, the investment cost of alkaline electrolysers has drastically dropped. Table 6-3 shows the cost estimates of hydrogen production through electrolysis as of 2020 using the alkaline electrolyser (AE), PEM, and solid oxide Electrolyser (SOE).

System Type	Scenario	CapEx Cost ($/kW)	OpEx @ 3% ($/kW)	Electrolyser Lifetime (hr)	Conversion Efficiency (%)	Improvement Rate (%/yr.)
AE	Min.	571	17	75,000	70	0.5
	Median	988	30			2.0
	Max.	1268	38			2.5
PEM	Min.	1200	12	60,000	81	0.5
	Median	1634	35			2.0
	Max.	2068	62			2.5
SOE	Min.	1429	43	20,000	85	0.5
	Median	1857	56			2.0
	Max.	2285	69			2.5

Table 6-3: *Estimates of electrolysers price parameters as at mid-year 2020* [29, 66]

Given the onshore wind power cost estimate values in section 6.1 and the hydrogen production cost estimates in table 6-3, it was possible to deduce cost estimates of the main components that would be used in the Djupvik wind electrolysis. Table 6-4 shows the rough estimates of the investment costs and Operation and maintenance costs of the leading equipment that would be required to make this project a reality.

Components	Investment Cost (CapEx) ($/kW)	O & M Cost (%)	Lifetime (yr.)
Wind Turbine	1591	2	25
Alkaline Electrolyser	1300	4	15
Gas Compressor	850	4	10
Storage Tank	800	2	15
Transmission Cables	1070	3	25
Power Converter	160	2	10

Table 6-4: *Cost estimates of components for wind electrolysis hydrogen production* [67]

6.3 Economic Cost Comparison of Different Hydrogen Production Methods

Having discussed the cost estimates of the wind electrolysis, it would be worthwhile to compare such findings with production cost estimates of other methods that are already well established globally and thereafter make a comparative analysis. Table 6-5 shows the global average investment costs comparison of different forms of hydrogen production.

Production Process	Energy Source	Feedstock	Capital Cost (Million $)	Hydrogen Cost ($/kg)
SMR with CCS	Fossil Fuels	Natural gas	226.4	2.27
SMR without CCS	”	Natural gas	180.7	2.08
CG with CCS	”	Coal	415.6	1.63
CG without CCS	”	Coal	335.9	1.34
ATR of CH_4 with CCS	Fossil Fuels	Natural gas	183.8	1.48
Biomass Gasification	Internally generated steam	Woody biomass	6.4 – 149.3	1.77 – 2.05
Wind Electrolysis	**Wind Energy**	**Water**	**499.6 – 504.8**	**5.89 – 6.03**

Table 6-5: *Global average investment costs of different hydrogen production methods* [19]

From table 6-5, it can be observed that the capital cost of wind electrolysis is exorbitantly high when compared to the methods that use fossil fuel sources of energy like steam methane reformation (SMR), coal gasification (CG), and Auto-thermal reformation (ATR). In fact, the cost of producing hydrogen through wind electrolysis is 6 to 10 times that of fossil fuel alternatives, according to [28]. This can be associated with the existence and establishment of fossil fuel-powered technologies for a much more extended period than electrolysis technologies. However, the cost of natural gas steam reformation (NG SR) and coal gasification technologies are slightly inflated when the carbon capture and sequestration (CCS) technologies are applied to help in minimising the CO_2 and other greenhouse gases (GHG) emissions. Such technology is not required in wind electrolysis as the process is producing pollution-free hydrogen. Figure 6-2 shows the comparison of the production cost of hydrogen from different methods.

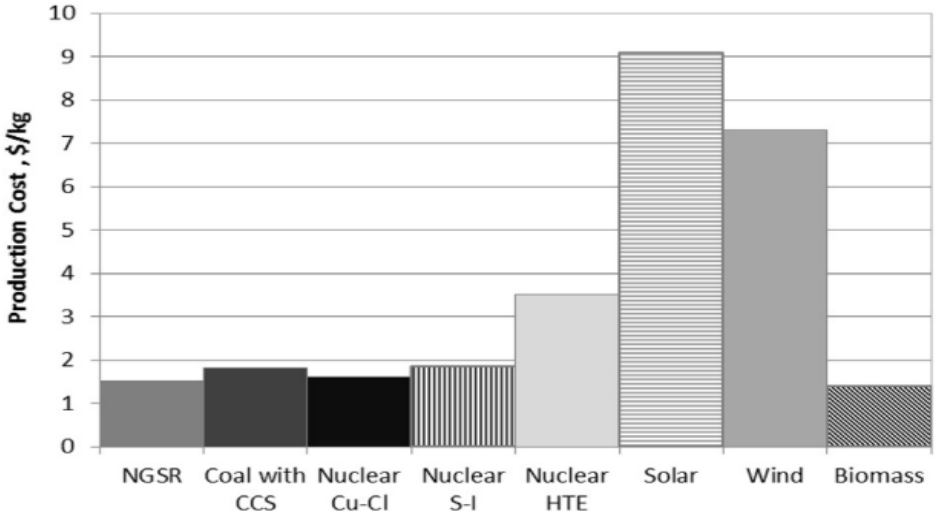

Figure 6-2: *Comparative analysis of hydrogen production cost from different technologies* [28]

From table 6-5 and figure 6-2, the methods with the lowest cost of hydrogen production are biomass gasification, Natural gas steam reformation (NG SR) methods, and nuclear reactors. However, their sustainability and environmental effect are serious issues that make everyone frown at them. The cost of production from renewable sources like wind and solar remains high, but because they are emission-free, they make up serious candidates for future consideration.

6.4 Environmental Impact Comparison of different Hydrogen Production Methods

Even though the cost of hydrogen production from the natural gas steam reformation (NG SR), coal gasification, and biomass gasification is lower, the ecological effect is much more significant compared to the renewable sources, as shown in figure 6-3.

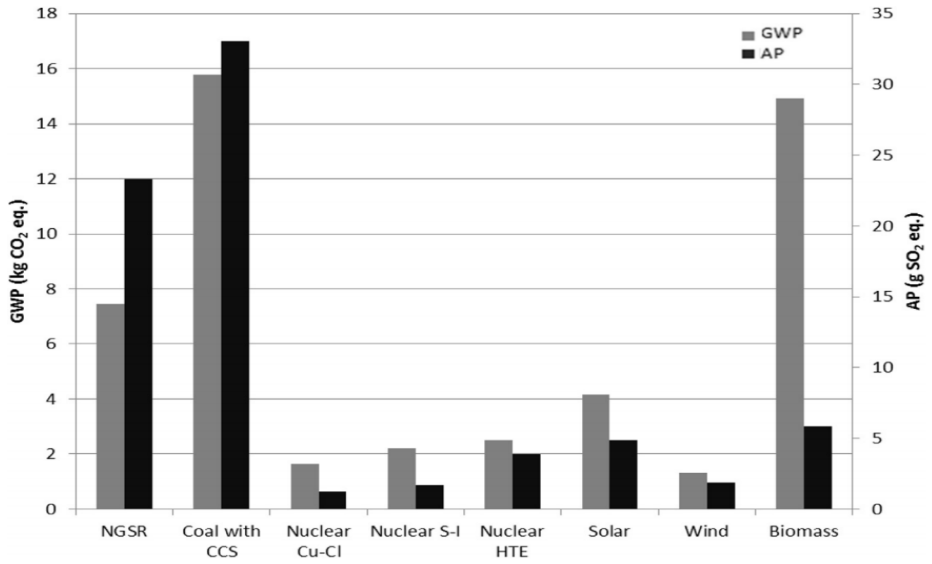

Figure 6-3: *GWP and AP of hydrogen production methods* [28]

Figure 6-3 shows that hydrogen produced from carbon-intensive sources like coal, biomass, and fossil fuel methods have extremely high global warming potential (GWP) and acidification potential (AP) to the environment, and such have negative impact on the ecological system in the long run. Such consequences can weigh heavily on the ecosystem such that the lower production costs are engulfed by very high costs incurred in correcting the long-term insidious environmental damages. On the other hand, wind electrolysis has the lowest GWP and AP emission to the environment compared to other methods, and this affirms that even though its hydrogen production cost is high, the aftermath ecological damage is minimal hence lower post-production costs incurred in correcting the environmental pollution.

7 CONCLUSION AND FURTHER RESEARCH

7.1 Conclusion

This master thesis project sort to investigate the green hydrogen production by way of wind electrolysis. The project was accomplished through wind resource assessment of the area around Djupvik using Windographer and WindSim tools to estimate the amount of electricity that would be generated for use in the water electrolysis process. Thereafter, the estimated electrical power output was used together with the existing electrolysers' specifications to calculate the possible hourly and daily hydrogen production rate.

Given that the minimum required demand for daily hydrogen consumption in Narvik and its environs was estimated at 20kg/day and comparing this demand against the findings on the rate of hydrogen production results from any of the electrolysers above, this study can authoritatively conclude that it would be feasible to meet the daily hydrogen consumption demand when a single Vestas V80-2.0MW wind turbine model is installed to generate power at the selected site location in table 4-25 operating at any hub height between 45m and 100m for the water electrolysis process. In particular, the highest hydrogen production rate would be experienced at a wind turbine installation hub height of 70m, where the electrical power generation is optimum.

To assert the above conclusion, the two case studies of the different alkaline electrolysers from Nel Hydrogen Company and Hydrogenics Corporation are evidence that if electrical power is generated from the selected site using the proposed wind turbine hoisted at any of the mentioned hub height range, the electrical power would be enough for use in water electrolysis to generate more than enough hydrogen to meet the daily approximated demand. On the other hand, in the invent that the future hydrogen consumption demand increases, translating to a possible increase in electrical power demand for electrolysis, an additional wind turbine might be installed at any of the remaining three locations in figure 4-18 to top up the additional hydrogen demanded.

Whereas the cost estimate findings of the wind electrolysis seemed relatively higher compared to the other renowned methods of hydrogen production, its ecological benefits outweigh the economic drawbacks. Furthermore, this method is highly sustainable and has long-term benefits compared to the short-term economic benefits of the fossil fuel-powered methods whose sustainability is volatile. In addition, the global warming and acidification potential of wind electrolysis is extremely low since the process is emission-free from greenhouse gases. To

crown it all, the economic cost of wind electrolysis might be an impediment in the short term, but the long term environmental impact will be exceptionally enormous. As a result, this study proposes an immediate investment in wind electrolysis project.

Finally, as part of this master thesis project scope, this study culminates in generating a scientific paper on green hydrogen production through wind electrolysis. I am currently working on a manuscript that once concluded will be submitted to a scientific journal.

7.2 Further Research

- Since the proposed hydrogen production site is on the slopes of a mountain, there was a limitation on wind resource simulation on the nearby areas where the actual site is located. The WindSim CFD software could not complete the entire module run for any location on the mountain even though the wind resource maps showed pleasant wind speed potential on the mountain top. This was associated with the complexity of the terrain and the presence of forested obstacles on the mountain, as it is known that CFD models have a weakness of application in complex terrains. Therefore, this study proposes further research on the application of more powerful simulation tools such as Meso-scale NWP models like Weather Research and Forecast (WRF) tools to ascertain the wind power potential on the slopes and peak of the mountain.

- In this project, only three different wind turbine models, were applied for comparative purposes. However, there are several models in the market. As a result, this study proposes a launch of further research on CFD simulation applications using various wind turbine models to compare their performance in the area under investigation.

- From the data analysis section of this project, I conclude that more wind energy will be harnessed in the winter season when the average wind speeds are higher than in summer. This calls for further investigation on the behavioral performance of wind turbines, electrolysers, and any other system used in power production, transmission, and hydrogen production in cold climates. In particular, the icing effect on the wind turbines' and electrolyser's performance is an area I would wish to vehemently pursue as an appendage of this project going into the future.

- Lastly, given that the wind speed potential is low during summer in the area and solar energy is optimal during this period, this study proposes a further research on possibility of using solar power as an alternative energy source for hydrogen production to supplement on the wind power and to bridge any supply shortfall during the summer season.

8 REFERENCES

[1] IEA. "World Energy Outlook 2020, ." IEA, Paris. https://www.iea.org/reports/world-energy-outlook-2020 (accessed 2021).

[2] E. Bryant, E. A. Bryant, and B. Edward, *Climate process and change*. Cambridge University Press, 1997.

[3] C. Acar and I. Dincer, "Review and evaluation of hydrogen production options for better environment," *Journal of cleaner production*, vol. 218, pp. 835-849, 2019.

[4] R. Annah and R. Max. "Emissions By Sector: Global Greenhouse gas Emissions." Our World in Data. https://ourworldindata.org/emissions-by-sector#energy-electricity-heat-and-transport-73-2 (accessed 2020).

[5] P. M. E. Solberg. "New Year Speech 2021." Office of the Prime Minister, Norway. https://www.regjeringen.no/en/aktuelt/new-year-speech-2021/id2826293/ (accessed January, 2021).

[6] UNEP and DTU, "Emissions Gap Report 2020," 2020. [Online]. Available: https://www.unep.org/emissions-gap-report-2020

[7] Explorer. "Green and Sustainable solutions from Norway: How Norway helps to commercialise environment-friendly energy techology." https://www.theexplorer.no/stories/energy/how-norway-helps-to-commercialise-environment-friendly-energy-techology/ (accessed November, 2020).

[8] EuropeanCommission, "HyWAyS Report: The European Hydrogen Energy Roadmap," 2008. Accessed: 2020. [Online]. Available: https://op.europa.eu/en/publication-detail/-/publication.

[9] S. Kumar, *Clean Hydrogen Production Methods*. New York Dordrecht London: Springer Cham Heidelberg, 2015, p. 75.

[10] S. A. Sherif, F. Barbir, and T. N. Veziroglu, "Wind energy and the hydrogen economy—review of the technology," *Solar Energy*, vol. 78, no. 5, pp. 647-660, 2005, doi: 10.1016/j.solener.2005.01.002.

[11] NREL. "The 2020 Transportation Annual Technology Baseline (ATB)." Golden, CO: National Renewable Energy Laboratory (NREL). https://atb.nrel.gov. (accessed January 2021).

[12] J. Turner *et al.*, "Renewable hydrogen production," *International journal of energy research*, vol. 32, no. 5, pp. 379-407, 2008.

[13] I. Dincer and C. Acar, "Review and evaluation of hydrogen production methods for better sustainability," *International Journal of Hydrogen Energy*, vol. 40, no. 34, pp. 11094-11111, 2015, doi: 10.1016/j.ijhydene.2014.12.035.

[14] V. Yaramasu and B. Wu, *Model predictive control of wind energy conversion systems*. John Wiley & Sons, 2016.

[15] GWEC. "Global Wind Report 2019: The flagship annual report for the global wind industry from GWEC Market Intelligence! ." https://gwec.net/global-wind-report-2019/ (accessed 2020).

[16] Nordkraft. "Datasenter." https://www.nordkraft.no/media/nyhetsarkiv/prosjekt/datasenter (accessed December 2020).

[17] S. T. Mirabal, "An economic analysis of hydrogen production technologies using renewable energy resources," University of Florida, 2003.

[18] A. Godula-Jopek, *Hydrogen Production: By Electrolysis*, First Edition ed. Weinheim, Germany: Wiley-VCH Verlag GmbH & Co. KGaA 2015.

[19] F. Calise, *Solar Hydrogen Production: Processes, Systems and Technologies* (Hydrogen Production Methods). London, United Kingdom: : Academic Press an imprint of Elsevier, 2019.

[20] "Fulfilling the Potential of Fuel Cell Electric Vehicles: The Impact of Hydrogen Production Methods on Global Warming Emissions," Union of Concerned Scientists, 2015. Accessed: 2021/02/26. [Online]. Available: http://www.jstor.org/stable/resrep17279

[21] Jan Vaes, "Hydrogen generators for energy storage and industrial applications: Water electrolysis state of affairs," *Hydrogenics On Site Generation: World of Energy Solutions*, 2016.

[22] M. Sankir and N. D. Sankir, *Hydrogen production technologies (Advances in Hydrogen Production and Storage)*. Beverly, MA: John Wiley & Sons, 2017.

[23] R. Yukesh Kannah, S. Kavitha, O. Parthiba Karthikeyan, G. Kumar, N. V. Dai-Viet, and J. Rajesh Banu, "Techno-economic assessment of various hydrogen production methods-A review," *Bioresour Technol*, pp. 124175-124175, 2021.

[24] D. Y. Goswami, S. T. Mirabal, N. Goel, and H. Ingley, "A review of hydrogen production technologies," in *International Conference on Fuel Cell Science, Engineering and Technology*, 2003, vol. 36681, pp. 61-74.

[25] E. I. Administration and E. Department, *Annual Energy Outlook with Projections: 2015 with Projections To 2040*. Government Printing Office, 2015.

[26] M. El-Shafie, S. Kambara, and Y. Hayakawa, "Hydrogen production technologies overview," *Journal of Power and Energy Engineering*, vol. 7, no. 01, p. 107, 2019.

[27] D. Gardner. "Hydrogen production from renewables." http://www.renewableenergyfocus.com/view/3157/hydrogen-production-from-renewables/ (accessed April 2021).

[28] C. Acar and I. Dincer, "Comparative assessment of hydrogen production methods from renewable and non-renewable sources," *International journal of hydrogen energy*, vol. 39, no. 1, pp. 1-12, 2014.

[29] R. Mark, M. Ahmad, and M. Maggie, "Manufacturing Competitiveness Analysis for PEM and Alkaline Water Electrolysis Systems," 11/08/2017.

[30] M. Brower, *Wind resource assessment : a practical guide to developing a wind project*. Hoboken, N.J.: Wiley, 2012, pp. xvi, 280 p.

[31] M. H. Zhang, *Wind resource assessment and micro-siting : science and engineering*. Singapore: China Machine Press : Wiley Blackwell, 2015, pp. xxv, 293 pages.

[32] J. F. Corbett, "RAMSIM: A fast computer model for mean wind flow over hills," *Risø-PhD*, vol. 17, p. 143, 2007.

[33] F. Sandro, G. M. Maria, and J. Pierre, "Wind Flow Models over Complex Terrain for Dispersion Calculations," *Cost Action 710: Pre-processing of Meteorological Data for Dispersion Models, Report of Working Group*, 1997.

[34] E. W. Hewson, J. E. Wade, and R. W. Baker, "Handbook on the use of trees as an indicator of wind power potential. Final report," Oregon State Univ., Corvallis (USA). Dept. of Atmospheric Science, 1979.

[35] K. Murthy and O. Rahi, "A comprehensive review of wind resource assessment," *Renewable and Sustainable Energy Reviews*, vol. 72, pp. 1320-1342, 2017.

[36] N. G. Mortensen, A. J. Bowen, and I. Antoniou, "Improving WAsP predictions in (too) complex terrain," in *Proceedings of the 2006 European Wind Energy Conference and Exhibition, Athens*, 2006, vol. 27.

[37] G. H. Galvez *et al.*, "Wind resource assessment and sensitivity analysis of the levelised cost of energy. A case study in Tabasco, Mexico," *Renewable Energy Focus*, vol. 29, pp. 94-106, 2019.

[38] P. Beaucage, M. C. Brower, and J. Tensen, "Evaluation of four numerical wind flow models for wind resource mapping," *Wind Energy*, vol. 17, no. 2, pp. 197-208, 2014.

[39] F. Daniele, "Wind Energy Resource Evaluation in A Site of Central Italy by CFD Simulations," 2007.

[40] R. Ebenhoch, B. Muro, J.-Å. Dahlberg, P. Berkesten Hägglund, and A. Segalini, "A linearized numerical model of wind-farm flows," *Wind Energy*, vol. 20, no. 5, pp. 859-875, 2017, doi: 10.1002/we.2067.

[41] R. M. Endlich, F. L. Ludwig, and C. M. bhumralkar, "A Diagnostic Model for Estimating Winds at Potential Sites for Wind Turbines," 1982.

[42] C. B. Moorthy and M. K. Deshmukh, "Wind Resource Assessment Using Computer Simulation Tool: A Case Study," *Energy Procedia*, vol. 100, pp. 141-148, 2016, doi: 10.1016/j.egypro.2016.10.156.

[43] H. M. Søren, V. H. Yavor, J. K. Sven, and S. O. Gregory, "Validation of CFD wind resource mapping in complex terrain based on WTG performance data," 2012.

[44] G. T. Philips, "A Preliminary User's Guide for the NOABL Objective Analysis Code," *U.S Department of Energy*, p. 121, 1979.

[45] C. A. Sherman, "A mass-consistent model for wind fields over complex terrain," *Journal of Applied Meteorology and Climatology*, vol. 17, no. 3, pp. 312-319, 1978.

[46] M. Boznar *et al.*, "Application of advanced and traditional diffusion models to an experimental campaign in complex terrain," *Transactions on Ecology and the Environment*, vol. 3, 1994.

[47] H. Jordan, H. Braden, S. Ashley, S. Kailyn, and D. Jason. "Energy Education - Wind Turbines." University of Calgary. https://energyeducation.ca/encyclopedia/Wind_turbine (accessed November, 2020).

[48] F. Todd. "Anatomy of a wind turbine: Analysing the key components involved." NS Energy. https://www.nsenergybusiness.com/features/wind-turbine-components/ (accessed November 2020).

[49] S. H. Song, S. I. Kang, and N. K. Hahm, "Implementation and control of grid connected AC-DC-AC power converter for variable speed wind energy conversion system," in

Eighteenth Annual IEEE Applied Power Electronics Conference and Exposition, 2003. APEC'03., 2003, vol. 1: IEEE, pp. 154-158.

[50] J. Andrews and N. Jelley, *Energy science: principles, technologies, and impacts*. Oxford university press, 2017.

[51] I. E. Commission, "Wind Energy Generation Systems—Part 12-1: Power Performance Measurements of Electricity Producing Wind Turbines," IEC 61400-12-1: 2017, 2007.

[52] X. Chen and R. Agarwal, "Optimal placement of horizontal-and vertical-axis wind turbines in a wind farm for maximum power generation using a genetic algorithm," *International Journal of Energy & Environment*, vol. 3, no. 6, pp. 927-938, 2012.

[53] L. Vermeer, J. N. Sørensen, and A. Crespo, "Wind turbine wake aerodynamics," *Progress in aerospace sciences*, vol. 39, no. 6-7, pp. 467-510, 2003.

[54] N. Moskalenko, K. Rudion, and A. Orths, "Study of wake effects for offshore wind farm planning," in *2010 Modern Electric Power Systems*, 2010: IEEE, pp. 1-7.

[55] "NORSK KLIMASERVICESENTER." https://seklima.met.no/observations. (accessed 2021).

[56] WindSim. https://windsim.com/about/history/ (accessed February 2021.

[57] A. Kangash, R. Ghani, M. S. Virk, P. Maryandyshev, V. Lubov, and M. Mustafa, "Review of energy demands and wind resource assessment of the Solovetsky Archipelago," *International Journal of Smart Grid and Clean Energy*, vol. 8, no. 4, pp. 430-435, 2019.

[58] T. J. Stehly and P. C. Beiter, "2018 Cost of Wind Energy Review," National Renewable Energy Lab.(NREL), Golden, CO (United States), 2020.

[59] S. Ram, "What are the Different Types of a Voltage Stabilizer?," in *http://www.saveawatt.in/*, ed: Saveawatt, 2019.

[60] K. Mulchandani, S. Bannore, S. Lambor, V. Parkhi, and V. Bhalerao, "Static Voltage Stabilizer," 2018.

[61] S. Venkatesh and K. Muthiah, "Power fluctuations-usage of servo voltage stabilizers in industries," *International Journal of Applied Engineering Research*, vol. 2, no. 1, p. 283, 2011.

[62] NelHydrogenElectrolysers. "The World's Most Efficient and Reliable Electrolysers." Nel Hydrogen, Norway. https://nelhydrogen.com/wp-content/uploads/2020/03/Electrolysers-Brochure-Rev-C.pdf (accessed April, 2021).

[63] HYDROGENICS. "Hydrogen generators: The HySTAT™ system is state-of-the-art technology that meets international safety and technical standards offers operational advantages."http://www.intech.eu/en/hydrogen-technology/products/hydrogen-generators (accessed March, 2021).

[64] M. I. Blanco, "The economics of wind energy," *Renewable and sustainable energy reviews*, vol. 13, no. 6-7, pp. 1372-1382, 2009.

[65] C. LICHNER. "Electrolyzer overview: Lowering the cost of hydrogen and distributing its production." https://pv-magazine-usa.com/2020/03/26/electrolyzer-overview-lowering-the-cost-of-hydrogen-and-distributing-its-productionhydrogen-industry-overview-lowering-the-cost-and-distributing-production/ (accessed March 2021).

[66] A. Christensen, "Assessment of hydrogen production costs from electrolysis: United States and Europe," *Retrieved from the International Council on Clean Transportation: https://theicct. org/publications/assessment-hydrogen-production-costs-electrolysis-united-states-and-europe,* 2020.

[67] C. J. Greiner, M. KorpÅs, and A. T. Holen, "A Norwegian case study on the production of hydrogen from wind power," *International Journal of Hydrogen Energy,* vol. 32, no. 10-11, pp. 1500-1507, 2007.